THE EFFECTS OF MASS TRANSFER AND ANGLE OF ATTACK ON HYPERSONIC TURBULENT BOUNDARY LAYER CHARACTERISTICS

A. L. Laganelli, et al

General Electric Company

Prepared for:

Air Force Flight Dynamics Laboratory

April 1975

AFFDL-TR-75-35

THE EFFECTS OF MASS TRANSFER AND ANGLE OF ATTACK ON HYPERSONIC TURBULENT BOUNDARY LAYER CHARACTERISTICS

GENERAL ELECTRIC COMPANY
RE-ENTRY AND ENVIRONMENTAL SYSTEMS DIVISION
PHILADELPHIA, PENNSYLVANIA 19101

TECHNICAL REPORT AFFDL—TR—75—35

APRIL 1975

FINAL REPORT FOR PERIOD NOVEMBER 1973 — APRIL 1975

Approved for public release; distribution unlimited.

AIR FORCE FLIGHT DYNAMICS LABORATORY
AIR FORCE SYSTEMS COMMAND
WRIGHT—PATTERSON AIR FORCE BASE, OHIO 45433

UNCLASSIFIED

SECURITY CLASSIFICATION OF THIS PAGE (When Data Entered)

REPORT DOCUMENTATION PAGE		READ INSTRUCTIONS BEFORE COMPLETING FORM
1 REPORT NUMBER AFFDL-TR-75-35	2 GOVT ACCESSION NO.	3 RECIPIENT'S CATALOG NUMBER
4 TITLE (and Subtitle) THE EFFECTS OF MASS TRANSFER AND AND ANGLE OF ATTACK ON HYPERSONIC TURBULENT BOUNDARY LAYER CHARACTERISTICS		5 TYPE OF REPORT & PERIOD COVERED Final Report November 1973 - April 1975 6 PERFORMING ORG. REPORT NUMBER
7 AUTHOR(s) A. L. Laganelli R. P. Fogaroli A. Martellucci		8 CONTRACT OR GRANT NUMBER(s) F33615-74-C-3016
9 PERFORMING ORGANIZATION NAME AND ADDRESS General Electric Company Re-entry and Environmental Systems Division Philadelphia, Pennsylvania 19101		10 PROGRAM ELEMENT, PROJECT, TASK AREA & WORK UNIT NUMBERS Project 1366
11 CONTROLLING OFFICE NAME AND ADDRESS Air Force Flight Dynamics Laboratory Air Force Systems Command Wright-Patterson Air Force Base, Ohio 45433		12. REPORT DATE April 1975 13. NUMBER OF PAGES 159
14 MONITORING AGENCY NAME & ADDRESS(if different from Controlling Office)		15. SECURITY CLASS (of this report) Unclassified 15a DECLASSIFICATION DOWNGRADING SCHEDULE

16 DISTRIBUTION STATEMENT (of this Report)

Approved for public release; distribution unlimited.

17 DISTRIBUTION STATEMENT (of the abstract entered in Block 20, if different from Report)

18 SUPPLEMENTARY NOTES

19 KEY WORDS (Continue on reverse side if necessary and identify by block number)

Turbulent Boundary Layers
Hypersonic Flow
Heat and Mass Transfer
Angle of Attack effects
Viscous Layer Thicknesses

20 ABSTRACT (Continue on reverse side if necessary and identify by block number)

Utilizing recent hypersonic flow experiments as a data base, several features of turbulent boundary layer characteristics were examined in order to provide improved engineering design capability, accounting for the effects of angle of attack, Reynolds number, compressibility, mass transfer and injectant molecular weight.

These features consisted of (1) the Crocco temperature-velocity relationship, (2) the boundary layer profile shape and viscous layer thickness relations, and (3) heat

DD FORM 1 JAN 73 1473 EDITION OF 1 NOV 65 IS OBSOLETE

UNCLASSIFIED

SECURITY CLASSIFICATION OF THIS PAGE (When Data Entered)

blockage and skin-friction reduction due to mass injection.

The classic Crocco temperature-velocity relation was examined at hypersonic flow conditions on a sharp porous cone. Departures from the linear Crocco relation were observed that tended to follow a modified quadratic distribution in velocity. In general, the data tended to follow the linear Crocco relation with a temperature overshoot resulting from the kinetic energy of the flow which is typical of flat-plate type flows previously investigated. A non-similarity parameter was introduced to account for the effects of mass transfer, pressure gradient and temperature potential.

An evaluation of the boundary layer profile shape (in terms of the velocity power-law exponent and viscous layer integral thickness relations) resulted in correlations for viscous layer thicknesses which account for the effects of Mach number, wall temperature, mass transfer, injectant molecular weight and angle of attack.

The effect of Mach number, wall temperature and injectant molecular weight on heat blockage and skin friction reduction resulting from mass injection was evaluated, resulting in semi-empirical correlations which are based on a modification of a compressibility transformation theory expanded to include the latest hypersonic data. The resultant heat blockage and skin friction reduction correlations were verified by comparison with data over a wide range of Mach number, wall temperature and injectant molecular weight.

The correlation development, based on an analytically derived compressibility transformation and an empirically derived viscous transformation, employed a critical blowaway parameter concept to provide a more tractable set of correlations for engineering design. Angle of attack heat transfer was satisfactorily predicted using an existing semi-empirical turbulent boundary layer code which utilized the aforementioned mass transfer correlations.

FOREWORD

This report presents a detailed examination of engineering design relationships for turbulent boundary layer flows which account for the effects of mass transfer, angle of attack, and Reynolds number. In particular, the study is concerned with turbulent boundary layer characteristics associated with energy profile shape (Crocco temperature-velocity relation), velocity power law exponent, viscous layer thickness, skin friction reduction, and heat transfer blockage. These tasks were selected as a consequence of their direct use in engineering design codes. The data base for this study consists of the experimental work obtained by GE-RESD under SAMSO Air Force contract F04701-70-C-0179 entitled "Strategic Re-entry Technology Program - Phase II" (STREET-G) Task 4.11 (1972) and Task 4.14 (1973) as well as data from the literature. The work supported herein was performed at the General Electric Company, Re-entry and Environmental Systems Division, Valley Forge, Pennsylvania.

This document represents the culmination of work performed under Contract Number F33615-74-C-3016, Project 1366; "Aerodynamic Empirical Techniques for Strategic Missiles." The work was performed in the time period November 1973 through April 1975. This investigation was conducted for the United States Air Force Flight Dynamics Laboratory under the technical direction of Mr. Richard R. Smith (AFFDL/FXG). The final report was submitted by the authors for publication approved on April 25, 1975.

The authors wish to acknowledge the following General Electric personnel for their assistance during this contract: Dr. A.M. Hecht for comments and suggestions, Mr. David Nestler and Ms. C. Dougherty for computational assistance and finally to Mr. R. Sweeney and Mr. W. Norman for computation and plotting.

TABLE OF CONTENTS

TABLE OF CONTENTS (Continued)

LIST OF ILLUSTRATIONS

LIST OF ILLUSTRATIONS (Continued)

LIST OF TABLES

LIST OF SYMBOLS

A - constant defined in Eq. (17), equal to 1.69

B - constant defined in Eq. (18), equal to 1.16

B_h - blowing parameter, $(C_{p_{inj}}/C_{p_{air}})\ (\lambda/St)$

B_u - blowing parameter, $(C_{p_{inj}}/C_{p_{air}})\ (2\lambda/C_f)$

b_{cr} - critical blowaway parameter

b_h - blowing parameter, $(C_{p_{inj}}/C_{p_{air}})\ (\lambda/St_o)$

b_u - blowing parameter, $(C_{p_{inj}}/C_{p_{air}})\ (2\lambda/C_{f_o})$

b_M - blowing parameter, $(2\lambda/C_{f_o})\ (\bar{M}_{air}/\bar{M}_{inj})^{2/3}$

$b_{M,\alpha}$ - blowing parameter, $\left[2\lambda(\alpha)/C_{f_o}(\alpha)\right]\ (\bar{M}_{air}/\bar{M}_{inj})^{2/3}$

C - velocity power law constant, defined in Eq. (22)

C_i - mass fraction of injectant gas (i)

C_f - skin-friction coefficient

C_p - specific heat, BTU/(lb_m ^oR)

F_c - compressibility transformation function

F_s - viscous transformation function based on Re_s

F_θ - viscous transformation function based on Re_θ

H - total enthalpy, BTU/lb_m

h - static enthalpy, BTU/lb_m

$K(n)$ - velocity power law parameter, defined in Eq. (24)

M - Mach number

$\bar{M}$ - molecular weight

MF - Mangler factor, defined in Eq. (28)

LIST OF SYMBOLS (Continued)

n	-	power law velocity profile exponent
P	-	pressure, psia
Pr	-	Prandtl number
$\dot{q}$	-	heat transfer rate, BTU/ft^2-sec
R_N	-	nose radius
$\bar{R}$	-	effective gas constant
Re_s	-	Reynolds number based on wetted length, $(\rho_e u_e s/\mu_e)$
Re_θ	-	Reynolds number based on momentum thickness, $(\rho_e u_e \theta/\mu_e)$
r	-	radius measured from axis of symmetry; recovery factor
s	-	wetted length along surface of body
St	-	Stanton number, $\dot{q}_w/(\rho u)_e \ (h_{aw} - h_w)$
St_∞	-	Stanton number, $\dot{q}_w/(\rho u)_\infty \ (H_\infty - h_w)$
T	-	temperature, ^oR
T^+	-	total temperature, defined in Eq. (5)
u	-	velocity component tangent to surface
v	-	velocity component normal to surface
x	-	axial distance from apex
y	-	distance normal to body surface
z	-	velocity ratio, u/u_e

GREEK SYMBOLS

α	-	angle of attack
β	-	kinetic energy parameter, $(T_{aw}-T_w) / (T_e^o-T_w)$
$\gamma, \bar{\gamma}$	-	ratio of specific heats, effective value
δ	-	boundary layer thickness
δ^*	-	boundary layer displacement thickness
ϵ_T	-	turbulent compressibility factor, defined in Eq. (25)

LIST OF GREEK SYMBOLS (Continued)

η	-	dimensionless coordinate, y/δ
θ	-	boundary layer momentum thickness
θ_c	-	cone half angle
λ	-	blowing parameter, $(\rho v)_w/(\rho u)_e$
λ_∞	-	blowing parameter, $(\rho v)_w/(\rho u)_\infty$
μ	-	molecular viscosity
ξ	-	non-similarity parameter, defined in Eq. (4)
ρ	-	density
τ	-	shear stress
χ_i	-	mole fraction of injectant gas (i)
ψ	-	constant defined in Eq. (34)
ω	-	viscous transformation exponent, defined in Eq. (58)

SUBSCRIPTS

air	-	air
aw	-	adiabatic wall value (recovery condition)
cr	-	critical value
e	-	boundary layer edge
i	-	incompressible flow value
inj	-	injectant
N	-	model nose tip
o	-	zero mass injection
r	-	recovery (adiabatic wall) condition
s	-	wetted length value
w	-	wall condition
∞	-	free stream condition

SUPERSCRIPTS

o	-	total conditions
*	-	properties based on Eckert reference enthalpy defined as: $h^*/h_e = 0.5\,(1 + h_w/h_e) + 0.11\,r\,(\gamma-1)\,M_e^2$

TECHNICAL SUMMARY

The problems examined in this study are concerned with turbulent boundary layer characteristics that are required for engineering design codes. These consist of: (1) boundary layer profile shape (velocity power law exponent), (2) energy profile shape (Crocco temperature - velocity relation), (3) viscous layer thicknesses (δ, δ^*, and θ), (4) skin friction reduction, and (5) heat transfer blockage. The above were investigated relative to improving existing engineering design capability for turbulent boundary layer flows that are associated with the effects of angle of attack, Reynolds number, compressibility, and mass transfer. This study serves to provide two primary functions: first, to upgrade industrial design codes that rely upon two-dimensional, low Mach number data correlations and secondly, to provide an insight to sophisticated 3-D finite difference or integral viscous boundary layer codes.

The classic Crocco temperature-velocity relation was examined at hypersonic flow conditions on a sharp, porous cone. The evaluation was made with the effects of mass transfer, angle-of-attack, and molecular weight variations of the injectant gas for a free stream Mach number of approximately 8.0. Departures from the linear Crocco relation were observed that tended to follow a modified quadratic distribution in velocity. In general, the data tended to follow the linear Crocco relation with a temperature overshoot resulting from the kinetic energy of the flow which is typical of flat plate type flows previously investigated.

Specifically, no apparent effect of Mach number or Reynolds number was noted. Mass transfer tended to depart from the linear relationship toward a modified quadratic velocity relation. The effect of boundary layer transition (up-stream history) should be considered when evaluating the Crocco variables. For windward angle of attack, the data tended to follow the linear distribution; whereas, for leeward conditions, the data were characterized by a quadratic behavior. Moreover, for laminar boundary layers the data was linearly oriented, and for turbulent flow conditions the data appeared to follow the quadratic relation. No specific conclusions could be made regarding the

Crocco relation for non-air injection cases. Finally, a non-similarity parameter is introduced to account for the effects of blowing, pressure gradient, and temperature potential.

This portion of the study is considered an important contribution to boundary layer behavior inasmuch as departures from similarity of the thermal and hydrodynamic (Pr $\neq$ unity) characteristics of the boundary layer can be accounted for with slight modifications to the linear Crocco relation. In particular, transformation functions which relate incompressible to compressible theory can be modified to account for departures from a unit Prandtl number that include longitudinal pressure gradient, mass transfer and temperature potential.

The turbulent boundary layer characteristic parameters δ, δ^*, θ, and n were also examined relative to the influence of Reynolds number, angle of attack, mass transfer, and molecular weight variations of the injectant gases. The study emphasized recently obtained data at hypersonic flow conditions on a sharp porous cone. In general, it was found that the state of boundary layer development was sensitive to the velocity power law exponent as well as the viscous layer thicknesses.

Specifically, the power law exponent showed significant variations from the classic fully-developed turbulent flow value of n = 7. As a consequence, reference momentum thickness relations (i.e., $\alpha = \lambda = 0$) had to be modified to include a generalized velocity power law exponent. Prediction capability for this reference situation is shown to be in excellent agreement with data. Concerning mass transfer effects, correlations were developed for the viscous layer thicknesses which include molecular weight effects. When combining angle of attack effects with blowing, a hyperbolic type correlation was developed that considers the viscous layer thickness (when normalized by its $\alpha = 0$ value) as a function of α/θ_c as well as the blowing parameter.

The development of the viscous layer thickness correlations is considered a significant advancement in the state of the art for turbulent flow engineering prediction capability. In particular, the ability to determine viscous layer parameters for three-

dimensional configurations, including the effect of mass transfer and molecular weight, affords the design engineer greater latitude than previously attained. Moreover, these correlations also allow for estimates of turbulent flow behavior over complex geometries such as control surfaces and surface discontinuities.

Finally, the effect of Mach number, wall temperature and injectant molecular weight on heat blockage and skin friction reduction resulting from mass injection was evaluated for turbulent flow over surfaces with negligible axial pressure gradients. The evaluation resulted in semi-empirical correlations which are based on a modification of a compressibility transformation theory expanded to include the latest hypersonic data up to a free stream Mach number of 8.0. The resultant heat blockage and skin friction reduction correlations were verified by comparison with data over a wide range of Mach number, wall temperature and injectant molecular weight. Emphasis was placed on recently acquired heat transfer data at hypersonic flow conditions on a porous sharp cone.

The correlation development, based on an analytically derived compressibility transformation and an empirically derived viscous transformation, employed a critical blowaway parameter concept to provide a more tractable set of correlations for engineering design. Angle of attack heat transfer was satisfactorily predicted using an existing semi-empirical turbulent boundary layer code which utilized the aforementioned mass transfer correlations.

By accounting for the effects of Mach number, wall temperature and injectant molecular weight on heat transfer and skin friction attenuation due to mass transfer, these correlations contribute significantly to the state of the art, effectively providing improved engineering design relationships suitable for inclusion in existing semi-empirical turbulent boundary layer codes. In addition, the theoretical compressibility transformation concept employed in this development has been shown to be effective and provides a sound fundamental base for future turbulent boundary layer studies.

SECTION 1

INTRODUCTION

The alleviation of the high heating rates encountered by surfaces of hypersonic vehicles has been recognized as an important problem. One of the cooling methods that has shown promise is mass-transfer cooling, wherein a "foreign" material is transferred from the vehicle surface into the boundary layer. This has a two-fold advantage in attenuating the heat-transfer problem. The transferred coolant may absorb heat from the boundary layer through a phase change (sublimation, evaporation, melting, etc.) as well as providing high thermal heat capacitance. In addition, it has been shown that the introduction of a material (with its normal velocity component) at the surface acts to decelerate the flow and, consequently, to reduce the skin friction which, in turn, reduces the heat transfer at the wall. The problem of coupling the fluid mechanics of boundary layer flow with material response is further enhanced when considering angle of attack effects. The evaluation of mass addition on the aerodynamic characteristics of re-entry vehicles at angle of attack is a complicated but definable process. Since the evaluation of viscous effects utilizing classical boundary layer theories requires knowledge of the inviscid flow conditions at the outer edge of the boundary layer, the inviscid streamline pattern of the flow and the resulting outer edge flow conditions must be determined. The angle of attack of the vehicle introduces local pressure gradients and cross flow effects which must be factored into the analysis. It is these effects which tend to dominate the flow computational procedures.

Within the aerospace community, very sophisticated computer programs have been developed for detailed computation of viscous flow properties. These programs provide rigorous solutions to many of the complex phenomena encountered by a re-entering vehicle, e.g., blunt body flows, separated flows, ablation, etc. However, they usually require significant computational time and can be sensitive to input values specified for configuration and flow conditions. Consequently, other classes of analytical methods have been developed. These techniques allow more rapid calculations for use in design

tradeoff studies, trajectory calculations, or evaluation of experimental data. These rapid design techniques (engineering type) make use of the results of the more sophisticated analyses and of experimental results either directly or in the form of correlations, to provide approximate but sufficiently accurate results. It is the engineering type of solution that will be examined in this study.

For turbulent flows, these engineering codes consider the heat transfer blockage, skin friction reduction, and boundary layer thickness growth with mass addition and angle of attack by semi-empirical means. In addition, it is customarily assumed that the velocity profile exponent (n) is 7 and that the Crocco integral is valid. Concerning the former, data obtained in the SAMSO sponsored Strategic Re-entry Technology (STREET-G) Program (corroborated in several other reports) indicate that a nonsimilar boundary layer exists downstream of transition (which could persist for 50 to 100 boundary layer thicknesses). In this region, which always exists on flight vehicles, there is a paucity of data. Furthermore, no data containing detailed boundary layer information for ablating bodies exists for the angle of attack case. On the other hand, the classic Crocco temperature-velocity relationship has been traditionally used to relate the density variations in a boundary layer to the velocity. In so doing, one must postulate an equation of state together with the boundary layer assumption for zero pressure gradient normal to the flow direction. One such method of relating the density and velocity is to assume unit Prandtl and Schmidt numbers throughout the boundary layer. Often referred to as the Reynolds Analogy, this assumption implies a relationship exists between shear stress, heat transfer, and mass transfer. Moreover, the Crocco relationship was developed from the two-dimensional boundary layer equations and its use in three-dimensional flows and flows with mass transfer must be carefully examined to determine its range of applicability for engineering prediction techniques.

As indicated above, the emphasis of this study is to upgrade and supplement data correlations that are required in engineering design codes. In particular, the recent hypersonic mean flow and surface data reported in References 1 and 2 will be emphasized.

The STREET-G experiment was performed at the Arnold Engineering Development Center in Tunnel B at Mach 8 using a five-degree half angle porous cone which is five feet long. The experiment considered mass addition rates which cover the ablation gas range for current heat shield materials (simulated ablation via gaseous mass injection of nitrogen, argon, Freon 12, and helium through the porous surface). Other significant parameters that were varied include molecular weight of the injectant, Reynolds number, and vehicle angle of attack (0° to 10°). These data are considered unique and represent an advancement in the state of the art for turbulent boundary layer characteristics.

The objectives of the proposed study are to provide improved engineering design relationships for turbulent boundary layer flows to account for the effects of mass transfer, angle of attack, and Reynolds number. Several correlations employing the effects of ablation (mass transfer) on local viscous flow properties have been reported in the literature. These correlations are, in general, based on incompressible "flat plate" type theory together with low and high speed data (supersonic). In the following tasks, commonly accepted correlations will be discussed and comparisons will be made to available data noting deficiencies in the relations.

When assessing the various engineering design codes, the integral technique appears to have received the most attention. Essentially, this prediction scheme is based on the incompressible momentum boundary layer equation which is subsequently modified for compressibility by a density transformation (such as the Eckert reference enthalpy method). Consider then the momentum integral equation for an irrotational flow, namely

$$\frac{C_f}{2} = \frac{\tau_w}{\rho_e u_e^2} = \frac{1}{r}\frac{d}{ds}(r\theta) - \frac{\theta}{\rho_e u_e^2}\frac{dP}{ds}\left[2 + \frac{\delta^*}{\theta} - M_e^2\right] - \frac{(\rho v)_w}{(\rho u)_e}$$

For a sharp cone with $(\rho v)_w$ and dP/ds equal to zero, one has

$$\frac{C_{f_o}}{2} = \frac{\tau_w}{\rho_e u_e^2} = \frac{\theta_o}{s} + \frac{d\theta_o}{ds}$$

where the subscript refers to a zero mass transfer state.

Keeping in mind that closed-formed solutions are desirable for expedient parametric studies, two concepts are available for design purposes. One is to assume a velocity power law together with the Blasius form of skin-friction and a reference enthalpy method for compressibility. Such a procedure yields the result

$$\frac{C_{f_o}}{2} = C_1 \frac{\rho^*}{\rho_e} \left(Re_s^* \right)^n = C_2 \frac{\rho^*}{\rho_e} \left(Re_\theta^* \right)^m$$

where C_1 and C_2 are constants, n and m are related to the power law selected and the starred properties are based on a reference state which is an average type between the wall and boundary layer edge conditions:

$$\rho^* \text{ and } \mu^* = \text{function } (h^*)$$

for

$$h^*/h_e = 1/2 + 1/2\, h_w/h_e + 0.11r\, (\gamma - 1)\, M_e^2$$

The second approach, which has been adopted by many authors, is somewhat more sophisticated and attempts to model more detail of the turbulent characteristics of the boundary layer. If one consideres either the von Karman or Prandtl forms of local shear distribution (the Prandtl form will be adopted here) there results

$$\tau_w = \bar{\rho}\, K^2 y^2 \, (d\bar{u}/dy)$$

For a constant pressure boundary layer together with the Crocco linear temperature-velocity relation and the equation of state, the density is related to the velocity giving

$$\frac{\bar{\rho}}{\rho_w} = \frac{T_w}{\bar{T}} = \frac{1}{1 + \tilde{B}\left(\frac{u}{u_e}\right) - \tilde{A}^2 \left(\frac{u}{u_e}\right)^2}$$

for

$$\tilde{A}^2 = \frac{r\,\frac{\gamma-1}{2}M_e^2}{T_w/T_e}, \quad \tilde{B} = \frac{1 + r\,\frac{\gamma-1}{2}M_e^2}{T_w/T_e} - 1$$

In this manner, skin-friction results can be generated for the non-blowing condition.

In both cases presented above, the design engineer has resorted to correlations of experimental data to determine the attenuation in skin-friction as well as the boundary layer characteristic thicknesses (δ, δ^*, θ) resulting from mass transfer. However, it should be noted that the analytical solutions suggest the form of the correlations.

In viewing these attendant difficulties to maintain simplicity in design codes, the features of the boundary layer characteristics that will require careful examination consist of:

(a) Boundary layer profile shape (velocity power-law exponent)

(b) Energy profile shape (Crocco temperature-velocity relationship)

(c) Viscous layer thicknesses (δ/δ_o, δ^*/δ_o^*, θ/θ_o)

(d) Skin-friction reduction (C_f/C_{f_o})

(e) Heat transfer blockage (St/St_o)

In particular, the above will be examined relative to improved engineering design capability for turbulent boundary layer flows that consider the effects of angle of attack and Reynolds number as well as mass transfer.

Because of the extensive scope of this study which examines the turbulent boundary layer features listed above, the body of this report is subdivided into four major sections. These sections are listed below in their order of appearance.

Section 2. Summary of STREET-G Experiment

Section 3. Crocco Temperature-Velocity Relationship

Section 4. Turbulent Viscous Layer Thicknesses

Section 5. Turbulent Heat Blockage and Skin-Friction Reduction Due to Mass Injection

The STREET-G experiment was summarized because it represents a unique set of data which heretofore was not available at hypersonic conditions and, appropriately, is emphasized in all phases of this study.

SECTION 2

SUMMARY OF STREET-G EXPERIMENT

The experimental investigation, which provides the main data base of the present study, represents a two year effort, the objective of which was to experimentally provide detailed turbulent boundary layer surface and profile data on a slender cone with mass transfer effects. The study represented a comprehensive investigation of the boundary-layer mean flow characteristics whose final product was a detailed documentation of the data including an assessment of pertinent trends and observations. The data obtained are to serve two functions which include: (1) long term, data base provision to validate sophisticated 3-D finite difference or integral viscous boundary layer computer codes; and (2) short term, data base provision to validate and upgrade engineering design codes which currently rely upon two-dimensional, low Mach number data correlations. These documents are included as References 1 and 2 of this report.

The experimental effort concentrated on surface and boundary layer behavior relative to the effects of mass addition (with uniform and non-uniform distributions), molecular weight, and angle of attack at a fixed Reynolds number condition. The injectant gases consisted of air, helium, argon, and Freon with blowing values $\lambda_\infty = (\rho v)_w/(\rho u)_\infty$ of 0, .0005, .0015 and .0035 at angles of attack of 0°, 3°, 5° and 10°. The basic model consisted of a 5° half angle porous cone which was 60 inches long and was constructed from sintered stainless steel so that ablation could be simulated by the injection of gases through the porous model walls. Tables I and II give a detailed listing of the type of profile data obtained in the two year period while Tables III and IV provide a detailed listing of the surface data.

2.1 EXPERIMENTAL APPARATUS

The test program was conducted in the Arnold Engineering Development Center (AEDC), Von Karman Gas Dynamics Facility, Tunnel B at Mach 8. This facility is a continuous flow, hypersonic wind tunnel with a 50-inch diameter test section. An

axisymmetric contoured nozzle provides flow at Mach 8 which corresponds to free stream unit Reynolds numbers from 0.30×10^6 to 3.8×10^6 per foot. The model used in this investigation was a 5 degree half angle cone which is nominally 60 inches long (10.5 inches base diameter). It consists of an impervious sharp nose ($R_N \simeq .002$ in) which is 9.47 inches long, a porous frustum which is 50 inches long, and a base plate which is 0.5 inches thick (see Figure 1). The porous section of the model is subdivided into four independent compartments, each with separate supply tubes which are 1/4 inch O.D. stainless tubing. The forward two chambers each have one supply tube; the two rear chambers each have two supply tubes. The porous frusta of the model are made of series 316 sintered stainless steel (using approximately 5 mil spherical powder) which is nominally 60% dense. The wall is approximately 1/4 inch thick. These porous elements are supported by a stainless steel substructure which contains all of the necessary internal plumbing and instrumentation routing ports.

The cone was instrumented with 26 heat transfer gages and 34 pressure orifices. The surface heat transfer was measured with a copper-constantan Gardon type heat gage. This gage operates on the principle that the heat flux input into the thin sensing foil is proportional to the difference in temperature between the center of the foil and its edge (where the foil edge is bonded to a copper heat sink). Heat transfer measurements were made with the model wall at both ambient temperature and at an elevated temperature (the latter while profile data were obtained). For the non-blowing case, with the model at an equilibrium wall temperature (approx. 1000° F), the surface heat transfer was approximately 0.40 BTU/ft^2-sec. To measure this small value of heat transfer, a gage with an extremely thin foil and a relatively large diameter was required. Both of these characteristics were undesirable for thick wall porous model instrumentation. Consequently, a gage with a diameter of 1/4" and a constantan diaphragm thickness of 5 mils was selected. Each sensor has the capability of measuring heat transfer (from a pre-determined calibration) as well as wall temperature. Surface pressure was recorded from conventional wall static pressure ports.

Boundary layer profile mean flow measurements were made with four discrete probes; namely, pitot pressure, total temperature, mass concentration (for foreign gas injection), and static pressure (via a cone probe). Each of these probes was connected to a strut, which in turn, was connected to the AEDC probe actuation mechanism. The probing was performed in general with the pitot and total temperature probes straddling the model centerline. The probe vertical height at $y = 0$ was ascertained by detecting continuity on each of two low voltage circuits when the probes touched the model surface. Since the lateral displacement of each of the probes (in the transverse direction) relative to the model radius is small, one would expect the data obtained at small values of the transverse coordinate to be the same as the data with each of the probes on the centerline of symmetry. This was verified experimentally and found to be true.

The pitot pressure was measured with a flattened tip hypodermic tube tip height opening approximately 0.020". The probe was designed to have a small probe tip height (y) relative to the local boundary layer thickness (i.e., $y/\delta < 0.050$), to minimize any influence of the probe size on the resulting measurements.

The mass concentration probe has the same external geometry as the pitot probe. This probe was connected to an evacuated gas analyzer system which contains an "alphatron" ionization gage. Alpha particles emitted from this gage ionize the gas molecules which are collected on a charged plate and produce an ionization current. Data are obtained by injecting a gas sample at a prescribed test point and determining the mixture concentration. From pre-test calibrations one can establish, with this system, the mole fraction χ_i of the mixture for each test point from the ionization potential of the gas mixture.

The stream total temperature was measured with a singly shielded thermocouple (tip height approximately 0.050"). This probe was calibrated in the free stream for several values of the Reynolds number and for a constant total temperature. Additional calibration points were obtained from measurements with the probe at the boundary

layer edge and for several values of the cone angle of attack. These data, although calibrated for a limited Mach number range, were assumed to apply for all M in the boundary layer.

One particular item of interest in this overall study was to examine the boundary layer assumption that $(\partial P/\partial y)_{b.l} = 0$. Consequently, static pressure profiles were measured in the boundary layer. Inasmuch as relatively thin boundary layers would be encountered on the cone (i.e., ~ 0.5" for $\lambda_\infty = 0$), conventional ogive-cylinder probes would be unsuitable because of attendant wall interference effects. As a result, a pointed cone probe was adapted. In principle, one can determine the local flow properties such as the Mach number and static pressure without making the classical assumption that $(\partial p/\partial y)$ across the boundary layer is zero (i.e., from the measurement of the pressure on the surface of the cone probe and the pitot pressure at that point and using conical flow theory and normal shock relations). However, in practice, the accurate measurement of the static pressure in a thin boundary layer for a hypersonic flow is no small task. Recognizing these difficulties, a careful assessment concerning probe geometry, lateral spacing, and application relative to obtaining quantitative data was made.

The probe lateral spacing was such that at a Mach number greater than approximately 1.5, the cone probe would not interfere with the total temperature probe which is immediately adjacent to it. For the turbulent boundary layer measurements made in Reference 1, this mutual interference did not present a problem. However, during the tests of Reference 2, where tests were made predominantly at a lower Reynolds number with measurements made in the laminar/transitional boundary layer region, interference effects were noted. As a consequence, the cone probe was removed from the probe assembly for the majority of the profile measurements.

Readers interested in more details of these probe measurements as well as model and instrumentation details should consult References 1 and 2.

2.2 DATA ACQUIRED AND DATA REDUCTION

In general, two categories of data were obtained in this test program, one involving transient heat transfer data, and the second pertaining to boundary layer profile measurements. In the former, the model was pulsed into the tunnel flow for a period of approximately five seconds and heat transfer data were obtained. The model was then retracted and cooled for the next test condition. For the profile data entry, the model was inserted into the tunnel flow and allowed to absorb heat until an equilibrium wall temperature was achieved (i.e., $\dot{q}_{rad} = \dot{q}_{conv.}$). Having reached thermal equilibrium, mean profile measurements were obtained. Boundary layer mean flow profile data were obtained for air, Freon-12, helium, and argon injection on the windward and leeward planes of symmetry. Measurements were made at several measuring stations at $\alpha = 0, \pm 3°, \pm 5°$, and $\pm 10°$.

For the prescribed free stream conditions and model mass injection rates used in the experimental study, the pitot pressure, total temperature and injectant mole fraction were measured across the boundary layer at several axial stations. In addition to these measurements in the boundary layer, the static pressure, heat transfer and the temperature at the model wall were also measured. Inasmuch as local flow properties deduced from the measured data are desired, equations describing parameters of a binary gas mixture, boundary layer characteristic distances and boundary layer properties are required. In particular, the parameters required are the mixture mass fraction, C_i, effective gas constant, $\bar{R}$, and the effective ratio of specific heats, $\bar{\gamma}$, for the injectant gases of helium, Freon, and argon. The boundary layer parameters consisted of the local Mach number, velocity, static temperature and density, viscosity of a binary mixture and the integral viscous layer thicknesses (δ^*, θ). The equations describing these parameters are given in References 1 and 2.

SECTION 3

CROCCO TEMPERATURE-VELOCITY RELATIONSHIP

3.1 BACKGROUND

In recent years an extensive amount of work has been undertaken for the purpose of predicting the behavior of compressible, turbulent boundary layers. This work has consisted of both sophisticated finite-difference type solutions as well as integral type codes, with the latter demonstrating a distinct advantage with respect to computational time. In examining the basic structure of the prediction techniques, one notes a significant number of simplifications which are required for reasonable solutions. Moreover, there is a very limited amount of high speed data available for the purpose of evaluating the prediction schemes.

One of the more popular concepts for predicting compressible turbulent boundary layer behavior is to extend the incompressible mixing-length formulation of Prandtl and von Karman to compressible flows as in the classic work of van Driest. Consequently, when density variations occur and kinetic-heating effects become appreciable, a relation between density and velocity is required. One such method of relating the density and velocity is to assume unit Prandtl and Schmidt numbers throughout the boundary layer. Often referred to as the Reynolds analogy, this assumption implies a relation between shear stress, heat transfer, and mass transfer. The linear expression relating the temperature (enthalpy) and velocity fields is the classic Crocco relation, namely:

$$\frac{H - h_w}{H_e - h_w} = \frac{u}{u_e}$$

The appendix of this report presents the pertinent assumptions and a formal derivation of similitude between temperature and velocity. Essentially, the equation above has been traditionally used to relate the density variations in a boundary layer to the velocity. In so doing, one must postulate an equation of state together with the boundary layer assumption for zero pressure gradient normal to the flow direction.

The development of the Crocco relationship was based on the two-dimensional boundary layer equations and is subject to the constraints of unit Prandtl number, zero pressure gradient (dP/ds), and constant wall temperature. Hence, the use of the Crocco relation to three-dimensional flows and flows with mass transfer must be carefully examined to determine its range of applicability for engineering prediction techniques. The Crocco expression will be evaluated using available experimental data, emphasizing in particular the recently acquired experimental data of Martellucci and Laganelli[1,2] at hypersonic conditions.

There have been several recent studies concerning experimental verification of the Crocco temperature-velocity relation. The experiments can be categorized into two types: (1) "flat plate" type flows (e.g., flat plates, sharp cones, and hollow cylinders) where the upstream pressure gradient is considered negligible and (2) nozzle wall type flows where an upstream pressure gradient exists. In the former, difficulty in obtaining fully developed turbulent boundary-layer flow at hypersonic speeds, and consequent small boundary layer thickness, has impeded experimental studies. On the other hand, nozzle walls have been extensively surveyed since more accurate measurements can be made in such a comparatively thicker boundary layer. While the nozzle wall features a flow that simulates expansion over a blunt nose body, it does not allow for a mathematically tractable solution for flat plate type flow.

As previously noted, several experimental investigations have been performed that examined the Crocco velocity-temperature relation (References 3, 4, and 5). These works were critically reviewed by Bushnell et al[6] who also performed an experimental investigation on nozzle walls. The work of Reference 6 is summarized in Figures 2 and 3. Here, two distinct characteristics are observed when relating the data to the Crocco variables. In Figure 2, the total temperature-velocity data are shown for "flat plate" type flows (negligible pressure gradient) with significant scatter about the linear relation. This scatter is attributed to inaccurate measurements as a consequence of small boundary layer thicknesses. Moreover, the short length of the models, compared to the length of wind tunnel nozzle walls, produced transition effects at the various measuring stations

which also contributed to the data scatter. The authors note a relatively good agreement about the linear, unit Prandtl number distribution. The data generally fall in a band of ±25% of the linear Crocco distribution.

In Figure 3 the Crocco variables are shown for both a linear (Pr = unity) and a quadratic distribution in velocity. Here, the data appear to scatter about the quadratic variation. The total-temperature-velocity data in this case were obtained on nozzle wall type flows which characteristically display upstream pressure gradient histories. In both cases no apparent effect of Reynolds number or Mach number was evident.

Since the work of Reference 6, another important extension of the Crocco relation has resulted from the experimental and analytical investigations of Fiore[7] who examined contoured and conical nozzles. Two distinct regions were observed, neither of which followed the linear Crocco relation. In the region close to the boundary layer edge, the data appeared to follow the parabolic velocity distribution; while near the wall, the data tended to follow a linear distribution with an off-set slope. The deviation from the classic Crocco relation was attributed to a combination upstream history effect and longitudinal pressure gradient.

Beckworth et al[8] performed an experimental investigation on the wall of an axisymmetric contoured nozzle. In that case, it was noted that a portion of the data tended toward the quadratic distribution as a consequence of the boundary layer development from a cold wall temperature condition at the throat of the settling chamber. The linear trend of another portion of the data ($u/u_e \sim 0.8$) in these experiments was attributed to the thick viscous sublayer that extended out to values of $u/u_e \sim 0.8$. It was also determined that the local density levels as well as flow history must be known to make theoretical predictions.

In a more recent publication, Gates[9] made a very comprehensive literature review and experimental investigation which was concerned with the effect of upstream conditions on the downstream state of flow. The experiment employed a half nozzle and a flat plate with the nozzle throat and flat plate leading edge being temperature controlled. Again the

importance of upstream heat transfer, with and without longitudinal pressure gradient, was observed. The energy removed from the upstream boundary layer tended to shift the downstream enthalpy profile with negligible effect on the corresponding velocity profile. For a favorable pressure gradient, the nozzle produced a fuller velocity profile than the flat plate case but relaxed to the flat plate downstream characteristic conditions. It was noted that the enthalpy profile tended to respond to local conditions near the wall (sublayer), whereas the energy profile responded to thermal history effects primarily in the turbulent outer region of the boundary layer. Finally, the recovery factor for a cooled flat plate leading edge was less than that of the adiabatic (nearly) leading edge case.

Demetriades and Laderman[10] have presented mean profile data in the Crocco variables using the model and the same basic tunnel conditions of References 1 and 2. While the emphasis of their work was to obtain fluctuating measurements in the boundary layer, mean profile data were also obtained. The Crocco energy-velocity relation for both the linear and quadratic distributions was compared with data including non-blowing, blowing, and angle-of-attack effects. The authors noted a small effect of blowing on the measured profiles. Moreover, at a free-stream unit Reynolds number of 1.7×10^6/ft. the data appeared independent of blowing, while the data in the laminar region tended toward linear distribution and the turbulent regime tended toward the quadratic behavior. While the authors noted that the validity of the measurements is questionable, there appears to be some irregularity in the probe data per se.

As previously noted, the authors used the same model and tunnel conditions as were used in the experiments of References 1 and 2. When examining the data of Reference 10, it is noted that the lack of temperature "overshoot" in the outer regions of the boundary layer render the total temperature probe design questionable. Further comments concerning the experiments of Reference 10 will be given in the text of this report.

In a very interesting study, Reda[11] conducted an experimental program that examined the effects of roughness and wavy walls on turbulent boundary layer skin friction and

velocity profiles in a compressible, adiabatic flow. Flat and contoured nozzle tunnel walls were used in the experiment. It was found that the Crocco relationship, for adiabatic flow, could be used to describe measured temperature profiles for both smooth and rough walls.

In assessing the analytical and experimental studies of the Crocco temperature-velocity relation, it becomes apparent that two distinct characteristics of the velocity distribution are exhibited. For flat plate type flows (geometries with negligible longitudinal pressure gradients), the energy distribution tends to follow a linear velocity relation; whereas, for tunnel wall (nozzle) type data, the energy distribution favors a quadratic type velocity distribution. It should be emphasized, however, that the above phenomena are not all-encompassing. For example, it has been demonstrated that the upstream thermal history has some effect on the downstream boundary layer characteristics. Although the Crocco relation does not appear to vary with a Reynolds number or Mach number variation, the state of the boundary layer should be included in any analysis. The history effect can be observed when considering a profile measuring station in the vicinity of the position of boundary layer transition. Here, the boundary layer has not been fully developed and exhibits an upstream history effect on the local properties.

As developed in the appendix of this report, the Crocco linear temperature (enthalpy) velocity relation is given by

$$\frac{H - h_w}{H_e - h_w} = \frac{u}{u_e} \tag{1}$$

which is subject to the constraints of unit Prandtl number, zero longitudinal pressure gradient, and constant wall temperature. Moreover, the above relation does not contain an explicit function for mass transfer, but one which enters implicitly through the boundary conditions. Inasmuch as similitude between the thermal and velocity fields does exist throughout a turbulent boundary layer (which would imply that a Reynolds analogy exists) departures from the linear relation are expected. Recognizing that the data

tended to deviate from the linear Crocco relation, Danberg[3] suggested the following empirical relation:

$$\frac{T^o - T_w}{T^o_e - T_w} = \beta \frac{u}{u_e} + (1 - \beta) \left(\frac{u}{u_e}\right)^2 \tag{2}$$

where

$$\beta = \frac{T_{aw} - T_w}{T^o_e - T_w} \tag{3}$$

In the above, for an adiabatic wall condition β approaches zero and the energy profile is characterized by a quadratic velocity relation which is typical of nozzle wall type data. However, one must keep in mind that these data are sensitive to upstream history effects (pressure gradient and thermal effects). On the other hand, for a unit Prandtl number ($T_{aw} = T^o_e$), β approaches unity, and the energy profile is characterized by the linear distribution.

Kutateladze and Leont'ev[12] also noted that departures from similarity (which are a consequence of the kinetic energy term, $(Pr-1)\frac{u^2}{2}$, in the energy equation as noted in the appendix) could be accounted for by the following modification

$$\frac{T+ - T_w}{T_{aw} - T_w} = \xi \left(\frac{y}{\delta}\right) \frac{u}{u_e} \tag{4}$$

where

$$T+ = T + r\left(\frac{y}{\delta}\right) \frac{u^2}{2gJCp} \tag{5}$$

The authors allowed the recovery factor to be constant, such that the parameter ξ was uniquely defined by Eqs. (4) and (5). Moreover, the parameter ξ which is a function of the normal coordinate depends, in general, on the longitudinal pressure gradient, the temperature difference imposed, and the magnitude of mass transfer. For

a constant value of the recovery factor, Eqs. (4) and (5) can be expressed in terms of the Crocco values, giving

$$\frac{T^o - T_w}{T^o_e - T_w} = \xi\beta\frac{u}{u_e} + (1 - \beta)\left(\frac{u}{u_e}\right)^2 \qquad (6)$$

One immediately recognizes the value of the work of Kutateladze and Leont'ev in the addition of the parameter ξ. Also, the above equation was later empirically verified by Danberg for the condition of a unit value of ξ.

The objective of the present study is to investigate the Crocco temperature-velocity relation relative to hypersonic flow conditions. The examination will include the effects of mass transfer, angle of attack, and molecular weight (i.e., with the injectant gas differing from the free stream gas). Moreover, the study will emphasize the STREET-G experimental data together with data from the scientific community. Finally, the suggested temperature-velocity relation of Kutateladze and Leont'ev will be examined with emphasis on the non-similarity parameter ξ.

3.2 DATA PRESENTATION

In order to assess the data and data reduction techniques, Figure 4 was constructed to show the velocity and temperature profile data compared with results from the equilibrium non-similar boundary layer program outlined in Reference 13. The comparison was made for laminar boundary layer conditions with and without mass transfer. For the non-blowing case one notes excellent agreement except for the region near the wall ($y \leq 0.1''$) where probe/surface flow interactions are present. For the blowing case the agreement is also good for both velocity and temperature profiles except for the region near the wall ($y \leq 0.1''$) where once again interference effects are present. It is also of interest to note that the measured total temperature profile shows a 5% overshoot whereas the theoretical value corresponds to an overshoot of less than 1%. The reason for this difference is not readily obvious. It is suspected that it is due to the numerical procedures in the boundary layer program. Nevertheless, relatively good overall agreement was achieved between theory and experiment.

When assessing the available data in the literature concerning the Crocco temperature-velocity characteristics, the importance of upstream history effects was noted. In particular, the relative distance of the measuring station to boundary layer transition occurrence must be carefully weighed. Consequently, Figures 5 and 6 were prepared to indicate the location of boundary layer transition, with and without blowing, for the zero angle of attack conditions. Shown in these figures are the axial distributions of heat transfer along the porous cone for both the transient and steady state mode. In the latter case, the model wall reaches an equilibrium temperature which is somewhat below the adiabatic wall value; and accordingly, the convective heating to the model surface is nominally balanced by the radiative losses.

There are two significant observations that can be deduced from Figures 5 and 6: first, the attenuation in heat flux with blowing and, second, the effect of blowing on transition. In the former, one notes a greater heat blockage effect in the laminar regime as compared to the turbulent case which, in general, is compatible with existing heat blockage correlations. On the other hand, the location of the transitional boundary layer regime (defined here as the region between the points of local minimum and maximum heat transfer rates) appears to be relatively insensitive to mass transfer from the free stream which is in direct agreement with the findings of Martellucci et al.[14] Finally, it should be noted that with foreign gas injection, an increase in the heat capacity of the injectant attenuates the convective heating level at the surface. Moreover, it appears that the location of the transition region is not materially affected by the frustum injectant gases.

Some comparisons of the transitional/turbulent data obtained at Re_∞ /ft = 3.8×10^6 and 1.3×10^6 for $\lambda_\infty = 0$ were made with the non-similar boundary layer theory.[13] The objective of these comparisons was to examine the characteristics of a non-similar theory with the validity of eddy viscosity models for predicting profile shapes. For convenience, the Smith-Cebeci model[15] was employed. Shown in Figure 7 are comparisons of theory with velocity and total temperature profile data for the high Reynolds number non-blowing case (i.e., Re_∞ / ft = 3.8×10^6). The bounds of the transitional flow regime as

deduced from the surface heat transfer data, are also shown. Excellent agreement between theory and experiment is noted for this case. Shown in Figure 8 are comparisons of theory with the profile data for the intermediate Reynolds numbers non-blowing case (Re_∞ / ft = 1.3 x 10^6). It is interesting to note the poor agreement between theory and experiment for this case. One can speculate on many reasons for the lack of agreement in the low Reynolds number condition. Without attempting to elaborate on these phenomena, it suffices to say that additional work is required to better understand the applicability of eddy viscosity models to flows which are not "fully-developed".

To illustrate the influence of mass transfer on the profile shape, comparisons of data for $\lambda_\infty = 0$ and $\lambda_\infty = 0.0015$ (air injection) were made. Shown in Figure 9 are the data for the velocity and total temperature profiles for the mass transfer case. The non-blowing data are represented by the dashed lines which were faired thru the data points. As was the case for the surface heat transfer, mass transfer at a constant blowing rate has a significantly greater influence on the laminar-transitional profile shape than for the turbulent case. Furthermore, it is of interest to note that the data obtained at stations 28 and 32 (i.e., in the transitional regime) clearly indicate that the profile can be divided into two parts. This observation is more evident when examining the temperature profile data of Figure 9. It appears that the laminar boundary layer has been "lifted" from the surface by the injected gases. As a result one obtains a region near the wall which has a quasi constant total enthalpy near the injectant value, while the outer part of the profile resembles a laminar-like profile.

One method of establishing whether the data obtained exhibit a fully developed characteristic is through examination of the velocity profile exponent, n. The velocity power law exponent, n, has been plotted as a function of Re_θ for the zero blowing, zero angle of attack case and is shown in Figure 10. Each of the data points is identified as to the type of flow experienced, i.e., laminar, transitional, or turbulent. When the data of Figure 10 are compared with the data band of References 16 and 17 it is seen that the turbulent flow points ($10^3 \cdot \quad Re_\theta \cdot 10^4$) all lie in the "overshoot" region where the turbulent boundary layer has not yet come to full equilibrium (i.e., fully developed).

This is a rather surprising result when considering the model length of 60 inches and maximum facility Reynolds number of 3.8×10^6/ft which yields over 3 feet of "turbulent" flow (i.e., the end of transition as depicted from surface heat transfer data is at 23 inches). This observation raises some speculation concerning published "turbulent" boundary layer data. This leads one to believe that the only available hypersonic "fully developed" turbulent boundary layer data may be those works obtained on nozzle walls.

Another item discussed in the assessment of the literature review is boundary layer thickness. This becomes of concern when the probe size relative to the boundary layer height and the potential interference effects of the probe and wall may produce questionable data. Shown in Figure 11 are the measured hydrodynamic thicknesses for several blowing values at both the free stream unit Reynolds numbers tested in the program. For convenience, the transition zones have also been shown. One notes the significant thickening of the boundary layer with mass transfer which allows an extended profile survey. However, the total pressure and total temperature probes used in the experiment (approximately 0.050 inches in diameter) are subject to erratic readings below station 35 (non-injectant cases) for the high Reynolds number case and below station 45 for the low Reynolds number conditions. It is also interesting to observe the change in slopes between the two Reynolds number cases. For the highest condition, the curves are convex and grow according to the 4/5 power of distance as expected. However, the low Reynolds number case exhibits curves that are concave. This is believed to be a consequence of the effects of transition occurring in the boundary layer over a larger section of the model.

Figure 12 exhibits the surface pressure variation as functions of axial distance. The data represent both uniform and non-uniform blowing conditions. Concerning the latter condition, one obvious region of discontinuity occurs at the juncture of the impermeable nose with the first porous chamber. In the tests of Reference 2, combinations of injection through the individually controlled chambers were devised to investigate a differential mass transfer process. In particular, chambers 1 and 2 were set at one blowing

distribution, while chambers 3 and 4 were controlled at twice the value and no injectant, respectively. Clearly a history effect is expected, and the relaxation phenomenon was evident. A detailed discussion concerning the non-uniform injection test was given by Laganelli and Martellucci[18] and will be discussed further herein. Concerning Figure 12 two distinctive characteristics are interesting to note here. First the step-down in blowing case (15/15/0/0) showed no effect on pressure compared to the step-up case (15/15/30/30). Secondly, an increase in pressure is apparent at the juncture of the impermeable tip and chamber 1 as a result of blowing ($s \simeq 10$ inches). The same effect is not observed at the juncture of discontinuity for the step-up injection case, but occurs in a distributed fashion downstream. This can be attributed to the thicker boundary layer which is more evident at the chamber 2/3 juncture than at the nose section.

3.3 CROCCO TEMPERATURE-VELOCITY DATA RESULTS

The Crocco temperature-velocity data will be presented in this section under five conditions of flow. These include uniform injection at zero, leeward, and windward angles of attack; non-uniform injection; and molecular weight behavior. Interpretation of these data will be provided in the penultimate section of this report. Finally, it should be noted that no attempt has been made to eliminate data points that are obviously in error as a consequence of probe interference.

3.3.1 Uniform Injection: $\alpha = 0°$

Figures 13 and 14 represent the Crocco variables with and without mass transfer effects at the high Reynolds number conditions of these tests (Re_∞ /ft = 3.7×10^6). In Figure 13, several profile stations are represented for zero mass transfer conditions. Here, one notes that the data tend to significantly deviate about the linear Crocco relation. For this condition (i.e., $Re_\infty/ft = 3.7 \times 10^6$) boundary layer transition onset and end are approximately located between stations 13 and 22. Hence, the relative size of the boundary layer thickness together with transition render the results questionable in this region. On the other hand, the data at stations 39 and 52, although not fully

developed, indicate a quadratic effect prior to the energy "overshoot" region. This latter condition is quite typical of supersonic/hypersonic flow behavior.

A significant increase in boundary layer thickness was noted with increasing mass transfer which allows for a more effective boundary layer survey. Figure 14 was constructed to observe the effect of mass transfer at a fixed station. Here, the data tend to follow a modified quadratic relation with temperature overshoot at approximately 90% of u/u_e. It should be noted that for this figure only, data points have been eliminated that reflect possible probe interference effects.

Figures 15 and 16 express the enthalpy (temperature) - velocity characteristics for a free stream Reynolds number of 1.3×10^6 per foot. For this condition, the transition zone (based on heating) was in the region of stations 20 to 30 ($\lambda_\infty = 0$) and stations 20 to 34 ($\lambda_\infty \neq 0$). In Figure 15 one notes that the data tend toward the classic Crocco linear distribution and are further characterized by the temperature overshoot at the outer region of the boundary layer. Moreover, there appears to be less scatter in the data than for the 3.7×10^6 Reynolds number tests (Fig. 13) even though the corresponding boundary layer thicknesses are smaller. In Figure 16, the data tend to exhibit a peculiar behavior. In particular, stations 28 and 32, which are the transition zone, deviate significantly close to the wall and then tend toward the quadratic distribution. On the other hand, the data in the downstream region of the transition zone appear to follow some type of modified quadratic distribution as was evident in the higher Reynolds number cases. It is interesting to note that the data in the transition zone for the non-injectant case (Figure 15) did not exhibit the odd behavior of the mass transfer/transition coupled case.

Figure 17 represents the enthalpy-velocity characteristics for a free stream Reynolds number of 0.4×10^6 per foot. This condition allows for an examination of data in a laminar boundary layer state. Owing to probe interference effects close to the wall, the data follow the linear distribution with the usual temperature overshoot. The same pattern is exhibited at the low Reynolds number condition as was experienced at the higher

Reynolds number values; namely, mass transfer tends to alter the data from the linear toward the quadratic distribution.

Figures 18 and 19 were constructed to examine a Reynolds number effect with and without mass transfer. In Figure 18, the data are shown for the region around station 39. Here, no discernible effect of Reynolds number is apparent. If one is allowed some license to speculate, it is possible that the laminar flow results (low Reynolds number) are showing a distinct variation from the unit Prandtl number result when compared with the turbulent and semi-turbulent data. (The latter, which is characterized by the mid-range Reynolds number, is subject to upstream transition effects.) For example, the laminar recovery factor is less than the turbulent value; hence, the data should reflect a larger variation for a non-unit Prandtl number condition. In Figure 19, the effect of Reynolds number with mass transfer is investigated in the vicinity of station 50. While the data tend to deviate from the linear distribution, there does not appear to be any dependence on Reynolds number.

3.3.2 Uniform Injection - Windward Angle of Attack

Figures 20 and 21 present typical Crocco enthalpy-velocity data for windward angles of attack at the high free stream Reynolds number condition. An inspection of these data indicates that the linear relation tends to fit the results with and without mass transfer effects. The data also display the energy overshoot characteristics; however, the level of overshoot is not as pronounced as for the zero angle of attack case. Moreover, there does not appear to be any distinction in the data trend from the linear distribution with increasing angle of attack. Another interesting aspect of these data is that no significant variation between the reported stations is apparent. This phenomenon, which was not characteristic for the zero angle of attack data, occurred with and without mass transfer (see, for example, Figure 21).

3.3.3 Uniform Injection - Leeward Angle of Attack

Typical leeward angle of attack data are presented in Figures 22 and 23 with and without mass transfer effects. A significant departure from the windward or zero angle

of attack results is observed. In the present case, the data tend to follow the quadratic behavior as well as exhibit variations between the measuring stations. Moreover, the data (station 39) also show a mass transfer effect, whereby increasing the mass transfer parameter λ_∞ shows departures from the quadratic relation ($\lambda_\infty = 0$) to some modified form of the quadratic relation. Once again, the level of energy overshoot is not as pronounced as in the zero angle of attack cases. The variation in data between stations 39 and 52 with (Figure 22) and without (Figure 23) blowing is not known.

3.3.4 Non-Uniform Injection: $\alpha = 0°$

One of the more interesting tests performed during the experimental program of References (1) and (2) consisted of non-uniform mass transfer along the sharp porous cone. Since each of the four compartments of the cone was individually controlled for blowing characteristics, various combinations of injection could be examined. In this manner, one can investigate upstream history effects primarily due to mass transfer. Figures 24 and 25 relate the Crocco variables to non-uniform injection data. Surface and profile data concerning the same, as well as several other combinations of injection can be found in References (1), (2), and (18). Figure 24 shows the injection combination for $\lambda_\infty = 0.0015$ in chambers 1 and 2 and $\lambda_\infty = 0$ in chambers 3 and 4. Also shown for comparison is the data band for the uniform injection case of $\lambda_\infty = 0.0015$. The data for the non-uniform case tend to follow the quadratic velocity relation and proceed through the energy overshoot region in the usual fashion. It is interesting to note that the data deviate slightly from the uniform injection case and, more importantly, show significant departures from the zero injection case (Figure 13). The latter condition indicates that the boundary layer, relative to the Crocco variables, does not tend to recover to the non-injection distribution. An examination of Figure 12 shows that the pressure distribution recovers to the zero injection value thereby indicating some other mechanism for the departures. It should also be noted that both uniform and non-uniform cases are subject to turbulent boundary layer conditions.

In Figure 25, a non-uniform, step-up injection case is presented. As in the previous figure, a data band for the uniform injection distribution is shown for comparison. Here, one notes still a different pattern; namely, a departure from the uniform case toward the linear Crocco distribution. These data are not significantly different from the uniform injection case (Figure 14) for the stepped-up injection rate. Furthermore, Figure 12 shows an increase in pressure as a consequence of the step in injection and recovers to the uniform lower distribution case. Hence, an apparent upstream pressure gradient effect tended to drive the data toward the linear distribution (the opposite of what may be expected) which indicates the blowing level is potentially in control of the profile characteristics.

3.3.5 Molecular Weight Effect

Figures 26 and 27 present the Crocco enthalpy-velocity relation for the situation where the injectant gas differs from the boundary layer fluid. In particular, injectants of helium, Freon-12, and argon were examined. The enthalpy was determined from a value of specific heat of the injectant-boundary layer gas mixture, which in turn, was calculated from mole fraction measurements. The results are difficult to interpret, but will be presented with further comments in the next section. In Figure 26, a significant departure from the linear relation is observed when the injectant gas differs from the main stream. There is no trend in the departure from the air/air result with either molecular weight or specific heat. While the argon data are close to the air results (their being similar) a substantial deviation is observed in the helium data.

Freon-12 data are compared to the air results in Figure 27 for stations 39 and 52. While no significant departures are recognized between stations, the Freon-12 data appear to follow the linear relation more closely than the air. Moreover, the energy overshoot region appears to be less magnified with the non-air injectant gases.

3.4 DISCUSSION OF RESULTS

As noted in the background section of this report, sharp cone type data tend to follow the linear Crocco relation. This is a consequence of a negligible longitudinal

pressure gradient and a Prandtl number (for an air free stream) close to unity. In general, this behavior prevailed in the tests of References 1 and 2 owing to the devi in data as a result of the small boundary layer thicknesses as well as attendant upstream transition effects. Moreover, Danberg[3] and Kutateladze and Leont'ev[12] recognized that departures from the linear relation could be attributed to the kineti energy of the stream and suggested modifications to the classic linear relation. Tl modified Crocco relation, which is discussed in the appendix, is given by

$$\frac{H - h_w}{H_e - h_w} = \beta \xi \left(\frac{u}{u_e}\right) + (1 - \beta) \left(\frac{u}{u_e}\right)^2$$

where $\beta = (h_{aw} - h_w)/(H_e - h_w)$. Figure 28 shows the parameter β as a functio the dimensionless injection term λ_∞ for zero angle of attack conditions. One wil that stations 39 and 52 represent the only stations for which data were reported at three Reynolds numbers. The curve was not drawn to express a functional form with λ_∞ , but to indicate the range of kinetic energy parameter for these tests. notes that blowing has an effect on the β parameter which is expected inasmuch wall enthalpy is reduced with mass transfer. Essentially, β varied between .8 .75 for the major portion of the tests.

Shown in Figure 29 are two groups typical of the data presented which are co with curves calculated using Eq. (6) for ξ equal to unity and the indicated valu β. Here, one notes that the modified quadratic relation is in concert with the dat but appears to overpredict the results. Moreover, the modified quadratic relat with ξ equal to unity does not compare with the data trend in the energy overs region. Consequently, Figure 30 was constructed using Eqs. (4) and (5) with th for several cases. Here, the parameter ξ is shown as a function of dimensi distance through the boundary layer. Two distinct regions are evident: first, t region close to the wall where departures from unity exist as well as reversal i presence of blowing; and secondly, the energy overshoot region ($y/\delta > .55$ - . While several of the data points in the wall region are subject to error, the dep from unity as well as the trend with injection are considered accurate.

As noted above, the similarity parameter shows a decrease with blowing in the region close to the wall. Other interesting effects on the similarity parameter ξ include molecular weight (Figure 30B), at fixed values of λ_∞ and Re_∞, where no apparent trend is obvious. Moreover, for λ_∞ equal to zero, there does not appear t › be any angle of attack effect (Figure 30C); however, with blowing the leeside data indicate a more significant variation than the windward data. Finally, a Reynolds number effect (Figure 30D) shows a significant departure between the laminar boundary layer and the combined transitional/turbulent boundary layer results.

With the exception of the region close to the wall, the parameter ξ appears to approach a value equal to the reciprocal of the recovery factor (no mass transfer). On the other hand, the recovery factor is expected to exhibit more of an effect toward the wall, with blowing, than at the edge of the boundary layer. Hence, for mass transfer the parameter ξ was assumed to take the form $\xi \simeq \frac{1}{r_o} - \left(\frac{r}{r_o}\right)$. These results are shown in Figure 31 where β was assumed to be 1/2, which is typical for zero injection data. Here, one notes that the trend correctly predicts what is observed in the data; that is, the modified quadratic relation tends toward the linear distribution in the presence of mass transfer. This trend is by no means a necessary consequence of mass transfer; but rather, a result of the temperature potential between the adiabatic and wall values. Finally, the inclusion of the parameter correctly predicts the energy overshoot behavior which is characteristic of high speed flow.

In the preceding discussion, it was noted that the linear Crocco relation could be expressed as

$$\frac{H - h_w}{H_e - h_w} = \left(\frac{u}{u_e}\right)^{\epsilon}$$

where $1 \leq \epsilon \leq 2$. Moreover, it was noted in Reference 19 that the use of the exponent, ϵ, is suitable for mass transfer conditions as well as non-injection conditions. A re-examination of the Crocco relation has shown that the assumed exponent dependence on

mass transfer (which is actually a boundary condition) was erroneous. This can be seen by an inspection of Eq. (6). Here, for the adiabatic condition ($h_{aw} \rightarrow h_w$), $\beta \rightarrow 0$ and results in the quadratic case. On the other hand, for $h_{aw} \rightarrow H_e$, $\beta \rightarrow$ unity, the linear case. Inasmuch as a mass transfer process tends to cool the wall (hence, drive toward an isothermal condition, $\beta \rightarrow 1$), the corresponding effect is to drive the enthalpy potential toward the classic linear distribution. The attempt in this study was to model the effect of mass transfer in the modified Crocco relation through the non-similarity parameter ξ.

3.5 CONCLUSIONS

The classic Crocco temperature-velocity relation has been evaluated experimentally at hypersonic flow conditions on a sharp, porous cone. The evaluation was made with the effects of mass transfer, angle-of-attack, and molecular weight variations of the injectant gas over a range of free stream Reynolds numbers of 0.4 to 3.7 x 10^6/ft and fixed free stream Mach number of approximately 8.0. Departures from the linear Crocco relation (which is constrained to unit Prandtl number, zero longitudinal pressure gradient, and constant wall temperature) were observed that tended to follow a modified quadratic velocity behavior. The data were compared to the suggested modified quadratic relation of Kutateladze and Leont'ev and appeared to agree favorably, including, as well, the energy overshoot region.

Several of the pertinent observations made in this study are as follows:

1. In general, the data tended to follow the linear Crocco relation with a temperature overshoot resulting from the kinetic energy of the flow. This result is typical of flat plate type flows (sharp cone) which have previously been investigated.
2. As a consequence of the small boundary layer thicknesses, the probe data in the region of $y < 0.1$" are considered questionable.
3. A comparison of the present test results with other data [6, 9] substantiates that the Mach number does not appear to have any effect on the temperature-velocity relations.

4. For these cases tested, as well as comparison to other reported data[6, 9] Reynolds number had no apparent effect on the Crocco relation.

5. Mass transfer effects (air-injection) tended to depart from the linear relation toward a modified quadratic velocity relation. It is believed that such departures are a consequence of the increased temperature potential (i.e., $T_{aw} - T_w$) as well as changes in the velocity profile. Essentially, increased blowing lowers the wall temperature value, with β increasing as well, and tends toward the quadratic Crocco relation.

6. As noted by several experimenters, upstream history effects should be considered when evaluating the Crocco relation. In flat plate type flows the relative distance of the measuring station to the boundary layer transition region must be considered. In the present tests, departures from the reporting stations were noted which can be attributed to flow development. The reporting stations in the transition region (Re_∞ / ft = 1.3 X 10^6) per se indicated interesting results. Without mass transfer, the data tended toward the linear relationship, while with blowing effects a significant departure was observed that eventually became quadratic.

7. Laderman[10] has reported that the laminar boundary layer flow tended to agree with the linear relation, while the turbulent flow state followed the quadratic relation. The data of the present study are too inconclusive to separate the state of flow relative to the Crocco relation. At the high Reynolds number conditions, the reporting stations (for $\alpha = \lambda_\infty = 0$) tended toward the linear relation except for station 52 (end of the model) which displayed quadratic characteristics. On the other hand, the data for the mid-range Reynolds number, for $\alpha = \lambda_x = 0$, appeared to agree quite well with the linear relationship which also characterized the low Reynolds number tests.

8. Angle of attack effects on the Crocco relation indicated a specific pattern; namely, windward orientation tended toward the linear relation while the leeward side was characterized by the quadratic behavior. It should be noted that the above is completely opposed to the observations of Reference 10. Keeping in mind that the same model and facility were used at slightly different Reynolds number, the difference in the data has not been clarified. Windward and leeward nomenclature was considered identical based on the relative sizes of the boundary layer thicknesses for the tests of Reference 10 and the present experiments.

9. For non-uniform injection, both a step-up and step-down in blowing followed a modified quadratic distribution. In the latter, the data were closer to the quadratic relation than the step-up case which exhibited more nearly linear characteristics.

10. No specific conclusions could be made for the non-air injection tests. The heavy molecular weight gases, argon and Freon-12, followed the linear Crocco relation, while helium injection showed a significant departure in the opposite direction of the quadratic relation. Further work is required before non-air injection cases can be used readily in Crocco coordinates.

11. It appears that the modified quadratic Crocco relation suggested by Kutateladze and Leont'ev can be used for engineering prediction techniques. In this situation, the non-similarity parameter ξ can be replaced by the reciprocal of the recovery factor; i.e. $\xi = Pr^{-1/3}$ is recommended for use in Eqs. (6) or (7).

SECTION 4

TURBULENT VISCOUS LAYER THICKNESSES

4.1 BACKGROUND

There are many problems associated with hypersonic flight for which the prediction of characteristic thicknesses of the boundary layer would be desirable. These include entropy gradient effects on convective heating rates, signal attenuation in plasma and wake studies, boundary layer separation (surface discontinuities and control surfaces), rocket engine nozzle flow, and acoustic phenomena. Information concerning the growth of the viscous layer thicknesses further enhances the design engineers capabilities to examine three-dimensional flows for complicated shapes. While our understanding and analysis of three-dimensional flows has steadily advanced in recent years, the difficulties involved in the theory of turbulent shear flow have resulted in inadequate engineering prediction capability. Moreover, integral techniques, which generally employ streamline coordinates with small cross flow and local similarity, have not been successfully developed for turbulent boundary layer flows.

As a consequence of these attendant difficulties, the design engineer has resorted to semi-empirical correlations based on available experimental data. However, these attempts have been impaired because of the lack of detailed data as well as an incomplete experimental definition of the mean profile characteristics across the boundary layers of hypersonic flows. Several engineering analyses have been developed within the scientific community which are concerned with computing the vehicle loads and drag (which implies an accurate definition of the local properties). However, an examination of these techniques is necessary inasmuch as recently acquired data has indicated that modifications are required in the concepts. In particular, the effects mass transfer (including non-air injectants) and angle of attack on the viscous layer thicknesses should be carefully assessed.

Inherent with the above phenomena is the requirement of the state of the boundary layer itself. Here, fully-developed turbulent flow regions should be considered separately from transitional flow regimes inasmuch as the semi-empirical correlations are based on fully-developed turbulent flow. Turbulent boundary layer velocity profiles are customarily characterized by a power law relation $u/u_e = (y/\delta)^{1/n}$ where the exponent, n, assumes the value of 7 for a fully developed turbulent boundary layer flow. However, an examination of the overshoot region, defined as the end of transition (where the point of maximum heat flux occurs), indicates that the parameter n is augmented to values as high as 16. Hence, the impact on the viscous layer thicknesses resulting from boundary layer development will also require careful assessment.

Inasmuch as the emphasis of this study is to verify/modify existing semi-empirical techniques based on experimental data, one is restricted to data availability. Recognizing this difficulty, Martellucci and Laganelli[1, 2] had undertaken an experimental study to provide detailed turbulent boundary layer profile data for an axisymmetric configuration at both zero and non-zero angle of attack. The model used for this investigation was a 5-degree half angle porous cone which was 60 inches long. Gases consisting of helium, argon, air, and Freon-12 were used to simulate ablative conditions at several Reynolds number conditions. These experiments were intended to augment the earlier work of Martellucci and Rie[19, 20] which found a significant departure from existing industrial code prediction capability to their experimental data.

An example of this disparity is depicted in Figures 32 through 34. It should be noted that the data of Reference 20 (open symbols) and the flat plate data of Danberg[3] (filled symbols) are shown together with zero angle of attack industrial prediction techniques. It is evident that each of the methods overpredicts the effect of mass transfer. Moreover, contrary to the assumptions made in these prediction techniques. the form factor δ^*/θ does vary with mass transfer rate. Although several early theories for turbulent boundary layer with mass addition were available,[24, 26, 26] experimental skin friction data did not agree with theories.[27, 28] Of paramount interest, however, is the fact that the industrial codes relied heavily on these early works and

often did not change as new information became available. Consequently, the early theories are not necessarily considered to provide adequate descriptions for turbulent boundary layer behavior.

The prediction of the turbulent viscous layer thicknesses at angle of attack relies on empirical curve fits of limited data (in the absence of mass transfer).[29-31] Moreover, the additional complication of mass transfer coupled with angle of attack on prediction capability is virtually non-existent.

As previously noted, the state of the boundary layer relative to its fully-developed characteristics should be known prior to assessing viscous layer thicknesses. A survey[16] of velocity profile data from turbulent boundary layers with zero and slightly favorable pressure gradients has been made where data obtained at Mach numbers up to about 20 have been investigated. The data were classified according to three basic types of test configurations; namely: (a) flat plate, cone and hollow cylinders; (b) two-dimensional nozzle wall; and (c) axisymmetric nozzle wall. The results show that n is primarily a function of Reynolds number and wall temperature. It was also observed that when measurements were made in the region of the beginning of turbulent flow (i.e., the end of transition defined as the point where $\dot{q}_{max}$ occurs) there is generally an overshoot in the parameter n ranging to values as high as 16. As a result of this survey, it appears that a relationship exists between n and Re_θ as shown in Figure 10, where it is noted that within the overshoot region non-similarly effects are prevalent.

For zero mass injection, an examination, of the data of Reference 20 indicated that the axial distribution is characterized by a value of n 9 at the forward (transitional flow) station and increases to some unknown value (n 12) at the end of transition. A decrease is then noted to values of the order of 7 at points sufficiently far removed from the end of transition. This behavior is characteristic of the results obtained by Johnson-Bushnell[16]. Moreover, the region where n decreases with increasing Re_θ persists for some 50 boundary layer thicknesses downstream of the point where $\dot{q}$ is a local maximum. This fact is significant in the design of ground test experiments where

turbulent separation data are desired. The boundary layer profile shape can have a gross impact on local flow characteristics (such as separation lengths) relative to the separated region. As a consequence of ground test facility Reynolds number limitations, data often are acquired where the end of transition is sufficiently close to the separated flow region. These data must be viewed as optimistic, in that separation lengths could be minimized due to the large concentration of high energy flow near the wall.

The effect of mass transfer on the turbulent boundary layer velocity profile tends to reduce its fullness (i.e., the exponent n is reduced). It is interesting to note that the axial distribution of n with blowing retains the same general characteristics as the non-blowing value which is noted by Reference 20 shown in Figure 35.

In assessing the analytical and experimental studies on viscous layer thickness for turbulent hypersonic boundary layers, the design engineer has had to rely on semi-empirical development based on experimental data. This is a consequence of the difficulty of modeling the turbulent shear structure in three-dimensional analyses as well as time consumption which is inherent in codes of this nature. On the other hand, recent data has shown that engineering codes (integral type) have a tendency to over-predict mass transfer effects (with $\alpha = 0°$). Moreover, the inclusion of the angle of attack effects on the viscous thicknesses has resorted to curve fitting of limited data while virtually no information has been available for the coupling of mass transfer and angle of attack.

The technical objective of the present study is to examine the effects of mass transfer and angle of attack on the viscous turbulent boundary layer parameters δ, δ^*, θ, and n. The data obtained from the SAMSO STREET-G study (References 1 and 2) will be used to define the modifications for including angle of attack effects into existing engineering codes which are expressed as functions of mass transfer only. The analyses will also include molecular weight effects.

4.2 DATA PRESENTATION

4.2.1 Viscous Layer Thicknesses: $\alpha = \lambda = 0$

Inasmuch as the empirical correlations developed in this study require a standard for normalization (i.e., non-blowing, zero angle of attack conditions), the current state of the art engineering prediction capability will be assessed. Essentially, the development of this work is classic in nature and employs the usual boundary layer assumptions. An equation of state is assumed for a constant pressure boundary layer that relates density to temperature (enthalpy). The Crocco linear velocity temperature expression is then used together with a power law velocity distribution. Bloom and Martellucci[32] adopted such an approach where a Dorodnitzyn type compressibility transformation was used on the coordinates with the velocity power law. The viscous layer thicknesses can then be expressed as

$$y = \Delta_o \int_o^{\eta} (\rho/\rho_e)^{-1} \, d\eta \tag{8}$$

$$\delta_o = \Delta_o \int_o^{1} (\rho/\rho_e)^{-1} \, d\eta \tag{9}$$

$$\delta_o^* = \Delta_o \int_o^{1} \left[(\rho/\rho_e)^{-1} - (u/u_e)\right] d\eta \tag{10}$$

and

$$\theta_o = \Delta_o \int_o^{1} (u/u_e)\left[1 - (u/u_e)\right] d\eta \tag{11}$$

Noting the equation of state $(\rho/\rho_e) \quad h_e/h$ and the velocity power law $u/u_e = \eta^{\frac{1}{n}}$, for n the velocity power exponent, one can write

$$\delta_o = \Delta_o \int_o^{1} h/h_e \, d\eta \tag{12}$$

$$\delta_o^* = \Delta_o \int_o^{1} \left[(h/h_e) - \eta^{1/n}\right] d\eta \tag{13}$$

The linear Crocco relation is then used for the static enthalpy, giving

$$\frac{\delta_o}{\Delta_o} = \frac{n}{n+2} + \left(1 - \frac{n}{n+1}\right)\frac{h_w}{h_e} + \left(\frac{n}{1+n} - \frac{n}{2+n}\right)\frac{h_{aw}}{h_e} \tag{14}$$

and

$$\frac{\delta_o^*}{\Delta o} = -\frac{n}{(n+1)(n+2)} + \frac{1}{(n+1)}\frac{h_w}{h_e} + \frac{n}{(n+1)(n+2)}\frac{h_{aw}}{h_e} \tag{15}$$

Equation (11) together with the velocity power law reduces to

$$\theta_o/\Delta_o = n/\left[(n+1)(n+2)\right] \tag{16}$$

and it is easily shown that

$$\frac{\delta_o}{\theta_o} = (n+1) + \left[\left(\frac{n+2}{n}\right)\frac{h_w}{h_{aw}} + 1\right]\left[1 + A\,r\,\frac{\gamma-1}{2}M_e^2\right] \tag{17}$$

$$\frac{\delta_o^*}{\theta_o} = -1 + \left[\left(\frac{n+2}{n}\right)\frac{h_w}{h_{aw}} + 1\right]\left[1 + B\,r\,\frac{\gamma-1}{2}M_e^2\right] \tag{18}$$

The above was developed in Reference 32 for A = B = unity. However Walker and Schumann[28] noted a disparity when comparing Eqs. (17) and (18) to data for A = B = unity. The parameters A and B were then arbitrarily placed into Eqs. (17) and (18) with the kinetic energy term. Walker then compared equation (17) with the parameter A to the numerical results of Persh[33], who used a power law velocity distribution together with the Crocco linear velocity-temperature relations, from the integration of the expression

$$\frac{\delta_o}{\theta_o} = \left[\int_o^1 \frac{\rho u}{\rho_e u_e}\left(1 - \frac{u}{u_e}\right) d\left(\frac{y}{\delta_o}\right)\right]^{-1}$$

Equation (17) was found to closely approximate the numerical results for A = 1.29. However, an examination of available data[28] indicated that a value of A = 1.69 showed agreement between theory and data to within 10%.

If one considers the reduced form of Eq. (17) from the Bloom-Martellucci result, one can write

$$\frac{\delta_o}{\theta_o} = (n+1) + \left[\left(\frac{n+2}{n}\right)\frac{h_w}{h_{aw}} - 1\right]\frac{h_{aw}}{h_e}$$

which would imply that the Walker-Schumann modification can be expressed as

$$h_{aw}/h_e = 1 + A\,r\,\frac{\gamma-1}{2}M_e^2$$

However, from a conservation of energy, the product A r must be $\leq$ one which is not the case when matching the data. This dilemma cannot be explained by the authors. An inspection of Figures 36 and 37 shows, for n = 7 at various values of h_w/h_{aw}, that Eqs. (17) and (18) are in good agreement with data for A = 1.69 and B = 1.16 (also suggested in Reference 28) including the recently acquired data of References 1 and 2.

An alternative to the approach used by Walker and Schumann is to employ the modified Crocco relation suggested by Kutateladze and Leont'ev[12]. Here, the authors choose to include a non-similarity parameter, ξ. which is defined as

$$\xi = \xi\left(\frac{y}{\delta}\right) \cdots \xi \text{ (pressure gradient, mass transfer, enthalpy potential)}$$

More specifically, ξ is defined by Eqs. (4) and (5) of Section 3. If one expresses Eq. (7) in terms of the static enthalpy, there results

$$\frac{h}{h_e} = \frac{h_w}{h_e} + \xi\left(\frac{h_{aw}}{h_e} - \frac{h_w}{h_e}\right)\frac{u}{u_e} + \left(1 - \frac{h_{aw}}{h_e}\right)\left(\frac{u}{u_e}\right)^2 \qquad (19)$$

Equation (19) can be substituted into Eqs. (12) and (13) and the normalized viscous layer thicknesses become (where ξ is assumed as a constant)

$$\frac{\delta_o}{\theta_o} = (n+1)\cdot\left\{\left(\frac{n+2}{n}\right)\left[1 + n(1-\xi)\right]\frac{h_w}{h_{aw}} + \left[\xi(n+2) - (n+1)\right]\right\}\cdot \left(1 + r\,\frac{\gamma-1}{2}M_e^2\right) \qquad (20)$$

and

$$\frac{\delta^*}{\theta_o} = -1 + \left\{\left(\frac{n+2}{n}\right)\left[1 + n(1-\xi)\right]\frac{h_w}{h_{aw}} + \left[\xi(n+2) - (n+1)\right]\right\}\cdot \left(1 + r\,\frac{\gamma-1}{2}M_e^2\right) \qquad (21)$$

where it is noted that for ξ = unity, Eqs. (20) and (21) reduce to Eqs. (17) and (18).

The important thing to note here is that the parameter ξ is correctly connected with the enthalpy potential term (i.e., h_w/h_{aw}) and not the kinetic energy term. Moreover, an examination of the STREET-G data indicates that the parameter ξ can be used to model the viscous layer thicknesses. Inasmuch as $\xi = \xi\,(y/\delta)$, further experimental information will be required to actually establish $\xi = \xi\,(\eta)$ in Eqs. (12) and (13). However, if one considers a value of ξ and n in the energy overshoot region (see, for example, Figure 30) good agreement is noted. Until further information can be obtained relative to the non-similarity parameter, it is suggested that the Walker-Schumann method be used for engineering purposes.

As noted in the preceding development, an accurate value of the momentum thickness will be required in order to determine the corresponding viscous thicknesses δ_o and δ_o^*. Moreover this value will also be required for the correlation of viscous layer thicknesses involving mass transfer (which will follow). Traditionally, the momentum thickness has been determined from the incompressible momentum equation and modified to include compressible effects through some type of transformation. Moreover, the skin-friction coefficient is replaced by a Blasius type solution of the coordinate Reynolds number (which implies a power law velocity distribution) and is subsequently modified to include compressibility with the Eckert reference enthalpy method. This can be expressed as

$$\frac{C_{f_o}}{2} = \frac{C_{f_i}}{2}\,\frac{\rho^*}{\rho_e} = \text{constant}\,\left(\frac{\rho^*}{\rho_e}\right)\,Re_s^{*\,-1/5}$$

where the constant assumes a value of 0.0296. Having established the skin-friction coefficient, one can then determine the momentum thickness from the momentum equation (for a flat plate: $d\theta_o/ds = C_{f_o}/2$).

In the above, no provision was made to account for velocity power-law distributions that are not 1/7 (as seen, for example, in Figure 10). If one considers the

classic Blasius equation[34], which will be generalized to include a variable power law[12], there results

$$\tau_w = (C)^{\frac{-2n}{1+n}} \rho u_\infty^2 \left(\frac{\mu}{\rho u_\infty \delta}\right)^{\frac{2}{1+n}} \tag{22}$$

Here, the parameter C is a function of n also (see Reference 12 or 34). The boundary layer thickness can be determined from a conservation of momentum which allows for a solution to the skin friction coefficient. The flat plate momentum equation becomes

$$\frac{d\theta_o}{ds} = \frac{C_{f_o}}{2} = K(n)\,\epsilon_T \left[Re_s\right]^{-2/(3+n)} \tag{23}$$

where

$$K(n) = (C)^{\frac{-2n}{1+n}} \Bigg/ \left[\frac{(3+n)\,(2+n)}{n} (C)^{\frac{-2n}{1+n}}\right]^{\frac{2}{(3+n)}} \tag{24}$$

and

$$\epsilon_T = \left(\frac{\rho^*}{\rho_e}\right)^{\frac{1+n}{3+n}} \left(\frac{\mu^*}{\mu_e}\right)^{\frac{2}{3+n}} \tag{25}$$

Integration of Eq. (23) yields

$$\theta_o\Big|_{F.P.} = \left(\frac{3+n}{1+n}\right) K(n)\, \epsilon_T s\, Re_s^{-\frac{2}{(3+n)}} \tag{26}$$

and for a sharp cone, the above becomes

$$\theta_o\Big|_{S.C.} = MF \left(\frac{3+n}{1+n}\right) K(n)\, \epsilon_T s\, Re_s^{-\frac{2}{(3+n)}} \tag{27}$$

where the Mangler Factor (MF) is given by

$$MF = \left[\frac{2(2+n)}{1+n}\right]^{-(1+n)/(3+n)} \tag{28}$$

It is important to note that the above formulation did not allow for n = n(s) which has been experimentally observed (Figure 10). If one considers the classic 1/7 power law, C has the value 8.74 (which has since been modified to 8.56 to agree with measured data) and the parameter K (n) is equal to 0.0296. Table V gives the values of C, K, and MF (as a function of n) that should be used in calculating viscous layer thicknesses.

4.2.2 Velocity Power Law Exponent

Data representing the velocity exponent as a function of Re_θ are shown in Figure 10 at two free stream Reynolds number conditions. Here, one notes that the exponent n increases through the transitional boundary layer region into the overshoot region as shown in References 16 and 17. It is interesting to note that the classic 1/7 distribution (n = 7) is never reached which is somewhat surprising when considering a 5-foot model. This leaves one to speculate on the validity of published data on models of the order of one foot in length relative to fully-developed turbulent flow characteristics.

Figure 38 shows the attenuation in the velocity exponent as a function of mass transfer and molecular weight. The data of STREET-G are shown together with data from References 19 and 35. The data have been correlated as a function of the blowing parameter in the form

$$\frac{n}{n_o} = f(b_M) = \left[1 + \frac{1}{4} b_M\right]^{-1} \qquad (29)$$

4.2.3 Viscous Layer Thicknesses with Mass Transfer: $\alpha = 0$

Figures 39 through 41 show the viscous layer thicknesses, normalized by non-injection values, as a function of the skin-friction blowing parameter. The data represent several injection rates with three injectant gases. In all cases, correlations were developed based on data fitting. It is noted that boundary layer thickness growth displays a slight curvature with blowing while the displacement and momentum thickness growth appears to be linear. Considering the various molecular weights and injectant rates, the data show a well-ordered behavior. The correlations developed for the viscous thicknesses with blowing are

$$\frac{\delta}{\delta_o} = 1 + \frac{0.264 \quad b_M}{1 + 0.03 b_M} \tag{30}$$

$$\frac{\delta^*}{\delta^*_o} = 1 + \frac{b_M}{3} \tag{31}$$

$$\frac{\theta}{\theta_o} = 1 + 0.41 \quad b_M \tag{32}$$

Figure 42 shows the viscous layer thicknesses data of References 1 and 2 compared to the prediction technique developed within. The method of prediction considers the analytical expressions given by Eqs. (17) and (18) together with Eq. (27) and the empirical relations represented by Eqs. (30) through (32). For example, the displacement thickness in the presence of blowing can be written as

$$\delta^* = \left(\frac{\delta^*_o}{\theta_o}\right) \theta_o \left(\frac{\delta^*}{\delta^*_o}\right)$$

$\left(\frac{\delta^*_o}{\theta_o}\right)$ → Eq. (18)

θ_o → Eq. (27)

$\left(\frac{\delta^*}{\delta^*_o}\right)$ → Eq. (31)

It should be noted that the curves shown in Figure 42 were based on a 1/7 power law with the Walker-Schumann[28] modification to the Bloom-Martellucci[32] results. Excellent agreement is noted which further substantiates the choice of the non-blowing viscous layer parameters.

4.2.4 Viscous Layer Thicknesses with Angle of Attack and Blowing

Several attempts were made to correlate the viscous layer thicknesses at angle of attack conditions. For example, the boundary layer thickness normalized by its zero angle of attack value as a function of α / θ_c (i.e., ratio of angle of attack to conical half-angle) were not successful. Moreover, the suggested correlation of Copper and Shaw[31] (shown in Figure 43) which defines

$$\bar{\delta} = \frac{\left[\delta(\alpha)/\delta(\alpha=0)\right]_{\text{MEASURED}}}{\left[\delta(\alpha)/\delta(\alpha=0)\right]_{\text{CALCULATED}}} = f(\alpha/\theta_c)$$

was also attempted with no further improvement.

Other attempts were made to correlate angle of attack data. Shown in Figures 44 through 46 is the correlation developed in this study. Here, the viscous layer thicknesses are shown normalized by their zero angle of attack value as a function α/θ_c and b_M. Moreover, the data shown represent various injectant gases. Unlike the correlation attempts with α/θ_c as the independent variable, the data shown in Figures 44 through 46 have a tendency to coalesce in a more orderly fashion. Inasmuch as the data appears to be characterized by a hyperbola, a correlation of this type was made and is shown by the curves in the figures. In each case the curve drawn through the data is the hyperbola for which the ordinate equals the reciprocal of the quantity $(1 + \alpha/\theta_c + b_{M,\alpha}^{1/5}/6)$, that is

$$\frac{\delta(\alpha)}{\delta(\alpha=0)}, \quad \frac{\delta^*(\alpha)}{\delta^*(\alpha=0)}, \quad \frac{\theta(\alpha)}{\theta(\alpha=0)} \cdots \left[1 + \frac{\alpha}{\theta_c} + \frac{b_{M,\alpha}^{1/5}}{6}\right]^{-1} \tag{33}$$

With the exception of the leeward angle of attack data, satisfactory agreement is accorded.

4.3 DISCUSSION OF RESULTS

In the work statement of the proposal (GE-RESD N72647 R1) concerning profile shapes, the velocity exponent was to be examined relative to the effects of Reynolds number, transition location, blowing, and angle of attack. After careful deliberation, it was found that the angle of attack dependence on n did not show any trends. Since no pattern could be ascertained, no further work was considered. Moreover, inasmuch as three reporting profile stations (in general) were recorded, no definitive conclusions could be made relative to transition location effects on the exponent n.

As noted in the development of the zero blowing viscous layer thicknesses, a dilemma existed concerning the arbitrary choice of the constants A and B of Walker

and Schumann (see Eqs. (17) and (18)). While the choice of the value A appears to violate the conservation of energy, the results were shown to be in good agreement with experimental data. On the other hand, one can arbitrarily recast Eq. (17) to read

$$\frac{\delta_o}{\theta_o} = (n + 1) + \psi \left[\left(\frac{n + 2}{n}\right)\frac{h_w}{h_{aw}} + 1\right]\left[1 + r\,\frac{\gamma - 1}{2}\,M_e^2\right] \qquad (34)$$

where the arbitrary constant ψ is now a multiplicative product to the enthalpy potential term (i.e., h_w/h_{aw}). One will note that the above is much in the same spirit as that proposed in Reference 12. When Eq. (34) is matched with Eq. (17), for A = 1.69, n = 7, and $h_w/h_{aw} = 1$, a value of the parameter ψ of 1.62 yields results to within 3% of Eq. (17) for $M_e \geq 5$. For values of $M_e < 5$, departures up to 25% are observed to values of M_e = unity.

4.4 CONCLUSIONS

Turbulent boundary layer characteristic parameters δ, δ^*, θ, and n have been examined relative to the influence of Reynolds number, angle of attack, mass transfer, and molecular weight variations of the injectant gas. It was found that the state of boundary layer development was sensitive to the velocity power law exponent as well as the viscous layer thicknesses. Several of the pertinent observations of this study are as follows:

1. The velocity power law exponent showed significant departures from the classic n = 7 value, characteristic of fully-developed flows, to values of n >12 in the overshoot region. The latter defined as the region just after transition. As a result, the reference momentum thickness relations had to be modified to include a general velocity exponent.

2. The prediction capability for the viscous layer thickness parameters has been shown to yield excellent agreement with data for the reference case ($\alpha = \lambda = 0$) where a modified Crocco relation was used with a generalized velocity power law. Specifically, the recommended correlations for θ_o, δ_o, and δ_o^* are given by Eqs. (27), (17), and (18), respectively, where n = 7, A = 1.69, and B = 1.16.

3. With mass transfer effects, the velocity power law exponent attenuated to values of $n < 3$. On the other hand, the viscous layer thicknesses were augmented above the non-injectant values as might be expected. Concerning the latter, correlations were developed which include both the mass transfer parameter and molecular weight ratio. Prediction capability was then afforded by combining zero injection analysis with the mass transfer data correlations. Specifically, the recommended mass transfer correlations are given by Eqs. (30), (31), and (32).

4. When angle of attack was combined with blowing, the viscous layer thicknesses did not appear to correlate using methods previously reported in the literature. However, a hyperbolic function was found to reasonably correlate the thicknesses (when normalized by their $\alpha = 0$ values) as a function of α/θ_c and the blowing parameter $b_{M,\alpha}$. The recommended correlation is expressed by Eq. (33).

SECTION 5

TURBULENT HEAT BLOCKAGE AND SKIN-FRICTION REDUCTION DUE TO MASS INJECTION

5.1 BACKGROUND

The alleviation of the high heating rates encountered by surfaces of hypersonic vehicles has been recognized as an important problem. One of the cooling methods that has shown promise is mass transfer cooling, wherein a foreign material is transferred from the vehicle surface into the boundary layer. This has a two-fold advantage in attenuating the heat transfer problem. The transferred coolant may absorb heat from the boundary layer through a phase change (sublimation, evaporation, melting, etc.) as well as providing high thermal heat capacitance. In addition, it has been shown that the introduction of a material (with its normal velocity component) at the surface acts to decelerate the flow and, consequently, to reduce the skin friction. This also implies a reduction in heat transfer at the wall.

When examining the available literature concerning mass transfer experiments, it is noted that (1) the bulk of the data was obtained under supersonic flow conditions ($M < 5$) and (2) the model geometries consisted primarily of flat plates, sharp cones, and cylinders in cross-flow, precluding pressure gradient effects. Moreover, a careful inspection of engineering heat transfer prediction techniques indicates that empirically derived correlations, developed from the transpiration experiments, have been employed to determine the level of heat attenuation resulting from blockage by the injectant gas. However, examination of the available hypersonic turbulent boundary layer data, where mass transfer effects are present indicate that the existing empirical correlations[39, 40, 41] for turbulent boundary layers do not sufficiently characterize the heat blockage because the effects of Mach number and wall temperature are not taken into account (see Figure 47).

In general most analytical investigations have centered around the flat-plate or sharp cone geometry to allow a more tractable mathematical solution. The most

successful approaches involve the solution of the momentum integral equation coupled with suitable compressibility transformations and Colburn's analogy to predict skin-friction and heat transfer. These approaches will be examined, modified, and expanded: first, to include the recently acquired experimental data of Martellucci et al [1, 2] at hypersonic (M > 5) conditions, and second, to account for the effects of both Mach number and wall temperature, with the objective of providing improved engineering design relationships suitable for inclusion in existing semi-empirical turbulent boundary layer codes.

(a) Heat Blockage

There have been many experiments performed on various geometric shapes in low and high speed tunnels to determine the effect of heat blockage on a transpiration-cooled surface. Experiments of this nature have been performed to simulate ablation effects experienced on re-entry vehicles. However, analytical predictions have weighed heavily on the Reynolds analogy to determine the attenuation of heat flux as a consequence of mass injection, thereby requiring recourse to experimental data and subsequent engineering correlations. Of the three empirical correlations alluded to previously (Figure 47), only that of Walker[39] was a direct curve-fit of the available experimental data at that time. Lees' [40] expression was derived analytically based on a Couette-flow assumption. Bartle and Leadon[41] correlated their experimental data in terms of an effectiveness parameter. They suggested that the heat blockage could be expressed in terms of the effectiveness as shown in Figure 47. A comparison of these correlations with the data of Martellucci et al [1] (STREET-G) at M = 8 and Pappas & Okuno[42] at M ≈ 0 shows a definite deficiency in accounting for the effect of Mach number.

Two of the most pertinent analytical investigations of turbulent boundary layer heat and mass transfer employing compressibility transformations are those of Spalding, Auslander, and Sundaram[43] and Kutateladze and Leont'ev.[12] Spalding et al introduced compressibility transformations for skin-friction, heat transfer (Colburn analogy) and Reynolds number (viscous effect). The developed technique utilized all the available experimental data at the time (zero pressure gradient, supersonic flow, M < 5).

Spalding et al did not include a Mach number or wall temperature effect in their viscous transformation but recognized its potential. On the other hand, Kutateladze and Leont'ev included the effect of Mach number in their theory but neglected the viscous effect.

Most of the turbulent experimental heat blockage data reported up to the present time were obtained for supersonic flow over flat plates and sharp cones (having negligible pressure gradients). Bartle and Leadon[41] and Leadon and Scott[44] reported data for heat blockage due to mass injection (air and foreign gas) for a Mach number range of M_e = 2.0 to 3.2 with corresponding wall temperature ratios (see Table VI). Pappas and Okuno[42] reported heat blockage data with air, helium, and Freon injection over a sharp cone for a Mach number range of M_e = 0.7 to 4.35 and $T_w \simeq T_r$. Tewfik et al [45] reported subsonic air injection data over a cylinder in cross-flow. More recently hypersonic air injection data on a flat plate were obtained by Danberg[46] at M_e = 6.7 which indicated a wall temperature effect on heat blockage.

The recent STREET-G data of Martellucci et al [1,2] obtained using a sharp porous cone at M_e = 7.1 (at two different wall temperatures for air, helium, argon, and Freon-12 injection) supplies the bulk of the hypersonic flow data required to take into account the effects of Mach number, wall temperature and injectant molecular weight on heat blockage. Extensive angle of attack heat transfer data are also reported in References 1 and 2.

An attempt to account for pressure gradient effects was made by Laganelli et al [47] in a porous blunt body investigation; however, the authors noted that the data obtained were questionable due to the sensitivity of the tunnel free-stream conditions and surface sensor reponse.

(b) Skin-Friction

Relative to the abundant heat blockage literature, there is a paucity of applicable skin-friction experiments. Only Dershin et al [48] in their flat plate air-injection investigation have measured local skin-friction reduction in a supersonic flow (M_e=3.18)

environment. Dershin's data tended to verify Reynolds analogy when correlated with the heat blockage data of Bartle and Leadon.[41] The subsonic flow measurements of local skin friction reduction with air injection performed by Kendall et al [49] and Goodwin[50] serve to complement the supersonic data of Dershin.

Pappas and Okuno[51] reported total (averaged over the body) skin-friction measurements over a porous sharp cone for the Mach number range of 0 to 4.3. Data was obtained for air, helium and Freon-12 injection. This data together with that of Tendeland & Okuno[52] (M_e = 2.55) exhibited a significant Mach number dependence causing a disparity with the local measurements of Dershin et al. Dershin suggested that the difference may be due to small local pressure gradient effects that become apparent for total skin-friction on a cone but may not be relevant for local flat plate skin-friction. Walker[39] directly correlated the total (or average) supersonic skin-friction reduction data reviewed above as a function of Mach number and injectant molecular weight without employing a theoretical base as did Spalding et al.[43]

In assessing the experimental investigations of heat blockage and skin-friction reduction in turbulent boundary layers, one notes that the bulk of the previously reported experimental data were obtained at supersonic ($M < 5$) flow conditions. Only the recent measurements of Danberg[46] and Martellucci et al [1,2] (STREET-G) supply the much needed hypersonic ($M > 5$) flow information required to critically examine state-of-the-art engineering design relationships. In addition the STREET-G experiments provide a wealth of heat transfer data for air and foreign gas injection obtained at angle of attack to be used in validating 3-D viscous heating design codes. The data of Pappas & Okuno[42, 51] and others together with the STREET-G data supply sufficient data for analysis of injectant molecular weight influence on heat blockage and skin-friction reduction.

A careful examination of the profile data obtained in the STREET-G study indicates that the local variations across the boundary layer (e.g., velocity and temperature) have not reached a fully-developed characteristic. Keeping in mind that the model used in the STREET-G experiments was five feet long, one must carefully weigh the

significance of "fully-developed turbulent characteristics". Moreover, the credibility of reported turbulent boundary layer data, as published in the literature on much smaller models raises many questions. In addition, the assemblage of all applicable data illustrates the sensitivity of the skin-friction coefficient and Stanton number data to the character of the flow. If the flow is not fully-developed, the question arises as to what is the proper value of St_o (or C_{f_o}) for normalization purposes. As the blowing rate increases, the transitional (overshoot) region moves forward along the surface of the cone (or plate). The problem then becomes to determine whether to normalize the blowing data with St_o (or C_{f_o}) at the same wetted length or other distance based on some equivalent boundary layer thickness parameter (such as Re_θ).

The two most pertinent analytical investigations, Spalding et al [43] and Kutateladze and Leont'ev[12] employ compressibility transformations to the solution of the momentum integral equation. The viscous transformation employed by Spalding et al was empirically developed from the supersonic data available at the time. The result was that the method did not satisfactorily take into account the effects of Mach number and wall temperature exhibited by the inclusion of the recently acquired hypersonic data of Danberg and Martellucci et al. They did, however, suggest that the viscous transformation could be modified to account for M_e and T_w as more data becomes available.

Kutateladze and Leont'ev did not include a viscous transformation but introduced the concept of a critical blowaway parameter based on an infinite Re_θ - limiting law. However, their derivation resulted in critical blowaway values decreasing with increasing Mach number which is contrary to the observed experimental data.

The technical objectives of the present study are to examine, modify and expand the aforementioned heat blockage and skin-friction reduction correlations (both analytical and experimental) in order to include the recently acquired data of Martellucci et al and Danberg obtained at hypersonic flow conditions ($M \cdot 5$) and to account for the effects of Mach number, wall temperature and injectant molecular weight. The resulting semi-empirical relations are then to be employed in updating the GE-RESD 3-D Viscous Code to predict angle-of-attack effects on surface heating. In addition,

this study serves to reduce the data of Martellucci et al to a form suitable for addition to the general literature on heat blockage.

5.2 ANALYSIS

5.2.1 General Approach

Considerable success in correlating heat transfer blockage and skin-friction reduction as a function of Mach number and wall temperature was obtained by adopting an approach similar to that of Spalding et al [43], which employs compressibility transformations to the solution of the momentum integral equation. For a cone with mass injection one may write

$$\frac{1}{r}\frac{d}{ds}(r\theta) = \frac{C_f}{2} + \lambda = \frac{C_f}{2}(1 + B_u) \tag{35}$$

where B_u is defined as $2\lambda/C_f$.

For a sharp cone: $r = s \sin\theta_c$, and the momentum integral equation in terms of Reynolds number becomes

$$\frac{d(Re_s Re_\theta)}{dRe_s} = Re_s \frac{C_f}{2}(1 + B_u) \tag{36}$$

Spalding et al introduced the following transformations in their method:

(a) Compressibility transformation

$$\frac{C_{f_i}}{C_f} \equiv F_c = F_c(M_e, T_w/T_e, B_u) \tag{37}$$

(b) Viscous transformation

$$\frac{Re_{\theta,i}}{Re_\theta} \equiv F_\theta = F_\theta(M_e, T_w/T_e, B_u) \tag{38}$$

$$\frac{Re_{s,i}}{Re_s} \equiv F_s = F_s(M_e, T_w/T_e, B_u) \tag{39}$$

When these transformations are applied to the momentum integral relation, Eq. (36), there results

$$\frac{d\,(F_\theta\ Re_\theta \cdot F_s Re_s)}{d\,(F_s Re_s)} = F_s Re_s \cdot F_c \frac{C_f}{2}\ (1 + B_u)\ \frac{F_\theta}{F_c F_s} \tag{40}$$

Spalding's basic postulate asserts that unique relations exist between $(F_c\ C_f/2)$, $(F_\theta\ Re_\theta)$ and $(F_s Re_s)$. This can only be true if, in Eq. (40), $(1 + B_u)\ F_\theta/(F_c F_s)$ is equal to a constant for all boundary layers. Consideration of the particular case of the uniform density zero mass transfer boundary layer shows that this constant must be equal to unity. Therefore

$$F_s = \frac{F_\theta}{F_c}\ (1 + B_u) \tag{41}$$

Thus, it is seen that F_s is not independent of the F_c and F_θ transformations. This means that only F_c and F_θ need be deduced, either analytically or empirically, to afford a solution of Eq. (40).

Rewriting Eq. (40) yields

$$\frac{d(F_\theta\ Re_\theta \cdot Re_s)}{dRe_s} = \frac{F_\theta}{F_c} Re_s\ (F_c \frac{C_f}{2})\ (1 + B_u) \tag{42}$$

The skin friction coefficient for an incompressible flat plate flow can be expressed as

$$\frac{C_{f_i}}{2} = \frac{E}{2} Re_{\theta,i}^{-m} \tag{43}$$

or

$$F_c \frac{C_f}{2} = \frac{E}{2} (F_\theta\ Re_\theta)^{-m}$$

where E and m are constants related to the velocity power law exponent; specifically, $E = 0.013$ and $m = 0.25$ for $n = 7$.

Eq. (42) then becomes

$$\frac{d(F_\theta \, Re_\theta \cdot Re_s)}{dRe_s} = \frac{E}{2} \frac{F_\theta}{F_c} (F_\theta \, Re_\theta \cdot Re_s)^{-m} Re_s^{m+1} (1 + B_u) \tag{44}$$

which integrates to (assuming B_u constant)

$$\frac{(F_\theta \, Re_\theta \cdot Re_s)^{m+1}}{m+1} = \frac{E}{2} \frac{F_\theta}{F_c} (1 + B_u) \frac{Re_s^{m+2}}{m+2} \tag{45}$$

Rearranging yields

$$(F_\theta \, Re_\theta)^{-m} = \left[\frac{E}{2} \left(\frac{m+1}{m+2} \right) \frac{F_\theta}{F_c} (1 + B_u) \, Re_s \right]^{-\frac{m}{m+1}} \tag{46}$$

Reintroducing Eq. (43) yields the result

$$F_c \frac{C_f}{2} = \frac{E}{2} \left[\frac{E}{2} \left(\frac{m+1}{m+2} \right) \frac{F_\theta}{F_c} (1 + B_u) \, Re_s \right]^{-\frac{m}{m+1}} \tag{47}$$

For the zero blowing case ($B_u = 0$), Eq. (47) reduces to

$$F_{c_o} \frac{C_{f_o}}{2} = \frac{E}{2} \left[\frac{E}{2} \left(\frac{m+1}{m+2} \right) \frac{F_{\theta_o}}{F_{c_o}} Re_s \right]^{-\frac{m}{m+1}} \tag{48}$$

which, when combined with Eq. (47), results in the skin-friction reduction relation

$$\left(\frac{C_f}{C_{f_o}} \right)_{Re_s} = \left(\frac{F_c}{F_{c_o}} \right)^{-\frac{1}{m+1}} \left(\frac{F_\theta}{F_{\theta_o}} \right)^{-\frac{m}{m+1}} \left(1 + B_u \right)^{-\frac{m}{m+1}} \tag{49}$$

If one employs the use of Reynolds' analogy ($St = C_f/2$) at this point, the heat blockage relation, analogous to Eq. (49), becomes

$$\left(\frac{St}{St_o}\right)_{Re_s} = \left(\frac{F_c}{F_{c_o}}\right)^{-\frac{1}{m+1}} \left(\frac{F_\theta}{F_{\theta_o}}\right)^{-\frac{m}{m+1}} (1 + B_h)^{-\frac{m}{m+1}} \tag{50}$$

where B_h is defined in terms of the Stanton number:

$$B_h \equiv \frac{\lambda}{St} \tag{51}$$

5.2.2 Deduction of the Transformation Functions

Spalding et al adopted a definition for F_c which has been commonly accepted in the scientific community, namely:

$$F_c \equiv \left[\int_0^1 \left(\frac{\rho/\rho_e}{1 + B_u z} \right)^{1/2} dz \right]^{-2} \tag{52}$$

where z is the velocity ratio u/u_e.

In the above, an equation of state is generally invoked together with the boundary layer assumption of zero pressure gradient normal to the surface. The linear Crocco relation is then applied and numerical integration is performed to evaluate Eq. (52). In order to simplify the complexity of the above integral, it will be assumed that F_c can be approximated by the expression

$$F_c \sim F_c^* = \frac{\rho_e}{\rho^*} \left[\int_0^1 \frac{dz}{\sqrt{1 + B_u z}} \right]^{-2} \tag{53}$$

where the starred quantity is based on the Eckert reference enthalpy; then

$$F_c^* = \frac{\rho_e}{\rho^*} \left[\frac{2}{B_u} \left(\sqrt{1 + B_u} - 1 \right) \right]^{-2} \tag{54}$$

Note that in the limit (using L'Hôpital's rule) as $B_u \rightarrow 0$

$$F_{c_o}{}^* = \frac{\rho_e}{\rho^*} \tag{55}$$

which is the transformation function for a non-injection case[54].

A comparison of the $F_c{}^*$ approximation with the numerically exact F_c solution from the tables of Spalding et al is given in Figure 48 for a realistic range of Mach numbers ($0 \leq M_e \leq 8$) and wall temperature ratios ($1 \leq T_w/T_e \leq 8$). The comparison indicates excellent agreement in the supersonic regime ($M < 5$) but a significant variation with increasing values of Mach number; however, this is to be expected as seen, for example, in a turbulent heating flight test analysis by Laganelli[54]. The important thing to keep in mind here is that this approximation is purely analytical while the F_θ viscous transformation function (as will be seen) is deduced from experimental data. The net effect of both of these transformations will satisfactorily account for the hypersonic situation.

While most authors agreed on the analytical form for the F_c transformation, significant disagreement prevailed in the formulation of the F_θ function. Since there existed considerable uncertainty about the nature of F_θ, Spalding et al deduced the following empirical relation (based on all the air injection data available at the time prior to 1962)

$$F_\theta = \frac{\mu_e}{\mu_w} (1 + B_u)^{-3/2} \tag{56}$$

which does not contain a Mach number effect.

Consequent modification of this relation to include the experimental air injection data of Martellucci et al.[1,2], Danberg[46] and Pappas & Okuno[42] along with the Eckert reference state concept resulted in the empirical relation

$$F_\theta = \frac{\mu_e}{\mu^*} (1 + B_u)^{-\omega} \tag{57}$$

where

$$\omega = (T_w/T_e)^{-\frac{1}{8}} + \frac{1}{8} M_e \tag{58}$$

Eq. (58) takes into account the effects of Mach number and wall temperature through a purely empirical correlation of experimental data and judicious use of the F_c tables of Spalding et al. Note, again, that in the limit as $B_u \rightarrow 0$, Eq. (57) reduces to

$$F_{\theta_o} = \frac{\mu_e}{\mu^*} \tag{59}$$

which is the correct zero injection viscous transformation using the Eckert approach[54].

Substitution of Eqs. (54), (55), (57), and (59) into the skin friction expression, Eq. (49), results in (for m = 1/4)

$$\left(\frac{C_f}{C_{f_o}}\right)_{Re_s} = \left[\frac{2}{B_u}\left(\sqrt{1 + B_u} - 1\right)\right]^{\frac{8}{5}} \left(1 + B_u\right)^{\frac{\omega - 1}{5}} \tag{60}$$

where it is noted that in the limit as $B_u \rightarrow 0$, C_f/C_{f_o} approaches unity as required.

The analogous equation for Stanton number is simply (by Reynolds analogy)

$$\left(\frac{St}{St_o}\right)_{Re_s} = \left[\frac{2}{B_h}\left(\sqrt{1 + B_h} - 1\right)\right]^{\frac{8}{5}} \left(1 + B_h\right)^{\frac{\omega - 1}{5}} \tag{61}$$

where B_h has replaced B_u.

5.2.3 Verification With Experimental Data

A comparison of predictions using Eq. (61) and a wide range of air injection experimental data is given in Figure 49 where the heat blockage (represented by the Stanton number ratio, St/St_o) is plotted as a function of the blowing parameter λ/St_o. All of the STREET-G[1] data points were obtained at the high Reynolds number (Re_∞/ft. = 3.7×10^6). The Danberg data points at $T_w/T_e = 4.1$ are not the exact St/St_o values reported in Reference 46. The data points in Figure 49 were obtained by normalizing

his reported St values with a second set of St_o values he reported at the same conditions. It was felt that the second set which consisted of a larger number of data points would prove more reliable. This conclusion seems to be borne out by the correlation curve ($M_e = 7$, $T_w/T_e = 4$) in Figure 49. The Pappas and Okuno[42] data plotted in Figure 49 are their "thermocouple no. 7" data which were measured at their highest reported Reynolds numbers. Further comments concerning the choice of the data included above will be reflected upon in the Results Section.

The wall temperature effects were taken into account (Eq. (58)) through the use of the F_c transformation function tables of Spalding et al.[43] As seen from the figure the correlation curves bracket the data very well, verifying the approximations for F_c (Eq. (54)) and F_{θ} (Eq. (57)).

The influence of injectant molecular weight on heat blockage has been taken into account utilizing the foreign gas injection data of Pappas and Okuno[42], Leadon and Scott[44] and Martellucci et al [1,2] (STREET-G). Correlation of heat blockage with foreign gas injection is presented in Figure 50 where data for helium, argon, and Freon-12 injection are compared with the correlation of Eq. (61) with the blowing parameter B_h redefined as

$$B_h = \frac{C_{p_{inj}}}{C_{p_{air}}} \frac{\lambda}{St} \tag{62}$$

Considering the data scatter, Eq. (61) does an excellent job of correlating the available data.

When the abscissa of Figure 50, (λ/St_o), is multiplied by the specific heat ratio $(C_{p_{inj}}/C_{p_{air}})$, the result is Figure 51. Attempts to correlate the data using molecular weight as a parameter were unsuccessful. However, the specific heat factor did

collapse the data to a band reasonably predicted by the correlation. The Cp values employed for the various injectants were:

Injectant	Molecular Weight	Cp(BTU/lb °F)
Air	28.966	.2401
Argon	39.944	.1244
Freon-12	120.93	.1458
Helium	4.003	1.2413

5.2.4 Zero-blowing Predictions

Consistent with this development is the use of the Eckert reference enthalpy concept in accounting for compressibility effects on the zero-blowing skin-friction and Stanton number values used as the normalization terms in Eq.'s. (60) and (61). These expressions (based on the velocity power-law concept for flat plate fully-developed turbulent flows) are [54]

$$\frac{C_{fo}}{2} = .0296\ (MF)\ \epsilon_T\ Re_s^{-\frac{1}{5}} \tag{63}$$

$$St_o = .0296\ (MF)\ \epsilon_T\ Pr^{-2/3}\ Re_s^{-1/5} \tag{64}$$

where MF is the Mangler factor, $(2.25)^{1/5} = 1.176$ for a sharp cone, and the compressibility term

$$\epsilon_T = \left(\frac{\rho^*}{\rho_e}\right)^{4/5} \left(\frac{\mu^*}{\mu_e}\right)^{1/5} \tag{65}$$

is totally consistent with the preceding analysis (see Eq.'s (49), (55) and (60) with $m = 2/(n+1) = 1/4$ for $n = 7$, the classic fully-developed turbulent velocity power law exponent). The STREET-G "cold wall" zero-blowing heat transfer data are plotted in Figure 52 as a function of wetted-length Reynolds number. Two groups of local Stanton number data are included to illustrate data repeatability. The data are compared with the prediction of Eq. (61) which is based on the one-seventh power-law profile approximation

and Colburn's analogy. Inspection of Figure 52 shows the transitional overshoot region prior to fully-developed turbulent flow. Excellent agreement is observed between the prediction and the data for the fully-developed region.

5.3 RESULTS

5.3.1 Mass Transfer Correlations

The skin-friction reduction relation, Eq. (60), and the heat blockage expression, Eq. (61), that have been developed are expressed in the implicit parameters B_u and B_h, which contain the terms C_f and St, not C_{f_o} and St_o. As engineering design correlations, these expressions would require iterative solutions in order to obtain the desired result. Therefore, more tractable correlations for design purposes should be expressed in terms of explicit blowing parameters (i.e., terms containing the a priori known values of C_{f_o} or St_o).

This was accomplished through the use of the critical blowaway parameter, b_{cr}, introduced by Kutateladze and Leont'ev.[12] They defined b_{cr} as the limiting value of the explicit blowing parameter when C_f/C_{f_o} or St/St_o vanishes. The explicit blowing parameters with provision made for foreign gas injection (analogous to B_u and B_h) are defined as

$$b_u = \frac{C_{p_{inj}}}{C_{p_{air}}} \frac{2\lambda}{C_{f_o}} \tag{66}$$

$$b_h = \frac{C_{p_{inj}}}{C_{p_{air}}} \frac{\lambda}{St_o} \tag{67}$$

The critical blowaway parameter b_{cr} was found to be related to Mach number and wall temperature through the ω parameter defined in Equation (58). The expression which relates b_{cr} to ω is given as

$$b_{cr} = \exp\left[1.676\ (\omega + 0.161)\right] \tag{68}$$

This result, Eq. (68), represents the approximation for b_{cr} that provides the most suitable agreement with the correlation Eqs. (60) and (61) developed in the Analysis Section. Equation (68) is plotted in Figure 53 and compared with all the available heat transfer and skin friction air injection data (See Table VI). Each symbol represents the average value of b_{cr} extracted from each data source. The massive blowing data of Fogaroli and Saydah[53] was included for comparison at higher values of b_{cr}. The incompressible value for b_{cr} (i.e. when $\omega = 1$) was determined to be $b_{cr} = 7$ in order to match the predictions of Eqs. (60) and (61). This value is at variance with the reported incompressible value of $b_{cr} = 4$ as derived by Kutateladze and Leont'ev.[12] However, their result (from the definition below)

$$b_{cr} = \left[\int_0^1 \left\{ \frac{\rho}{\rho_e} \cdot \frac{1 + 2\,(y/\delta)}{z} \right\}^{1/2} dz \right]^2 \tag{69}$$

was based on the assumption that

$$1 + 2(y/\delta) \approx 1 \tag{70}$$

If, instead, an effective or weighted value for (y/δ) was employed in Eq. (69), a larger value of b_{cr} would result. For example, if an effective value of $(y/\delta) = 1/3$ were assumed, a value for b_{cr} of approximately 7 would result.

Utilizing this concept of b_{cr}, the skin-friction reduction and heat blockage equations may be expressed in terms of the explicit blowing parameters b_u and b_h as follows:

$$\frac{C_f}{C_{f_o}} = \left(1 - \frac{b_u}{b_{cr}} \right)^{2.5\omega} \tag{71}$$

$$\frac{St}{St_o} = \left(1 - \frac{b_h}{b_{cr}} \right)^{2.5\omega} \tag{72}$$

The form of these expressions was inspired by a correlation of a series of exact analytical solutions (for a wide range of Mach number and blowing rate) performed by Kutateladze and Leont'ev.[55]

In Figure 54 the heat blockage correlation, Eq. (72), is compared with the air injection data reviewed previously in the discussion of Figure 49. The curves generated from Eq. (72) provide slightly better agreement with the data than do the equivalent curves generated from Eq. (61). Overall, excellent agreement is observed for the air injection comparison over the Mach number range $0 < M_e < 7$ for three different geometrical surfaces.

A comparison of the skin-friction reduction correlation, Eq. (71), with all available air injection data is presented in Figure 55. The data of Dershin et al[48], Kendall et al[49], and Goodwin[50] represent direct measurements of local flat plate skin friction. The data of Pappas and Okuno[51] and Tendeland and Okuno[52] represent total (averaged over the body) skin friction measurements on a cone which are denoted by C_F as distinguished from C_f. Note the disparity between the local skin-friction data of Dershin et al ($M_e = 3.18$) and the total or average skin-friction data of Pappas and Okuno ($M_e = 3.21$). Dershin suggests that the difference may be due to small local pressure gradient effects that become apparent for total skin-friction on a cone but may not be relevant for local flat plate skin friction. In any event the curves generated from Eq. (71) for the range $0 < M_e < 5$ are in reasonable agreement with the reported data, considering the disparity in the data itself. The curves were generated assuming $T_w = T_e$ since the data sources did not report the experimental wall temperatures.

Foreign gas injection data for b_{cr} (molecular weight influence) were added to the air injection data depicted in Figure 53 with Figure 56 as the result. Data for helium and Freon-12 injection over a wide range of Mach numbers were included with relatively insignificant scatter around the air injection data and the correlation curve, Eq. (68).

Finally, the correlations for heat blockage and skin-friction reduction with foreign gas injection are illustrated in Figures 57 and 58 where St/St_o and C_f/C_{fo} are plotted as a function of b_h/b_{cr} and b_u/b_{cr}, respectively. Most of the data for air, helium and Freon-12 injection are bracketed by the correlation curves for ϵ

= 1 (subsonic flow) and $\omega = 2$ (hypersonic flow) which represent a realistic flight condition range. Some of the helium injection data fall outside the subsonic limit ($\omega = 1$) in both figures. Overall, however, the two Figures 57 and 58 verify the success of the correlation equations derived for heat blockage (Eq. (72)) and skin friction reduction (Eq. (71)).

5.3.2 Angle of Attack Predictions

The heat blockage and skin friction reduction correlations developed in this study have taken into account the effects of Mach number, wall temperature and injectant molecular weight (foreign gas injection). These correlations have been incorporated into the GE-RESD 3-D Viscous Code[56] in order to generate viscous flow solutions for angle of attack comparisons with applicable STREET-G[1] data.

The Three-Dimensional Viscous Code applies an integral boundary layer type solution for heating and wall shear stress to sharp cone, sphere-cone, and bent sphere-cone, configurations at angle of attack. The integral boundary layer solutions are carried out along streamlines calculated in the inviscid sense from an imposed pressure field. The small cross-flow approximation is made, and the effects of angle of attack on heat transfer arise from the streamline divergence effect. This is included in the calculation as a scale factor or metric which describes the rate of spread, and which at zero angle of attack reduces to the local body radius.

The effect of angle of attack on surface heat transfer was examined by comparing solutions from the GE 3-D Viscous Code with STREET-G cold wall ($T_w = 580\ ^\circ R$) turbulent heating data obtained on the windward meridian of a sharp cone (5° half-angle) at $M_e = 7.1$. The surface heat transfer rate as a function of wetted length along the cone for three values of angle of attack ($\alpha = 0°, 5°$, and $10°$) is presented in Figure 59 (zero injection) and Figure 60 (injection rate $\lambda = .0015$). A comparison of the code prediction with the STREET-G data shows excellent agreement for the cases with and without injection. The slight disagreement in the zero injection case at $\alpha = 10°$ (Figure 59) is offset by the remarkable predictive capability at the same angle of attack case with injection (Figure 60).

5.3.3 Further Comments

(a) Reynolds Analogy

Since the STREET-G program provided both surface heat transfer data and boundary layer profile measurements, with and without blowing, an attempt was made to investigate the validity of the Reynolds analogy experimentally for hypersonic flow. Here, directly measured Stanton number data were to be compared with skin friction data derived from the profile measurements. The skin-friction coefficient was to be determined from the momentum integral equation (for a sharp cone)

$$\frac{C_f}{2} = \frac{d\theta}{ds} + \frac{\theta}{s} - \lambda \qquad (73)$$

where the blowing rate and momentum thickness were measured. Since the momentum thickness was recorded at three stations along the cone surface, the slope ($d\theta/ds$) was obtained from a plot of θ as a function of the wetted length, s.

However, because of the low enthalpy potential provided by the AEDC facility, all the terms on the right hand side of Eq. (73) were found to be of the same order of magnitude, requiring subtraction of numbers of the order of 10^{-3}. This numerical sensitivity rendered the acquisition of meaningful skin friction data impossible. As a consequence, the attempt to experimentally verify Reynolds analogy at hypersonic conditions had to be abandoned.

(b) Concept of Fully-Developed Flow

The STREET-G experiments have demonstrated that a fully-developed turbulent boundary layer did not exist (from a velocity profile power low exponent point of view; i.e. for n = 7) on a five-foot model. This point has been discussed extensively in Sections 3 and 4 of this report. This knowledge induces one to speculate on the validity of experiments previously performed using models on the order of one foot in length. Several attempts were made to correlate the STREET-G heat transfer data in terms of Reynolds numbers based on equivalent momentum thickness, enthalpy deficit thickness and wetted length along the surface. It was found that the last choice contributed

the best behavior in the correlation for heat transfer attenuation. However, only the data toward the end of the model were emphasized since they were the least likely to be influenced by the velocity exponent overshoot region. It was for this reason that only the data reported at the last station (and highest Reynolds number) of the models of other experimental investigators were included for use in this study.

5.4 CONCLUSIONS

The effect of Mach number, wall temperature and injectant molecular weight on heat blockage and skin friction reduction resulting from mass injection has been evaluated for turbulent flow over surfaces with negligible axial pressure gradients. The evaluation resulted in semi-empirical correlations which are based on a modification of a compressibility transformation theory expanded to include the latest hypersonic data up to a free stream Mach number of 8.0. Angle of attack effects on heat transfer were examined utilizing the mass transfer correlations developed in this study.

Several of the more important conclusions derived from this study are as follows:

1. It has been shown that heat transfer attenuation due to mass injection is heavily influenced by Mach number and, to a lesser degree, by wall temperature.

2. A semi-empirical technique was developed that predicts heat blockage and skin friction reduction due to mass injection as a function of Mach number and wall temperature. This method was based on an analytically derived compressibility transformation and an empirically derived (based on experimental data) viscous transformation. A critical blowaway parameter concept was employed to provide a more tractable set of correlations for engineering design.

3. The analytically derived compressibility transformation made use of the Eckert reference enthalpy concept with considerable success, while the viscous transformation development met with success aided by the suggestions of Spalding et al and the inclusion of recently acquired hypersonic flow data.

4. The resultant heat blockage and skin friction reduction correlations produced in this study were verified conclusively by comparison with data over a wide range of Mach number ($0 \leq M_e \leq 7$) and wall temperature ($1 \leq T_w/T_e \leq 8$). The effects of injectant molecular weight were adequately accounted for by a specific heat ratio ($C_{p_{inj}}/C_{p_{air}}$) factored into the blowing parameter. The recommended correlations for C_f/C_{f_o} and

St/St_o are expressed as Eqs. (71) and (72) where the blowing parameters are defined by Eqs. (66) and (67), respectively. The exponent ω and the parameter b_{cr} are determined from Eqs. (58) and (68), respectively.

5. The use of the Eckert reference enthalpy concept and Colburn's analogy resulted in satisfactory prediction of the zero injection STREET-G heat transfer data.

6. Angle of attack heat transfer was satisfactorily predicted (when compared with STREET-G data) by the GE-RESD 3-D Viscous Code which utilized the heat blockage and skin friction reduction correlations developed in this study.

APPENDIX

DERIVATION OF THE CROCCO TEMPERATURE (ENTHALPY) - VELOCITY RELATIONSHIP

Consider a steady, two-dimensional, compressible boundary layer where the equations of momentum and energy can be expressed as

$$\rho\left(u\frac{\partial u}{\partial x} + v\frac{\partial u}{\partial y}\right) = -\frac{\partial P}{\partial x} + \frac{\partial}{\partial y}\left(\mu\frac{\partial u}{\partial y}\right) \tag{A-1}$$

and

$$\rho\left(u\frac{\partial h}{\partial x} + v\frac{\partial h}{\partial y}\right) = u\frac{\partial P}{\partial x} + \mu\left(\frac{\partial u}{\partial y}\right)^2 + \frac{\partial}{\partial y}\left(k\frac{\partial T}{\partial y}\right) \tag{A-2}$$

The thermal conductivity can be expressed as

$$k = u C_p / Pr,$$

such that

$$k\frac{\partial T}{\partial y} = \frac{\mu C_p}{P_r}\frac{\partial T}{\partial y} \tag{A-3}$$

and $h = h(p, T)$

Differentiating the above term, one has

$$dh = \left(\frac{\partial h}{\partial T}\right)_p dT + \left(\frac{\partial h}{\partial p}\right)_T dP \tag{A-4}$$

where

$$\left(\partial h/\partial T\right)_p = C_p \tag{A-5}$$

Since $h = f(x, y)$, then

$$dh = \frac{\partial h}{\partial x}dx + \frac{\partial h}{\partial y}dy \tag{A-6}$$

If one equates Equations (A-4) and (A-6) and expands the total derivatives dT and dP, there results

$$\frac{\partial h}{\partial x} dx + \frac{\partial h}{\partial y} dy = C_p \left[\frac{\partial T}{\partial x} dx + \frac{\partial T}{\partial y} dy \right] + \left(\frac{\partial h}{\partial p} \right)_T \left(\frac{\partial P}{\partial x} dx + \frac{\partial P}{\partial y} dy \right) \quad \text{(A-7)}$$

Considering the enthalpy dependence on the coordinates, one has

$$\frac{\partial h}{\partial y} = \left(\frac{\partial h}{\partial T} \right)_p \frac{\partial T}{\partial y} + \left(\frac{\partial h}{\partial p} \right)_T \frac{\partial P}{\partial y} = C_p \frac{\partial T}{\partial y} + \left(\frac{\partial h}{\partial p} \right)_T \frac{\partial P}{\partial y} \quad \text{(A-8)}$$

and

$$\frac{\partial h}{\partial x} = C_p \frac{\partial T}{\partial x} + \left(\frac{\partial h}{\partial P} \right)_T \frac{\partial P}{\partial x} \quad \text{(A-9)}$$

However, from the boundary layer assumptions, $\partial P/\partial y \simeq 0$; hence,

$$\frac{\partial h}{\partial y} = C_p \frac{\partial T}{\partial y} \quad \text{(A-10)}$$

where it is understood that $\left(\frac{\partial h}{\partial p} \right)_T \neq 0 \left[\frac{1}{\partial P/\partial y} \right]$ (A-11)

If Equation (A-11) is satisfied, Equations (A-3) and (A-10) yield

$$k \frac{\partial T}{\partial y} = \frac{\mu}{Pr} C_p \frac{\partial T}{\partial y} = \frac{\mu}{Pr} \frac{\partial h}{\partial y} \quad \text{(A-12)}$$

Thus, the last term on the RHS of Equation (A-2) becomes

$$\frac{\partial}{\partial y} \left(k \frac{\partial T}{\partial y} \right) = \frac{\partial}{\partial y} \left(\frac{\mu}{Pr} \frac{\partial h}{\partial y} \right) \quad \text{(A-13)}$$

Multiplying Equation (A-1) by u and rewriting Equation (A-2) using the definition $Pr = \mu C_p/k$ and $h = C_pT$ and finally adding the resulting two equations, one has

$$\left(\rho u \frac{\partial}{\partial x} + v \frac{\partial}{\partial y} \right) \left(h + \frac{u^2}{2} \right) = \frac{\partial}{\partial y} \left(\frac{\mu}{Pr} \frac{\partial h}{\partial y} \right) + u \frac{\partial}{\partial y} \left(\mu \frac{\partial u}{\partial y} \right) + \mu \left(\frac{\partial u}{\partial y} \right)^2 \quad \text{(A-14)}$$

Noting the relationship

$$u\frac{\partial}{\partial y}\left(\mu\frac{\partial u}{\partial y}\right) + \mu\left(\frac{\partial u}{\partial y}\right)^2 = \frac{\partial}{\partial y}\left[u\frac{\partial}{\partial y}\left(\frac{u^2}{2}\right)\right]$$

and unit Prandtl number, Eq. (A-14) reduces to

$$\left(\rho u\frac{\partial}{\partial x} + \rho v\frac{\partial}{\partial y}\right)\left(h + \frac{u^2}{2}\right) = \frac{\partial}{\partial y}\left[\frac{\partial}{\partial y}\left(h + \frac{u^2}{2}\right)\right] \qquad \text{(A-15)}$$

which has the solution

$$h + \frac{u^2}{2} = \text{constant}$$

The constant can be evaluated using the wall condition $u = 0$, such that

$$h_w = \text{constant}$$

and we can write

$$h = h_w - \frac{u^2}{2} \qquad \text{(A-16)}$$

The enthalpy gradient at the wall becomes

$$\left(\frac{\partial h}{\partial y}\right)_w = \left[-u\frac{\partial u}{\partial y}\right]_w = 0$$

Using Eq. (A-10), we can write

$$\left(\frac{\partial T}{\partial y}\right)_w = 0 \qquad \text{and} \qquad q_w = -k\left(\frac{\partial T}{\partial y}\right)_w = 0$$

which implies an adiabatic wall condition. Thus, the arbitrary constant becomes

$h_w = h_{aw}$, and Eq. (A-16) is written as

$$h = h_w - \frac{u^2}{2} \qquad \text{(A-17)}$$

It should be noted that Eq. (A-17) was developed without restricting the pressure gradient to zero. Moreover, an examination of Eq. (A-9) indicates that for a non-zero pressure gradient, the temperature is not necessarily constant along the surface even though the enthalpy must be constant along the surface. On the other hand, if the temperatures are fairly low, the function $(\partial h/\partial p)_T$ will be essentially zero such that from Eq. (A-9), regardless of the pressure gradient, the surface temperature must also be constant. Now at high temperatures, the corresponding surface condition does not have to be constant for non-zero pressure gradients but must be constant for zero pressure gradient. Finally, it should be kept in mind that Eq. (A-17) is valid only for unit Prandtl number.

For generality, Eq. (A-1) can be multiplied by a constant, say, c, which yields

$$\left(\rho u \frac{\partial}{\partial x} + \rho v \frac{\partial}{\partial y}\right) (cu) = \frac{\partial}{\partial y}\left(\mu \frac{\partial}{\partial y} (cu)\right) - c \frac{\partial P}{\partial x} \qquad \text{(A-18)}$$

Combining Eqs. (A-18) and (A-15) there results

$$\left(\rho u \frac{\partial}{\partial x} + \rho v \frac{\partial}{\partial y}\right)\left(h + cu + \frac{u^2}{2}\right) = \frac{\partial}{\partial y}\left[\mu \frac{\partial}{\partial y}\left(h + cu + \frac{u^2}{2}\right)\right] - c \frac{\partial P}{\partial x} \qquad \text{(A-19)}$$

which, for zero pressure gradient conditions, reduces to

$$\left(\rho u \frac{\partial}{\partial x} + \rho v \frac{\partial}{\partial y}\right)\left(h + cu + \frac{u^2}{2}\right) = \frac{\partial}{\partial y}\left[\mu \frac{\partial}{\partial y}\left(h + cu + \frac{u^2}{2}\right)\right] \qquad \text{(A-20)}$$

As before, one possible solution to the above is

$$h + cu + \frac{u^2}{2} = \text{constant}$$

where at the wall, $u = 0$, one has

$$h + cu + \frac{u^2}{2} = h_w$$

and $(\partial h/\partial y)_w = -c\,(\partial u/\partial y)_w \neq 0$. Employing the conditions at the edge of the viscous layer, there results

$$c = \frac{h_w - h_e - \frac{u_e^2}{2}}{u_e} \qquad \text{(A-21)}$$

Inasmuch as the derivation of Eq. (A-21) made use of Eq. (A-15), the same conditions apply to Eq. (A-21); namely, that Pr = unity. Moreover, if Pr = unity, the recovery factor, defined as

$$r = \frac{h_{aw} - h_e}{H_e - h_e}$$

must also be unity. Hence

$$h_e + \frac{u_e^2}{2} = h_{aw} = H_e \qquad \text{for Pr = unity}$$

and

$$c = \frac{h_w - h_{aw}}{u_e} \qquad \text{(A-22)}$$

The static enthalpy can then be expressed as

$$h = h_w - cu - \frac{u^2}{2} \quad h_w - \frac{(h_w - h_{aw})}{u_e} u - \frac{u^2}{2} \qquad \text{(A-23)}$$

and, noting the definition $h_{aw} - h_e \quad \frac{u_e^2}{2}$ for unit Prandtl number, the static enthalpy distribution is written as

$$h = h_w + (h_{aw} - h_w)\frac{u}{u_e} - (h_{aw} - h_e)\left(\frac{u}{u_e}\right)^2 \qquad \text{(A-24)}$$

In terms of total enthalpy, the above reduces to the familiar classic linear Crocco temperature-velocity relationship, namely

$$\frac{H - h_w}{H_e - h_w} \quad \frac{u}{u_e} \qquad \text{(A-25)}$$

It should be noted that the wall enthalpy must be constant, and, since the pressure gradient is zero, it is seen from Eq. (A-9) that the wall temperature must also be constant. Thus, the conditions that must be satisfied for Eq. (A-24) or (A-25) to be valid are:

(i) unit Prandtl number

(ii) constant pressure (zero pressure gradient)

(iii) constant surface temperature

In Eq. (A-25) one notes a linear relationship between H and u which implies the existence of a local Reynolds analogy. Moreover, the boundary conditions used to obtain Eq. (A-25) also imply that the relationship is valid across the entire boundary layer. It is also noted that mass transfer is not an explicit function in Eqs. (A-1) and (A-2), and hence Eq. (A-25) as well, and would enter only through the boundary conditions.

As a consequence of the kinetic energy contribution in high speed flow, Eq. (A-14) can be re-expressed as

$$\rho u \frac{\partial h}{\partial x} + \rho v \frac{\partial h}{\partial y} = u \frac{\partial}{\partial y}\left(\mu \frac{\partial u}{\partial y}\right) - \rho u^2 \frac{\partial u}{\partial x} - \rho v u \frac{\partial u}{\partial y} + \frac{\partial}{\partial y}\left(\frac{k}{C_p} \frac{\partial h}{\partial y}\right) + \mu \left(\frac{\partial u}{\partial y}\right)^2$$

Using the definition of total enthalpy, $H = h + \frac{u^2}{2}$, the above becomes

$$\rho u \frac{\partial H}{\partial x} + \rho v \frac{\partial H}{\partial y} = \frac{\partial}{\partial y}\left\{\frac{k}{C_p} \frac{\partial}{\partial y}\left[H + (Pr - 1) \frac{u^2}{2}\right]\right\} \qquad \text{(A-26)}$$

For gases, the Prandtl number is close to unity which is a basic condition for the existence of similarity between the hydrodynamic and thermal profiles (i.e., Eq. (A-25)). However, departures from similarity, which are a consequence of the kinetic energy term $(Pr-1)\frac{u^2}{2}$, can be accounted for by considering the work of Kutateladze and Leont'ev. In their work, the authors suggested a relationship of the form

$$\frac{T^{+} - T_w}{T_{aw} - T_w} = \xi \left(\frac{y}{\delta}\right) \frac{u}{u_e} \qquad \text{(A-27)}$$

where

$$T^{+} \equiv T + r\left(\frac{y}{\delta}\right) \frac{u^2}{2g\, J\, C_p} \qquad \text{(A-28)}$$

The parameters ξ and r (recovery factor) are both functions of the coordinate and depend, in general, on the pressure gradient, the temperature difference imposed, and the magnitude of mass transfer. Spalding noted that one superfluous function had been introduced in the definitions of Eqs. (A-27) and (A-28). If one defines the recovery value as a constant, then Eq. (A-27) together with Eq. (A-28), defines the parameter $\xi\ (\frac{y}{\delta})$. If, on the other hand, r is allowed to vary with ξ, then the definitions are incomplete.

By considering the recovery factor to be constant, Eq. (A-27) can be re-written in terms of the static and total temperature (Crocco variables) as

$$\frac{T}{T_e} = \frac{T_w}{T_e} + \xi\left(\frac{T_{aw} - T_w}{T_e}\right)\frac{u}{u_e} + \left(1 - \frac{T_{aw}}{T_e}\right)\left(\frac{u}{u_e}\right)^2$$

and

$$\frac{T^o - T_w}{T_e^o - T_w} = \xi\left(\frac{T_{aw} - T_w}{T_e^o - T_w}\right)\frac{u}{u_e} + \left(\frac{T_e^o - T_{aw}}{T_e^o - T_w}\right)\left(\frac{u}{u_e}\right)^2$$

If we define

$$\beta = \frac{T_{aw} - T_w}{T_e^o - T_w}$$

then the total temperature becomes (Crocco variables)

$$\frac{T^o - T_w}{T_e^o - T_w} = \xi\beta\,\frac{u}{u_e} + (1 - \beta)\left(\frac{u}{u_e}\right)^2$$

Equation (A-32) is recognized as that obtained empirically by Danberg (when ξ is unity).

In the above, it is noted that for adiabatic wall conditions ($T_{aw} = T_w$), β is zero and one obtains the parabolic distribution that is characteristic of nozzle wall data (for Pr $\neq$ unity). On the other hand, when considering a unit Prandtl number condition where $T_{aw} = T_e^o$ and β is unity, Eq. (A-32) reduces to

$$\frac{T^o - T_w}{T_e^o - T_w} = \xi \frac{u}{u_e} \qquad \text{(A-33)}$$

which is representative of the classic linear Crocco relation (for ξ = unity). Thus the important contribution of Kutateladze and Leont'ev is the parameter $\xi = \xi\left(\frac{y}{\delta}\right)$.

REFERENCES

1. Martellucci, A., Hahn, J., and Laganelli, A., "Effect of Mass Addition and Angle of Attack on the Turbulent Boundary Layer Characteristics of a Slender Cone", Vol's. I, II and III, SAMSO TR-73-147, also GE-RESD Document No. 73SD210 and AD911347L, April 1973.

2. Martellucci, A., Laganelli, A. L., and Hahn, J., "Hypersonic Turbulent Boundary Layer Characteristics with Mass Transfer", Vol's I, II and III, SAMSO TR-74-112, also GE-RESD Document No. 74SD2039, April 1974.

3. Danberg, J. E., "Characteristics of the Turbulent Boundary Layer with Heat and Mass Transfer at M = 6.7", NOLTR-64-99 (Naval Ordnance Laboratory), Oct. 1964.

4. Bertram, M. H., and Neal, L., "Recent Experiments in Hypersonic Turbulent Boundary Layers, NASA TMX-56335 also N65-22565, May 1965.

5. Hopkins, E. J., Rubesin, M. W., Inouye, M., Keener, E. R., Mateer, G. L., and Polek, T. E., "Summary and Correlations of Skin-Friction and Heat Transfer Data for a Hypersonic Turbulent Boundary Layer on Simple Shapes", NASA TN D-5089, June 1969.

6. Bushnell, D. M., Johnson, C. B., Harvey, W. D., and Feller, W. J., "Comparison of Prediction Methods and Studies of Relaxation in Hypersonic Turbulent Nozzle-Wall Boundary Layers", NASA TN D-5433, Sept. 1969.

7. Fiore, R. W., "Turbulent Boundary Layer Measurements at Hypersonic Mach Numbers", ARL 70-01666 (Aerospace Research Laboratories), Aug. 1970.

8. Beckworth, J. E., Harvey, W. D., and Clark, F. L., "Comparisons of Turbulent Boundary Layer Measurements at Mach Number 19.5 with Theory and an Assessment of Probe Errors", NASA TND-6192, June 1971.

9. Gates, D. F., "Measurements of Upstream History Effects in Compressible Turbulent Boundary Layers", NOLTR-73-152 (Naval Ordnance Laboratories), July 1973.

10. Demetriades, A. and Laderman, A. J., "Effect of Mass Addition and Angle of Attack on the Hypersonic Boundary Layer Turbulence Over a Slender Cone", Philco Ford Pub. No. U-6047, Also SAMSO TR-73-397, Sept. 1973.

11. Reda, D.C., "Compressible Turbulent Skin Friction on Rough and Rough/Wavy Walls in Adiabatic Flow", NOLTR-74-34 (Naval Ordnance Laboratories), Feb. 1974.

12. Kutateladze, S. S. and Leont'ev, A. J., Turbulent Boundary Layers in Compressible Gases, Academic Press, New York, 1964.

13. Rie, H., "The GE-RESD Equilibrium Non-Similar Boundary Layer Program (ENSBL)", GE-RESD TIS 71SD212, February 1971.

14. Martellucci, A., Maguire, B. L., and Neff, B., "Analysis of Flight Test Transition and Turbulent Heating Data: Part 1 - Boundary Layer Transition Results", NASA CR 129045, Nov. 1972.

15. Smith, A. M. O., and Cebeci, T., "Numerical Solution of the Turbulent Boundary Layer Equations", Douglas Aircraft Division Report DAC 3375 (ASTIA AD 656430), May 1967.

16. Johnson, C. B., and Bushnell, D. M., "Power-Law-Velocity-Profile-Exponent Variations with Reynolds Number, Wall Cooling, and Mach Number in a Turbulent Boundary Layer", NASA TN D-5753, April 1970.

17. Hopkins, E. J., Keener, E.R., Polek, T. E., and Dwyer, H.A., "Hypersonic Turbulent Skin-Friction and Boundary Layer Profiles on Nonadiabatic Flat Plates," AIAA Journal, Vol. 10, No. 1, January 1972, pp. 40-48.

18. Laganelli, A. L. and Martellucci, A., "Experimental Surface and Boundary Layer Measurements in a Hypersonic Boundary Layer with Non-Uniform Blowing", Presented at AIAA/ASME 1974 Thermophysics and Heat Transfer Conf., Boston, Mass., July 1974 Paper No. 74-699.

19. Martellucci, A., "Effects of Mass Transfer on Hypersonic Turbulent Boundary Layer Properties", AIAA Jour. Vol. 10, No. 2, Feb. 1972, pp. 181-187.

20. Martellucci, A., and Rie, H., "Effects of Mass Addition on Viscous Flow Parameters", GE TIS 71SD205, January, 1971, also SAMSO TR-71-60.

21. Studerus, C. J., Dienna, E.A., "Viscous Interaction Zero Angle of Attack Drag (VIZAAD) Program", GE TIS 64SD292, November 1964.

22. Timmer, H.G., Arne, C.L., Stokes, T.R., Jr., Tang, H.H., "Ablation Aerodynamics for Slender Re-entry Bodies, Vol. I Theoretical Analyses and Results", McDonnell-Douglas Astronautics Co., AFFDL-TR-70-27, March 1970.

23. Grabow, R.M., "Hypersonic Drag Coefficients for Cones with Mass Transfer and Bluntness Effects", Philco-Ford Report No. METN 112 January 1967.

24. Rubesin, M.W., "An Analytical Estimation of the Effect of Transpiration Cooling on the Heat-Transfer and Skin-Friction Characteristics of a Compressible Turbulent Boundary Layer", NACA TN 3341, December 1954.

25. Ness, N., "Distributed Injection of Air into a High-Temperature, Equilibrium Air, Turbulent Boundary Layer", GE MSVD AOTM #141, August 1959.

26. Dorrance, W.H., and Dore, F.J., "The Effect of Mass Transfer on the Compressible Turbulent Boundary-Layer Skin Friction and Heat Transfer", JAS, June 1954.

27. Pappas, C.C., "Effect on Injection of Foreign Gases on the Skin Friction and Heat Transfer of the Turbulent Boundary Layer", IAS Report #59-78, January 1959.

28. Walker, G.K. and Schumann, B.A., "A Discussion of Ness's Analysis for a Turbulent Boundary Layer with Mass Addition", GE-MSVD TIS #61SD49, April 1961.

29. Tracy, R.R., "Hypersonic Flow Over a Yawed Circular Cone", GALCIT Memo No. 69, August 1963, California Institute of Technology, Pasadena, California.

30. Rainbird, W.J., "Turbulent Boundary Layer Growth and Separation on a Yawed Cone", AIAA Journal, Vol. 6, No. 12, December 1968, pp. 2410-2416.

31. Copper, J.A., Shaw, W.J., Jr., "Turbulent Boundary Layer Thicknesses on Yawed Cones," AIAA Journal, Vol. 8, No. 6, June 1970, pp. 1138-1140.

32. Bloom, M.H. and Martellucci, A., "A Method for Calculating Turbulent Boundary Layer Properties in High Speed Flow", G.A.S.L. Technical Report 27A, March 1957.

33. Persh, J. and Lee, R., "Tabulation of Compressible Turbulent Boundary Layer Parameters", NAVORD Report 2482, 1956.

34. Schlichting, H., Boundary Layer Theory, McGraw-Hill Book Co., New York 6th Ed., 1968.

35. Kent, R., Martellucci, A., and George, F.C., "Static Force and Pressure Measurements on a Slender Porous Cone with Gas Injection", Data Memo ALDM 69-75, General Electric Co., February 1969.

36. Matting, F.W., Chapman, D.R., Nyholm, J.R., and Thomas, A. ` "Turbulent Skin Friction at High Mach Numbers and Reynolds Numbers in Air a.. 'elium", NASA TR-R-82, 1960.

37. Sterrett, J.R. and Emery, J.C., "Extension of Boundary Layer Separation Criteria to a Mach Number of 6.5 by Utilizing Flat Plates with Forward-Facing Steps", NASA TND-618, December 1960.

38. Adcock, J.B., Peterson, J.B., Jr., and McRee, D.I., "Experimental Investigation of a Turbulent Boundary Layer at Mach 6, High Reynolds Numbers and Zero Heat Transfer", NASA TN-D-2907, July 1965.

39. Walker, G. K., "Turbulent Boundary Layers with Mass Addition", G. E. Document No. TFM-8151-021, November 1963.

40. Lees, L., "Combustion and Propulsion, Third AGARD Colloquim", pp 451-498. Pergamon Press, New York, 1959.

41. Bartle, E. R., and Leadon, B. M., "The Effectiveness of a Universal Measure of Mass Transfer Cooling for a Turbulent Boundary Layer", Proceedings of the 1962 Heat Transfer and Fluid Mechanics Institute Stanford University Press, June 1962.

42. Pappas, C. C., and Okuno, A. F., "Measurement of Heat Transfer and Recovery Factor of a Compressible Turbulent Boundary Layer on a Sharp Cone with Foreign Gas Injection", NASA TN D-2230, April 1964.

43. Spalding, D. B., Auslander, D. M. and Sundaram, T. R., "The Calculation of Heat and Mass Transfer Through the Turbulent Boundary Layer on a Flat Plate at High Mach Numbers, with and without Chemical Reaction," AGARD Combustion and Propulsion Colloquium, London, 1963.

44. Leadon, B. M., and Scott, C. S., "Transpiration Experiments in a Turbulent Boundary Layer at M = 3", Journal of the Aeronautical Sciences, Vol, 23, No. 8, August, 1956.

45. Tewfik, O. E., Jurewicz, L. S., and Eckert, E. R. G., "Measurements of Heat Transfer from a Cylinder with Air Injection into a Turbulent Boundary Layer" ASME Paper No. 63-HT-45, August 1963.

46. Danberg, J. E., "Characteristics of the Turbulent Boundary Layer with Heat and Mass Transfer: Data Tabulation", NOLTR 67-6 (Aerodynamics Research Report No. 280), January 1967, Naval Ordnance Lab., White Oak, Maryland.

47. Laganelli, A. L., Kyriss, C. L., and Martellucci, A., "An Experimental Investigation of Mass Transfer Effects on a Porous Blunt Body", GE-RESD Document No. 74SD208, April 1974.

48. Dershin, H., Leonard, C. A., and Gallaher, W. H., "Direct Measurement of Skin Friction on a Porous Flat Plate with Mass Injection", AIAA Journal, Vol. 5, No. 11, 1967.

49. Kendall, R. M., Rubesin, M. W., Dahm, T. J., Mendenhall, M. R., "Mass Momentum, and Heat Transfer Within a Turbulent Boundary Layer with Foreign Gas Mass Transfer at the Surface", Vidya Report No. 111, February 1964, ASTIA AD 619209.

50. Goodwin, B. M., "The Transpired Turbulent Boundary Layer with Zero Pressure Gradient", MIT Doctor of Science Thesis, May 1961.

51. Pappas, C. C., Okuno, A. F., "Measurement of Skin Friction of the Compressible Turbulent Boundary Layer on a Cone With Foreign Gas Injection", Journal of the Aero/Space Sciences, Volume 27, No. 5, May 1960.

52. Tendeland, Thorval, and Okuno, A. F., "The Effect of Fluid Injection on the Compressible Turbulent Boundary Layer - The Effect on Skin Friction of Air Injected into the Boundary Layer of a Cone at M - 2.7," NACA RM A56D05, 1956.

53. Fogaroli, R. P., and Saydah, A. R., "Turbulent Heat Transfer and Skin-Friction Measurements on a Porous Cone with Air Injection at High Mach Numbers", AIAA J., Vol. 4, No. 6, June 1966.

54. Laganelli, A. L., "Analysis of Flight Test Transition and Turbulent Heating Data, Part II - Turbulent Heating Results", NASA CR 130251, November 1972 (also GE-RESD Document No. 72SD229).

55. Kutateladze, S. S., and Leont'ev, A. I., "Heat-Mass Transfer and Friction in a Turbulent Boundary Layer", NASA TT F-805, September 1974.

56. Hecht, A., and Nestler, D., "The General Electric Three Dimensional Boundary Layer Computer Program" GE-RESD Document (to be published).

47. Laganelli, A. L., Kyriss, C. L., and Martellucci, A., "An Experimental Investigation of Mass Transfer Effects on a Porous Blunt Body", GE-RESD Document No. 74SD208, April 1974.

48. Dershin, H., Leonard, C. A., and Gallaher, W. H., "Direct Measurement of Skin Friction on a Porous Flat Plate with Mass Injection", AIAA Journal, Vol. 5, No. 11, 1967.

49. Kendall, R. M., Rubesin, M. W., Dahm, T. J., Mendenhall, M. R., "Mass Momentum, and Heat Transfer Within a Turbulent Boundary Layer with Foreign Gas Mass Transfer at the Surface", Vidya Report No. 111, February 1964, ASTIA AD 619209.

50. Goodwin, B. M., "The Transpired Turbulent Boundary Layer with Zero Pressure Gradient", MIT Doctor of Science Thesis, May 1961.

51. Pappas, C. C., Okuno, A. F., "Measurement of Skin Friction of the Compressible Turbulent Boundary Layer on a Cone With Foreign Gas Injection", Journal of the Aero/Space Sciences, Volume 27, No. 5, May 1960.

52. Tendeland, Thorval, and Okuno, A. F., "The Effect of Fluid Injection on the Compressible Turbulent Boundary Layer - The Effect on Skin Friction of Air Injected into the Boundary Layer of a Cone at M - 2.7," NACA RM A56D05, 1956.

53. Fogaroli, R. P., and Saydah, A. R., "Turbulent Heat Transfer and Skin-Friction Measurements on a Porous Cone with Air Injection at High Mach Numbers", AIAA J., Vol. 4, No. 6, June 1966.

54. Laganelli, A. L., "Analysis of Flight Test Transition and Turbulent Heating Data, Part II - Turbulent Heating Results", NASA CR 130251, November 1972 (also GE-RESD Document No. 72SD229).

55. Kutateladze, S. S., and Leont'ev, A. I., "Heat-Mass Transfer and Friction in a Turbulent Boundary Layer", NASA TT F-805, September 1974.

56. Hecht, A., and Nestler, D., "The General Electric Three Dimensional Boundary Layer Computer Program" GE-RESD Document (to be published).

Table II. Hot Wall Profile Data Test Summary of Reference 2.

$X 10^{-6}$ R_{e_∞}/FT	(Deg.) θ	Inj. Gas	Injectant Distribution				Molecular Wt. Distribution				Surface Group No.	Profile Data Group No. — Axial Station (Inches From Apex)										
			λ_{w_1}	λ_{w_2}	λ_{w_3}	λ_{w_4}	M_{i_1}	M_{i_2}	M_{i_3}	M_{i_4}		28	29	32	33	36	39	40	44	48	52	53.5
3.82	0	-	0	0	0	0	-	-	-	-	83	-	82	-	-	-	-	-	-	-	-	-
	0	Freon	.0005	.0005	.0005	.0005	120.9	→	→	→	109	-	110	-	-	-	111	-	-	-	112	-
	-3°	Freon	.0005	→	→	→	120.9	→	→	→	116	-	113	-	-	-	114	-	-	-	115	-
	-3°	Freon	.0005	→	→	→	120.9	→	→	→	108	-	105	-	-	-	106	-	-	-	107	-
	0	Air/He	.0005	→	→	→	28.9	28.9	4	28.9	109	-	-	-	96	-	97	-	-	$^{45}_{98}$	99	-
	0	Air/He	.0005	.0005	.0015	.0005	28.9	28.9	4	28.9	101	-	-	-	-	-	104	-	-	$^{45}_{103}$	102	-
	0	Air	.0015	.0015	.0030	.0030	28.9	→	→	→	95	-	-	-	92	-	93	-	-	-	94	-
	0	Air	.0015	.0015	0	0	28.9	28.9	-	-	88	-	-	-	91	-	90	-	-	-	89	-
	0	Air	0	.0015	0	0	-	28.9	-	-	87	-	-	-	84	-	85	-	-	-	86	-
1.3	0	-	0	0	0	0	-	-	-	-	61	-	65	-	-	-	-	64	-	63	-	62
	0	-	0	0	0	0	-	-	-	-	132	74	-	75	-	76	-	77	78	79	-	-
	0	-	0	0	0	6	-	-	-	-	138	121	-	122	-	123	-	124	-	125	-	-
	0	Air	.0015	→	→	→	28.9	→	→	→	66	73	-	72	-	71	-	70	69	68	-	67
	0	Air	.0015	→	→	→	28.9	→	→	→		129	-	128	-	127	-	126	-	-	-	-
	0	He	.0015	→	→	→	4	→	→	→	133/137	-	-	136	-	-	-	135	-	134	-	-
	0	Freon	.0015	→	→	→	120.9	→	→	→	120	-	-	117	-	-	-	118	-	119	-	-
	0	Air	.0030	→	→	→	28.9	→	→	→	81	-	-	130	-	-	-	131	-	80	-	-
0.39	0	-	0	0	0	0	-	-	-	-	139	-	-	-	-	-	140	-	-	-	-	-
	0	Air	.0010	→	→	→	28.9	→	→	→	60	-	-	-	-	-	59	-	-	-	-	-
	0	Air	.0010	→	→	→	28.9	→	→	→	142	-	-	-	-	-	141	-	-	-	-	-

Summary of Free Stream Conditions									
Re_∞/FT $X 10^{-6}$	M_∞	P_0 (psia)	T_0 (°R)	P_∞ (psia)	T_∞ (°R)	ρ_∞ LBM/Ft^3 X 10^{-3}	μ_∞ LBF-Sec/Ft^2 X 10^{-8}	u_∞ Ft/Sec	$(\rho u)_\infty$ LBM/Ft^2 Sec
3.82	7.90	854.0	1350.6	.0949	100.2	2.556	8.061	3877.4	9.909
1.288	7.87	249.6	1236.5	.0284	92.36	.8304	7.432	3708.9	3.08
0.389	7.80	69.82	1194.2	.0081	90.69	.2506	7.298	3642.5	0.913

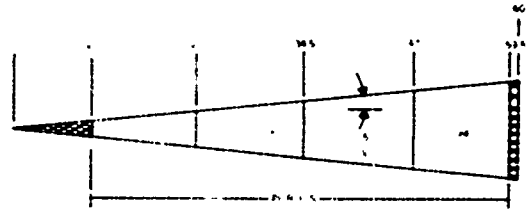

Table III. Cold Wall Heat Transfer Test Summary of Reference 1.

r_n (in)	Re_∞/ft x 10^{-6}	λ_∞	α (Deg.)	Data Group Number						
				Leeward ← $\alpha < 0$ → ϕ				← $\alpha > 0$ → Windward		
				0	30	60	90	120	150	180
0	3.7	0	0	1, 129						
			0	136						
			3	130	61	30	19	31, 32	62	133
			5	131	60	29	20	33	63	134
			10	132	59	28	21	34	64	135
		.0005	0	18 →						
		.0015	0	2, 14 →						
			3	13	55	37	22	38	56	15
			5	12	54	36	23	39	57	16
			10	11(B)	53	35	24	40	58	17
		.0030	0	3, 6						
			3	9	49	43	25	44	50	7
			5	10	48	42	26	45	51	8
			10	11(A)	47	41	27	46	52	4
		.0050	0	5 →						
0.1		0	0	65 →						
0.2		0	0	66 →						
0.3		0	0	67 →						
0	1.7	0	0	127 →						
0	0.36	0	0	128 →						

Table IV. Cold Wall Heat Transfer Test Summary of Reference 2.

$M_\infty = 7.9$
$\theta_C = 5°$
$r_N = 0$

$Re_\infty FT^{-1} \times 10^{-6}$	Inj. Gas	Injectant Distribution				Molecular Wt. Dist.				Angle-Of-Attack			
		λ_1	λ_2	λ_3	λ_4	1	2	3	4	0	± 3°	± 5°	± 10°
1.3	-	0	→	→	→	-	→	→	→	6*	7/5	8/4	9/3
1.3	Air	.0005	→	→	→	28.9	→	→	→	53	-	-	-
1.3	Air	.0015	→	→	→	28.9	→	→	→	52	-	-	-
1.3	Air	.0030	→	→	→	28.9	→	→	→	48	49/47	50/46	51/45
1.3	He	.0015	→	→	→	4	→	→	→	30	31/29	32/28	-
1.3	Freon	.0015	→	→	→	120.9	→	→	→	41	-	-	-
1.3	Air	.0015	.0015	.0030	.0030	28.9	→	→	→	43	44/42	-	-
3.7	Air	.0005	→	→	→	28.9	→	→	→	20	21/19	-	-
3.7	He	.0005	→	→	→	4	→	→	→	35	36/34	37/33	-
3.7	Freon	.0005	→	→	→	120.9	→	→	→	40	-/39	-/38	-
3.7	Air	.0015	.0015	.0030	.0030	28.9	→	→	→	11	12/2, 10	-	-
3.7	Air	.0015	.0015	0	0	28.9	28.9	-	-	14	15/13	-	-
3.7	Air	0	.0015	0	0	-	28.9	-	-	17	18/16	-	-
3.7	Air/Fr	.0005	→	→	→	28.9	28.9	120.9	28.9	26	27/25	-	-
3.7	Air/Fr	.0005	.0005	.0015	.0005	28.9	28.9	120.9	28.9	23	24/22	-	-
3.7	-	0	→	→	→	-	→	→	→	1	-	-	-
0.36	-	0	→	→	→	-	→	→	→	55	56/54	-	-
0.36	Air	.0010	→	→	→	28.9	→	→	→	58	-	-	-
0.36	Air	.0015	→	→	→	28.9	→	→	→	57	-	-	-

*Data Group No.

Table V. Velocity Power - Law Parameters

n	7	7	8	9	10
C	8.56	8.74	9.71	10.6	11.5
K(n)	0.0297	0.02884	0.02276	0.01852	0.0153
$K'(n)$	0.03712	0.03605	0.02781	0.02222	0.01878
MF	0.5227	0.5227	0.5203	0.51838	0.5168
ζ	0.0194	0.01885	0.01447	0.01152	0.009342

$$K'(n) = K(n)\ (3 + n)/(1 + n)$$

$$\zeta = MF\ K'(n)$$

Table VI. Definition of Data Symbols

Symbol	Source	Reference	M_e	T_w/T_e	Surface
	Heat Transfer				
◇	Fogaroli & Saydah	53	8.1	3.0-5.8	Cone
□	Martellucci et al	1	7.1	4.8	Cone
⊠	Martellucci et al	1	7.1	8.9	Cone
○	Danberg	46	6.7	4.1	Flat Plate
⊗	Danberg	46	6.7	5.2	Flat Plate
△	Pappas & Okuno	42	4.35	∠ 4	Cone
▽	Pappas & Okuno	42	3.67	3.3	Cone
◇	Bartle & Leadon	41	3.2	3.3	Flat Plate
○	Leadon & Scott	44	3.0	3.3	Flat Plate
◇	Bartle & Leadon	41	2.0	1.9	Flat Plate
☆	Pappas & Okuno	42	0.7	1.1	Cone
▯	Tewfik et al	45	0	1.0	Cylinder
	Skin Friction				
⏢	Pappas & Okuno	51	4.3	(4.4)	Cone
▽	Pappas & Okuno	51	3.21	(3.3)	Cone
⬭	Tendeland & Okuno	52	2.55	(1.0)	Cone
⬡	Dershin et al	48	3.18	(3.3)	Flat Plate
◺	Kendall et al	49	0	(1.0)	Flat Plate
◫	Goodwin	50	0	(1.0)	Flat Plate
◇	Pappas & Okuno	51	0.7	(1.1)	Cone

Open symbols denote AIR injection
Filled symbols denote HELIUM injection
Half-filled symbols denote FREON injection

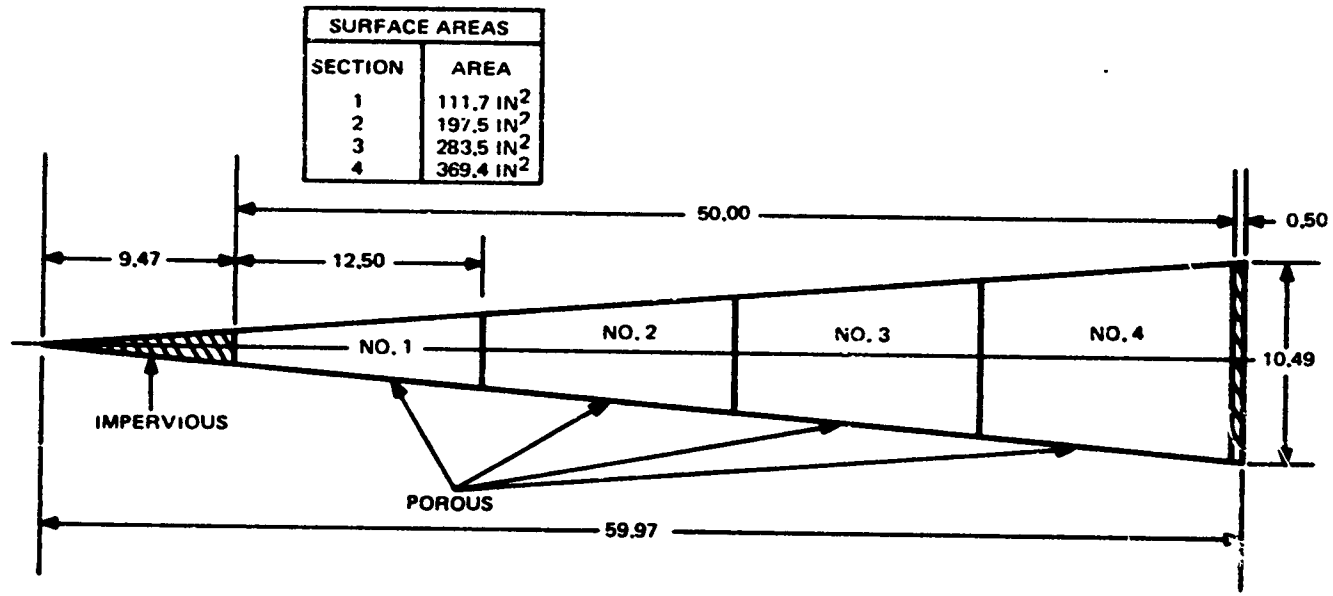

Figure 1. Model Schematic

	M_∞	Re_θ	T_W/T°_∞	Model
○	5.2	1.7×10^3–3.5×10^3	.56–.84	Flat plate
◇	6.4	6×10^3	.52	Flat plate
△	6.0	1.1×10^4	.38, .49	Hollow cylinder
◇	5.1	3.1×10^3–4.0×10^3	.72–.83	Flat plate
○	10.2	2.3×10^3	.28	Cone
△	3.67	9×10^4	.42	Parabolic, fineness ratio of 10
▷	5.75	3.8×10^4	.63	Hollow cylinder
▷	10.5	1.3×10^3	.3	Flat plate
▷	5,6,8	2×10^3–1.3×10^4	.4–.7	Hollow cylinder
◇	6.5	2.2×10^3–5.9×10^3	.3–.38	Flat plate

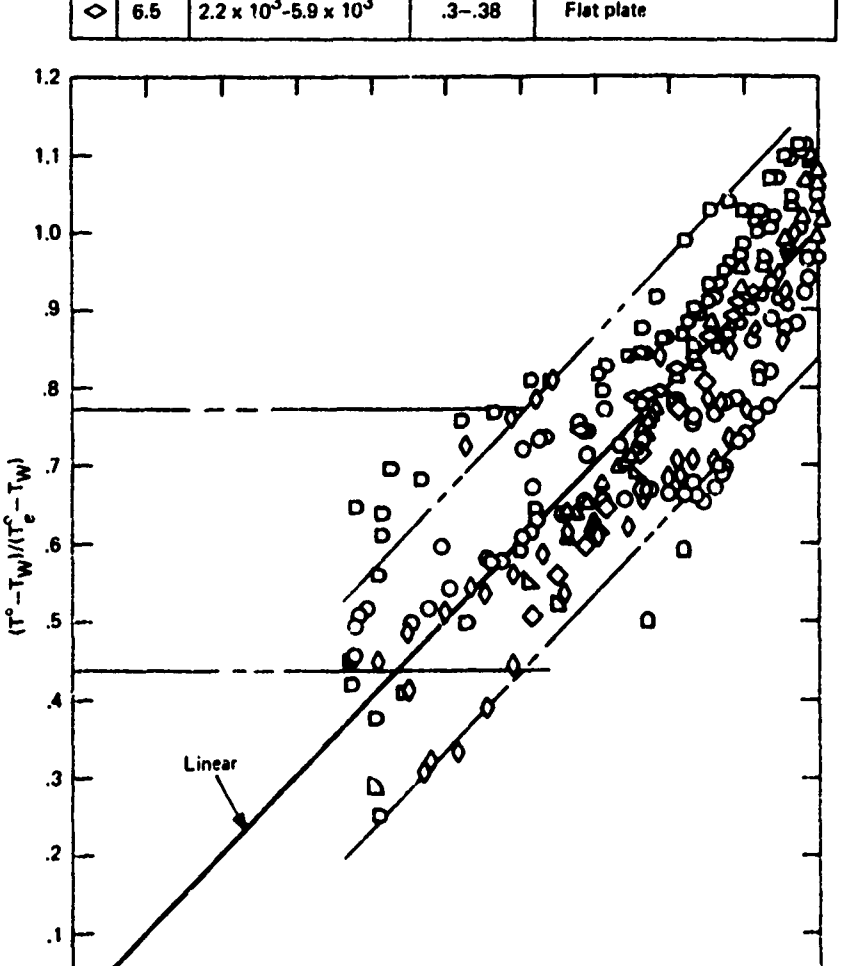

Figure 2. Total Temperature - Velocity for "Flat Plate" Flows $3.67 \lesssim M_\infty \lesssim 10.5$; $0.28 \lesssim T_W/T^0_\infty \lesssim 0.84$ (Ref. 6)

	M_∞	Re_9	T_w/T_∞°	MODEL
○	6	$1.9 \times 10^4 - 4.9 \times 10^4$	.63	Nozzle Wall
◇	11.5	1.6×10^4	.28	Nozzle Wall
▽	6.8	1.3×10^4	.5	Nozzle Wall
△	9.1	1.9×10^3	.48	Nozzle Wall
◇	5.1 – 8.2	$7.4 \times 10^3 - 1.26 \times 10^4$	.46 – .53	Nozzle Wall
□	4.7	6×10^3	.6	Nozzle Wall
◁	2.9	1.1×10^4	.77	Plate With Nozzle $\frac{dp}{dx}$
▽	≈14	$\approx 2 \times 10^3$	.2	Cone With Nozzle $\frac{dp}{dx}$
△	6.5	$2.1 \times 10^3 - 4.5 \times 10^3$	.31, .43	Nozzle Wall
◁	11.7	$2.6 \times 10^3 - 4.5 \times 10^3$	.27, .30	Nozzle Wall
□	8.2 – 8.9	$3.7 \times 10^3 - 9.4 \times 10^3$	.07 – .16	Nozzle Wall
◆	19,47	$3.4 \times 10^3 - 5.1 \times 10^3$	.17	Nozzle Wall
■	7.9	$1.1 \times 10^4 - 3.1 \times 10^4$	.44	Nozzle Wall

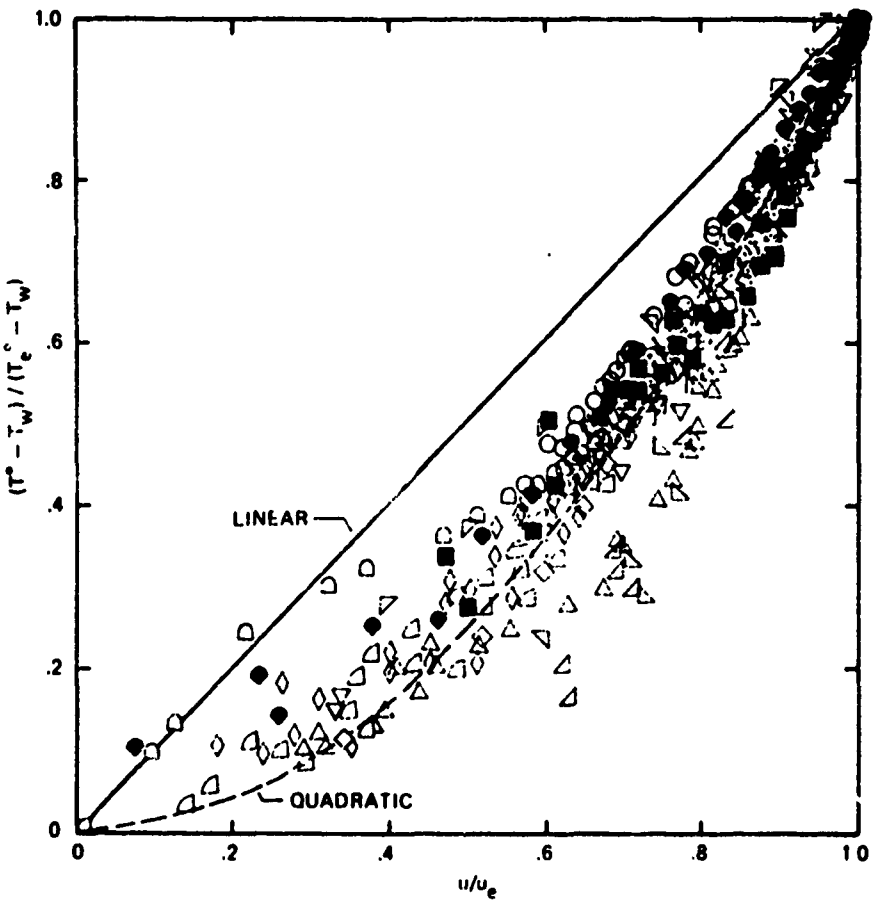

Figure 3. Total Temperature-Velocity Data for "Nozzle Wall" Flows $3 \leq M_\infty \leq 19$; $0.1 \leq T_w/T^0_\infty \leq 0.8$ (Ref. 6)

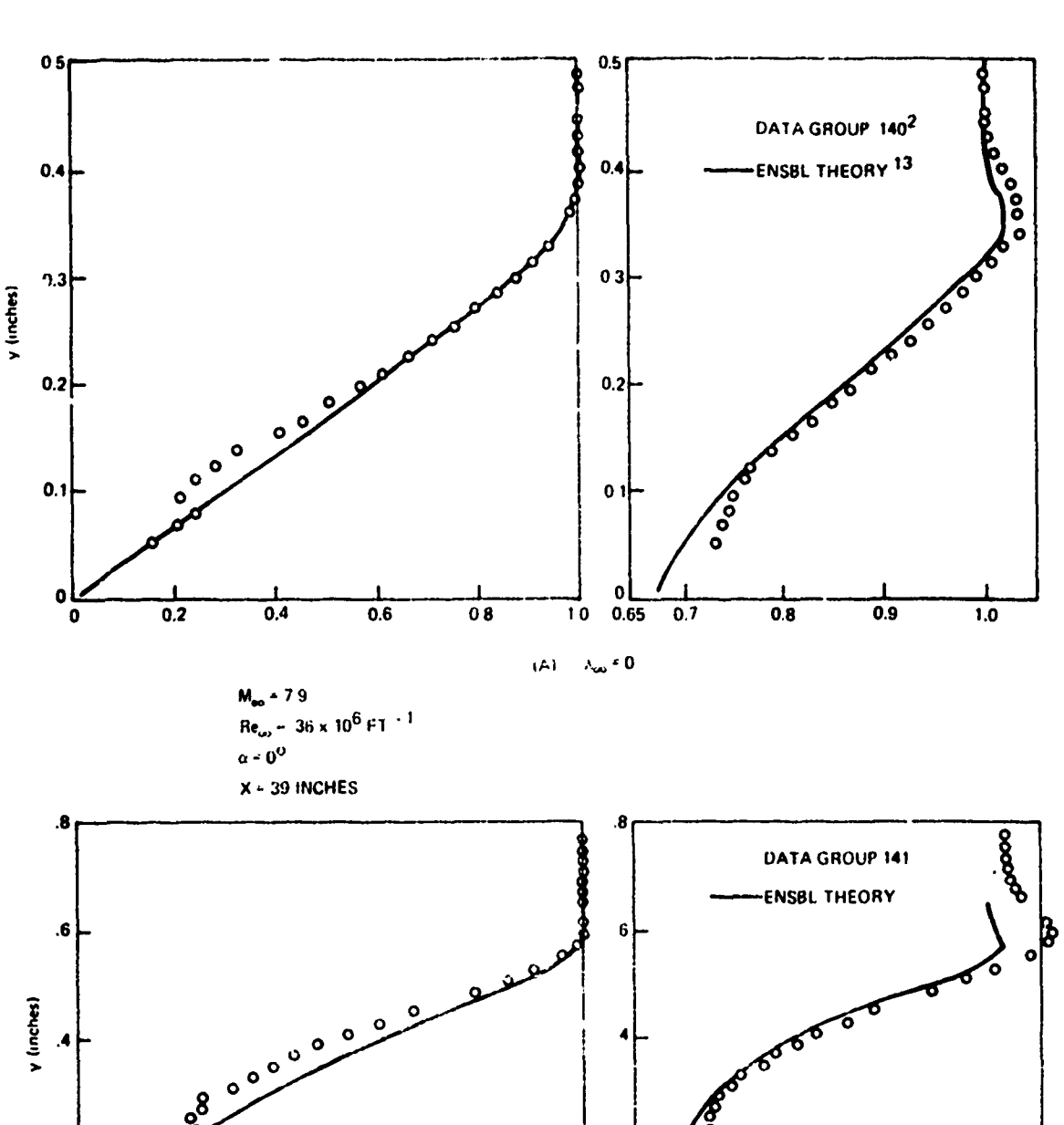

Figure 4. Comparison of Non-Similar Theory with Boundary Layer Profile Data - Laminar

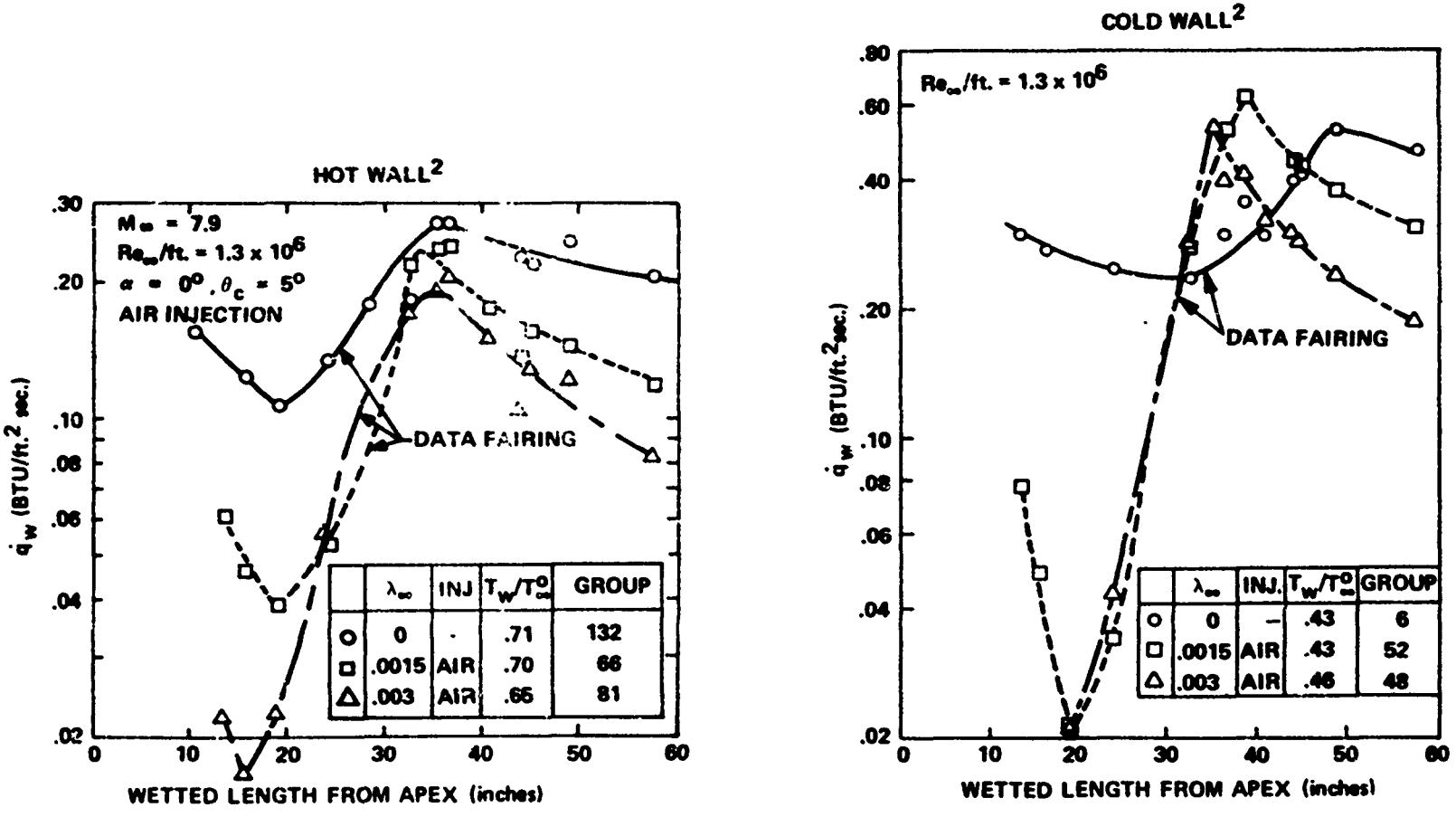

Figure 5. Effect of Mass Addition on the Surface Heat Transfer

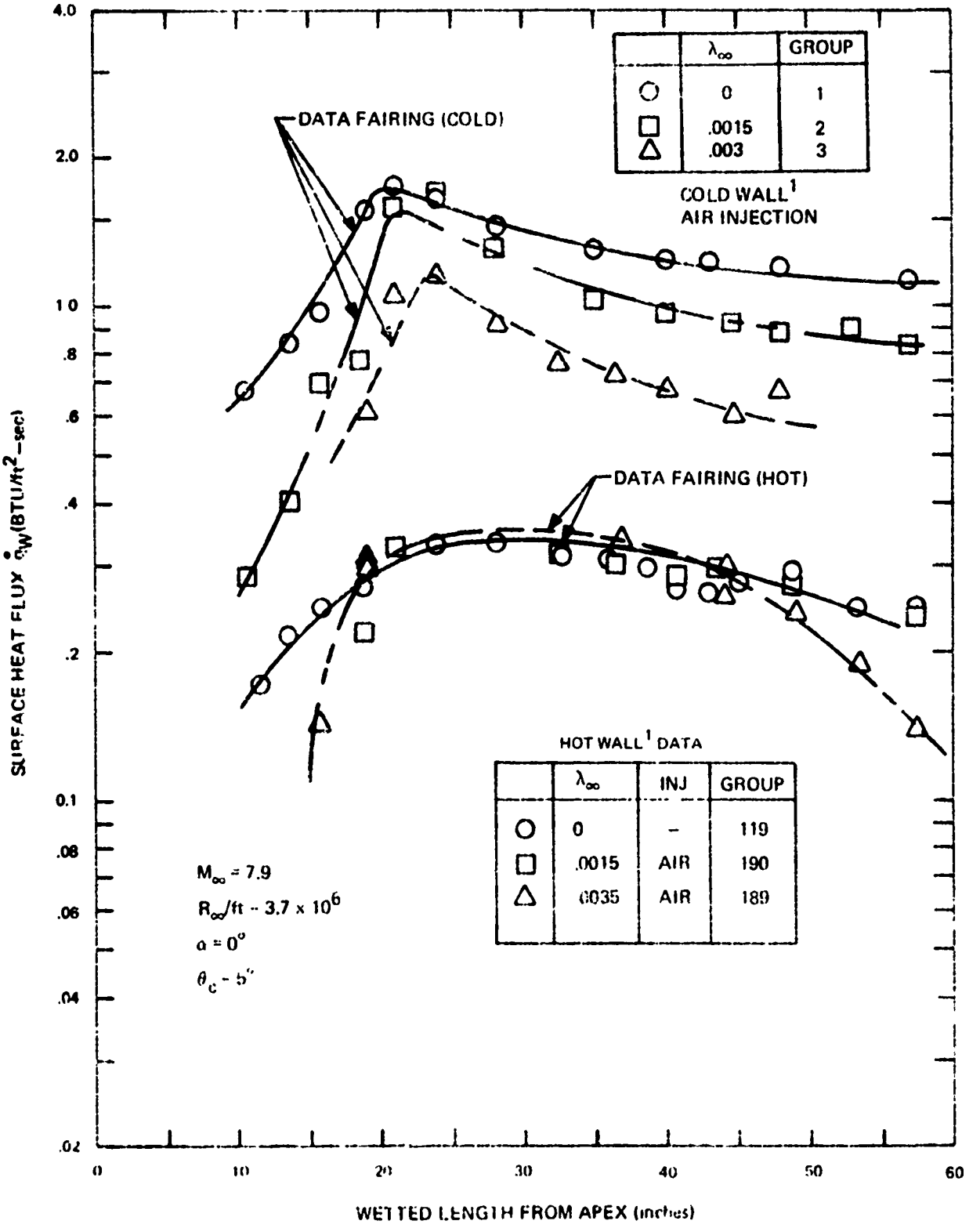

Figure 6 Effect of Mass Addition on Surface Heat Transfer

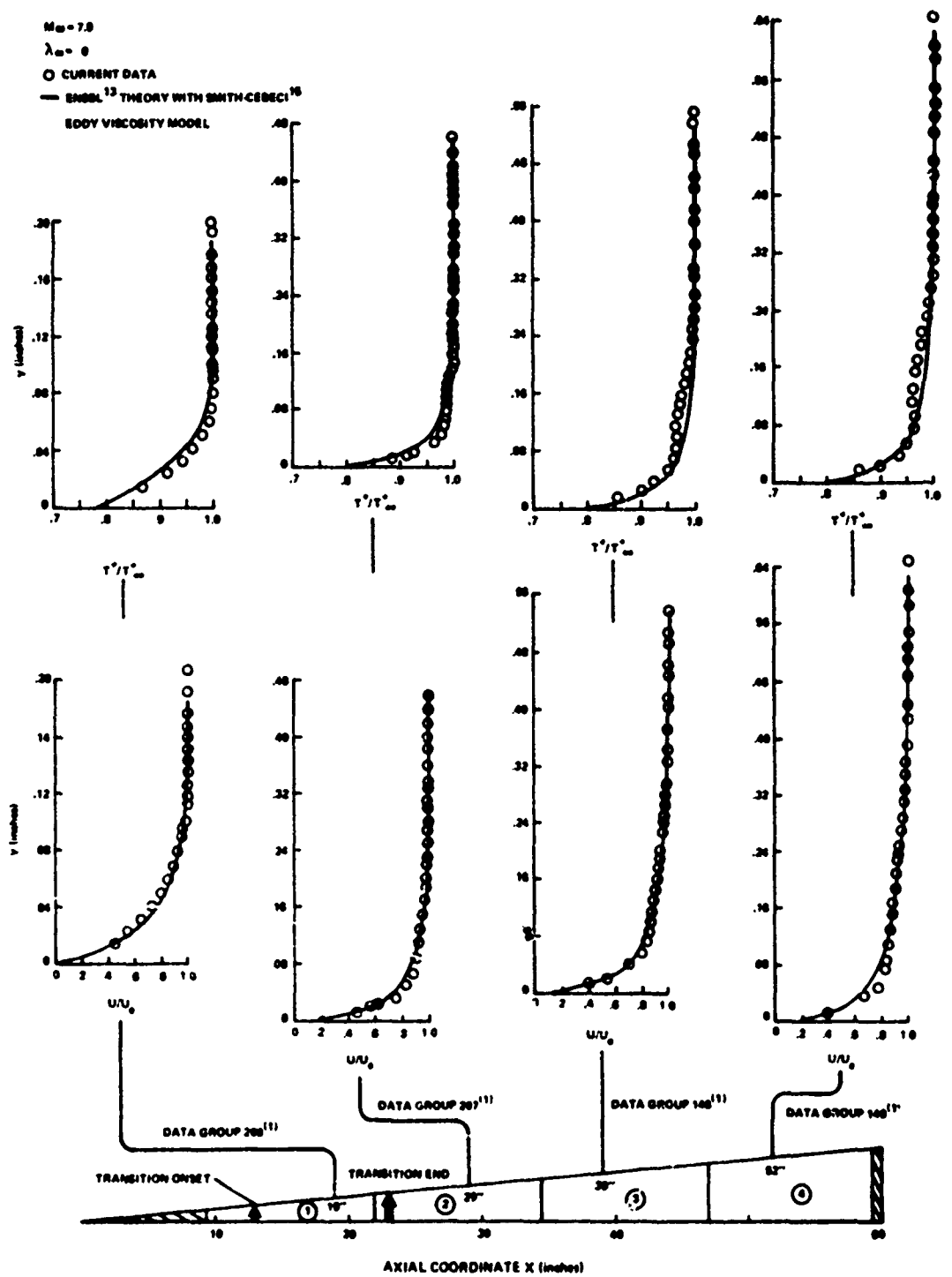

Figure 7. Profile Summary for a Zero Blowing Transitional-Turbulent Boundary Layer ($\alpha = 0°$)

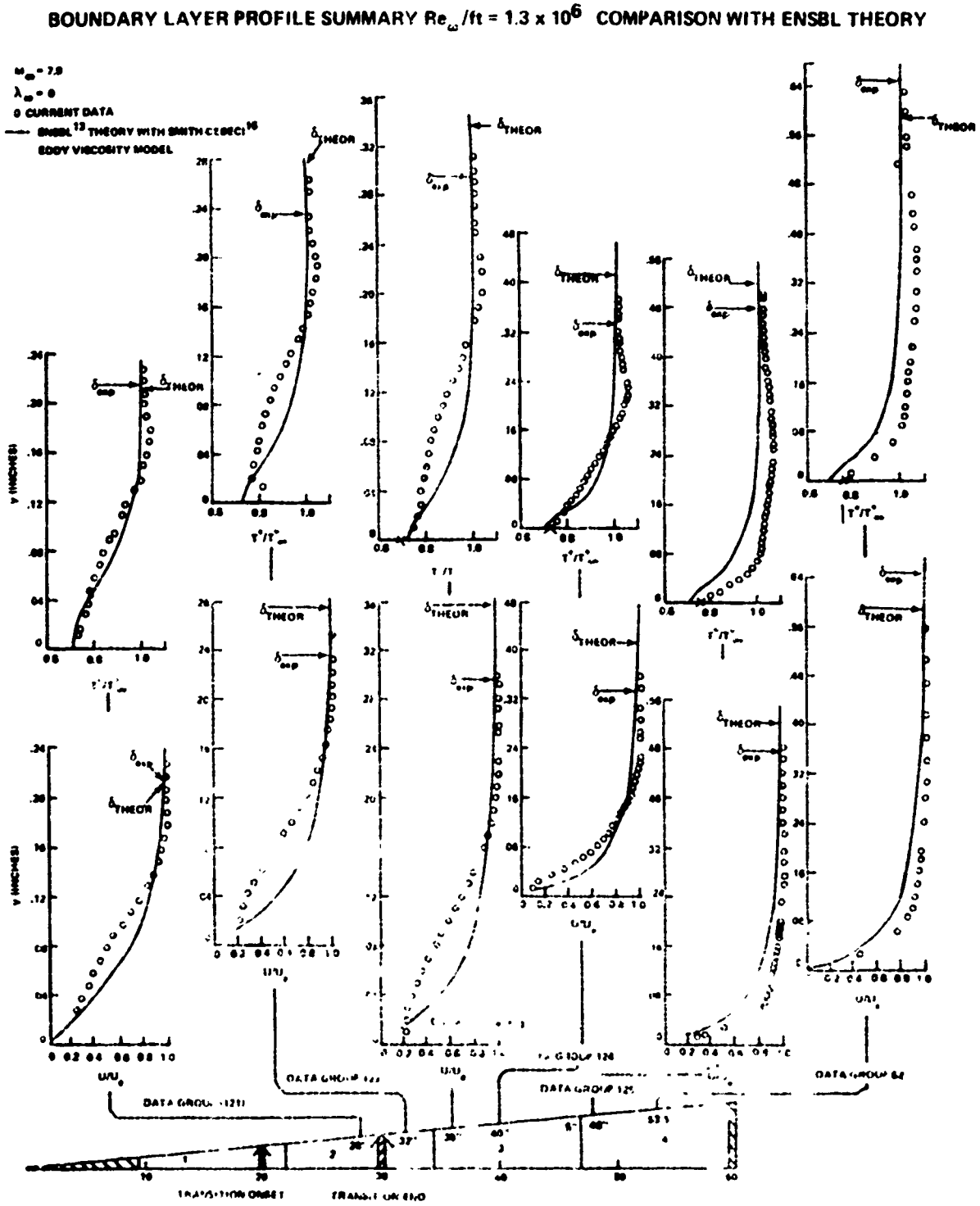

Figure 8. Profile Summary for a Zero Blowing Transitional-Turbulent Boundary Layer ($\alpha = 0°$)

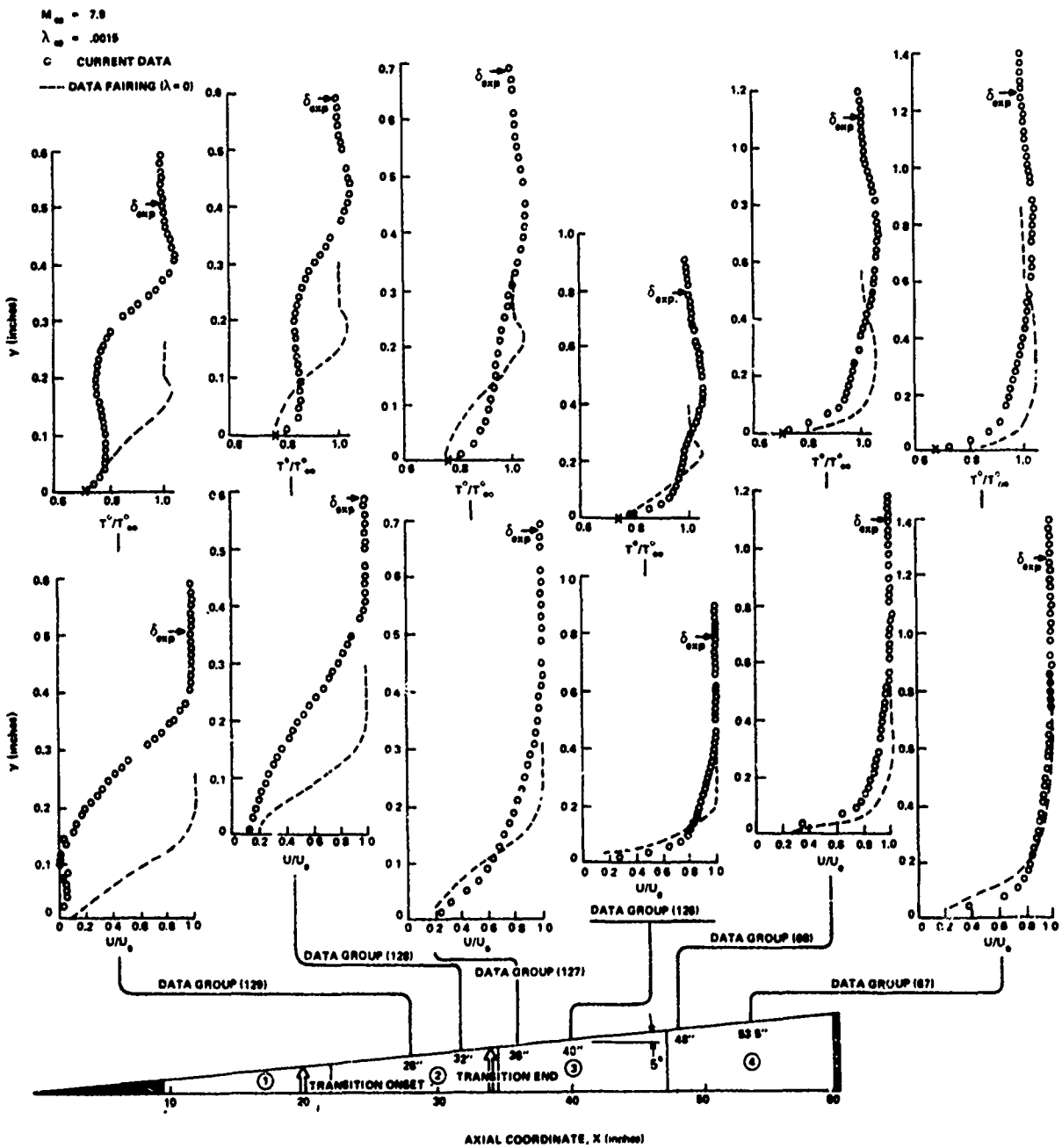

Figure 9. Profile Data Summary for a Transitional-Turbulent Boundary Layer with Air Injection ($\alpha = 0°$)

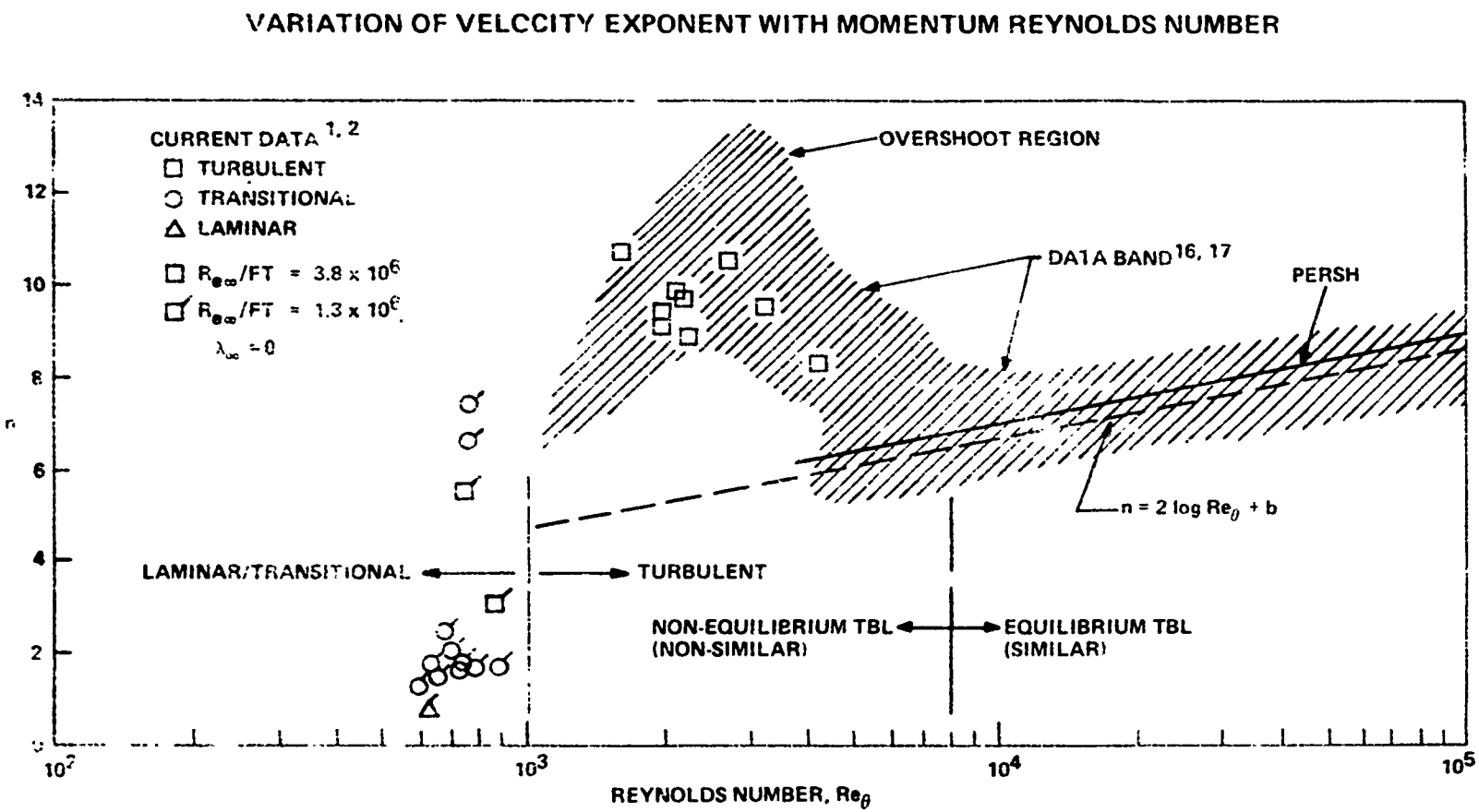

Figure 10. Variation of Velocity Exponent with Momentum Reynolds Number

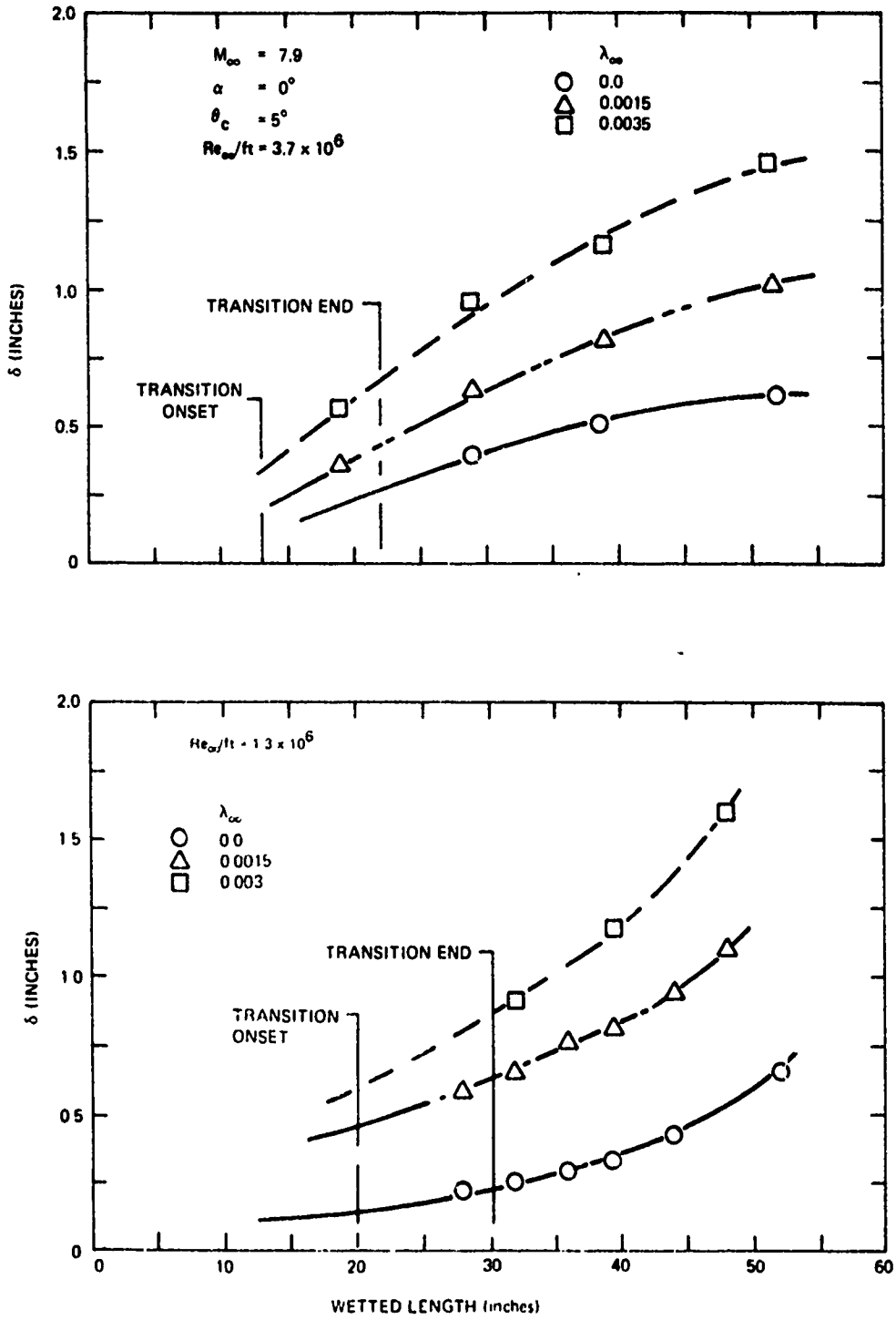

Figure 11. Effect of Blowing on Boundary Layer Thickness

SYMBOL	DATA GROUP	$\lambda_\infty \times 10^4$ CHAMBER				INJECTION GAS CHAMBER			
		1	2	3	4	1	2	3	4
△	88(2)	15	15	0	0	AIR →			
□	95(2)	15	15	30	30	AIR →			

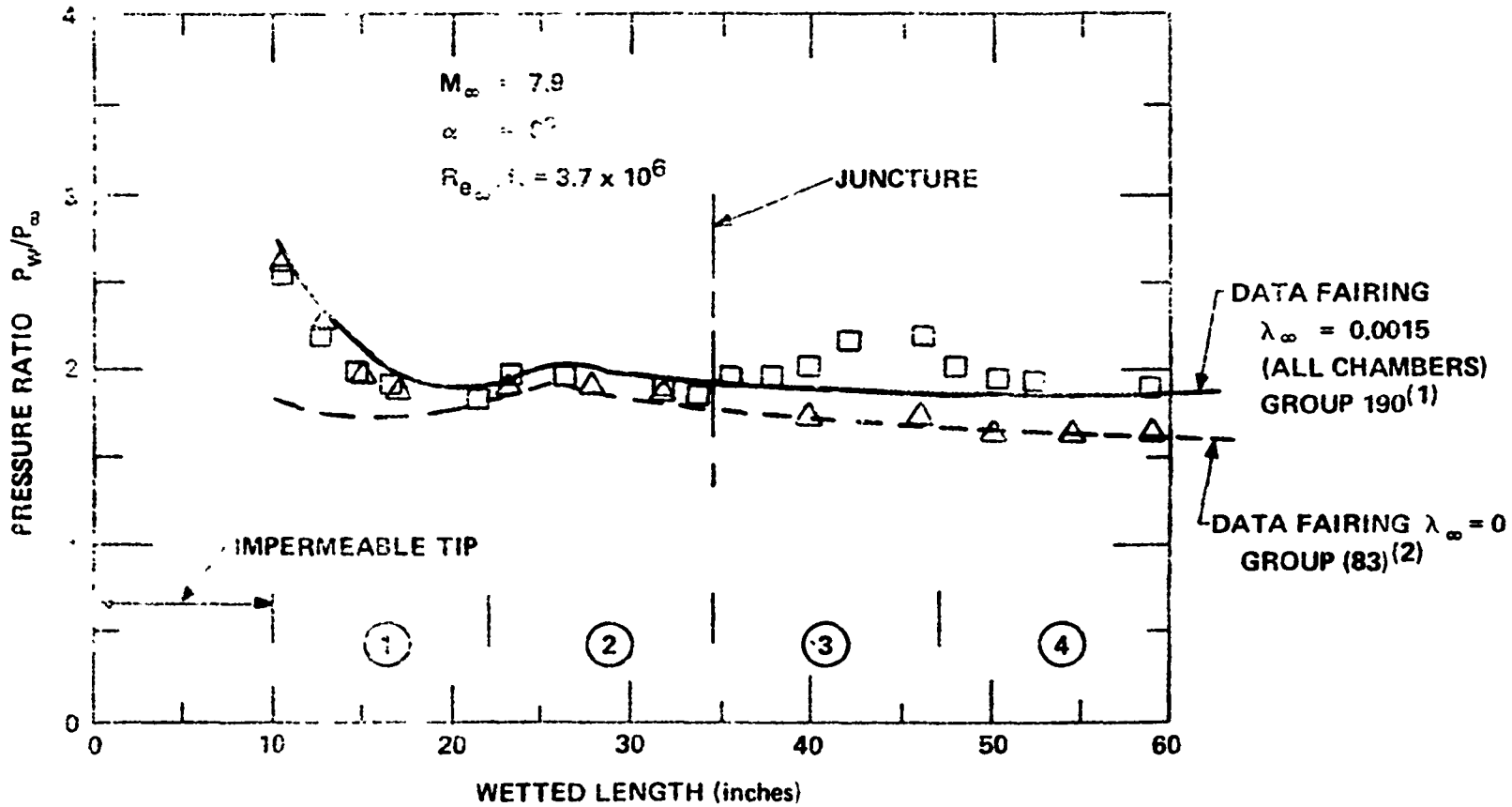

Figure 12. Non-Uniform Air Injection Effects on the Pressure Distribution

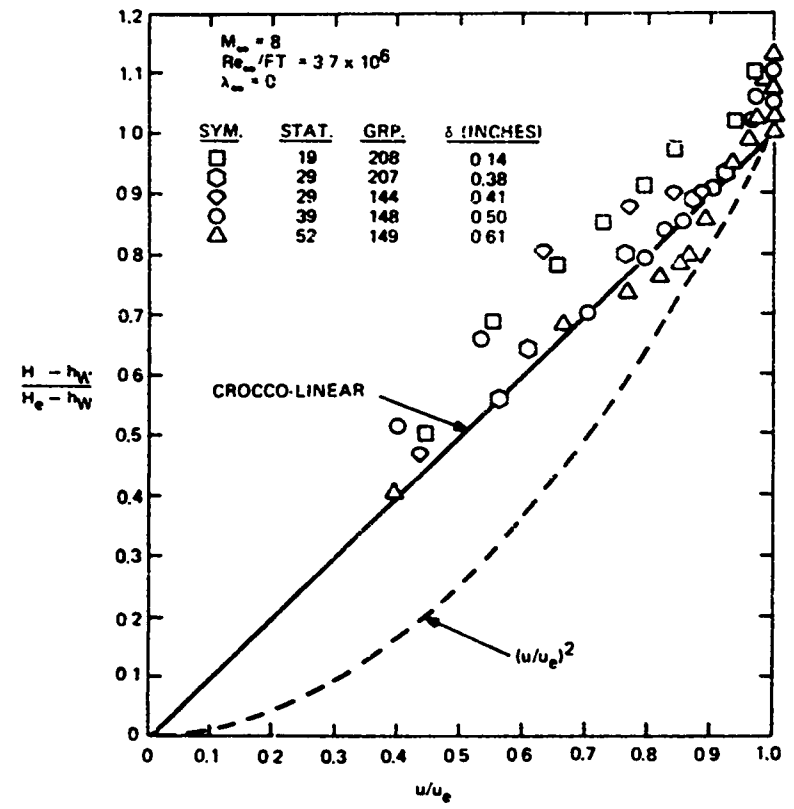

Figure 13. Crocco Total Enthalpy-Velocity Distribution along Surface

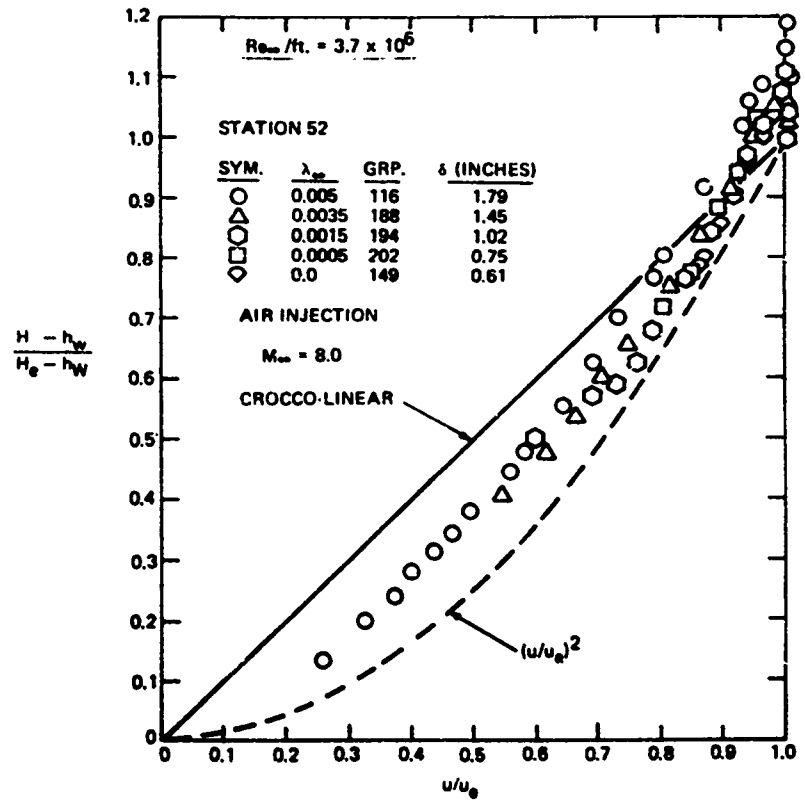

Figure 14. Crocco H-u with Blowing Effects

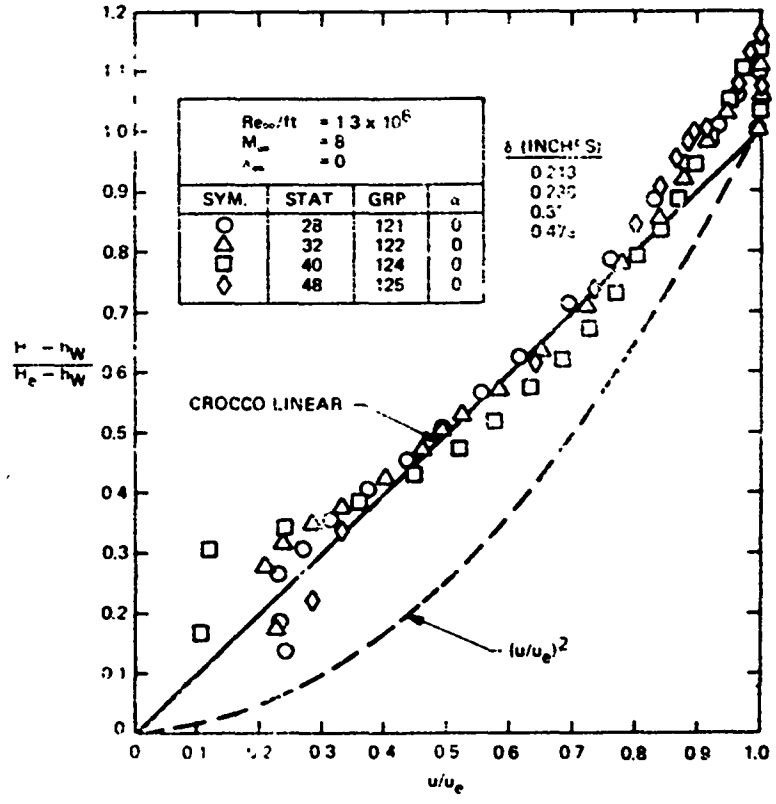

Figure 15. Crocco H-u along Surface with Transition Effects

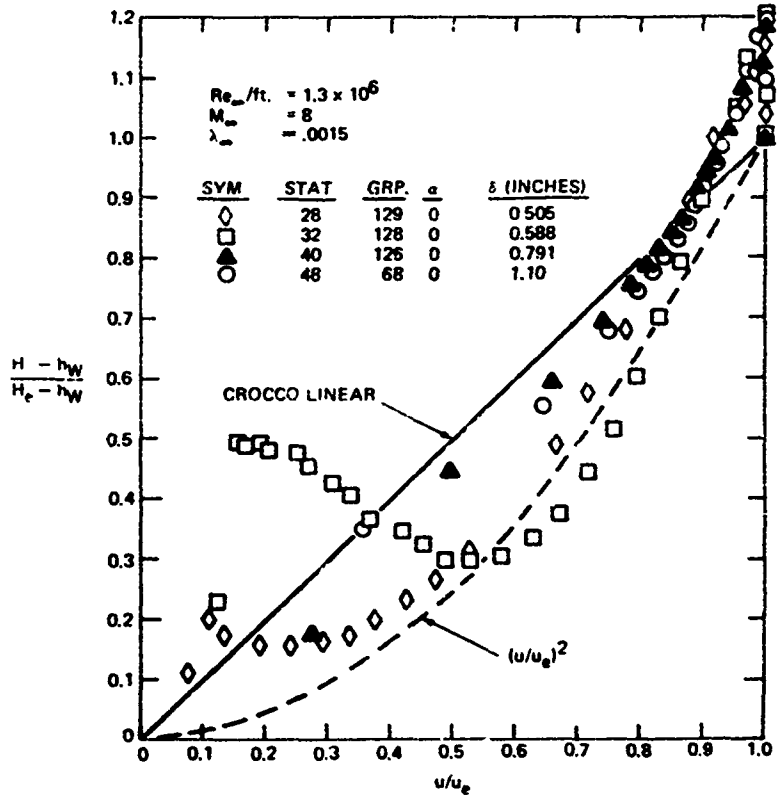

Figure 16. Crocco H-u with Blowing Transition Effects

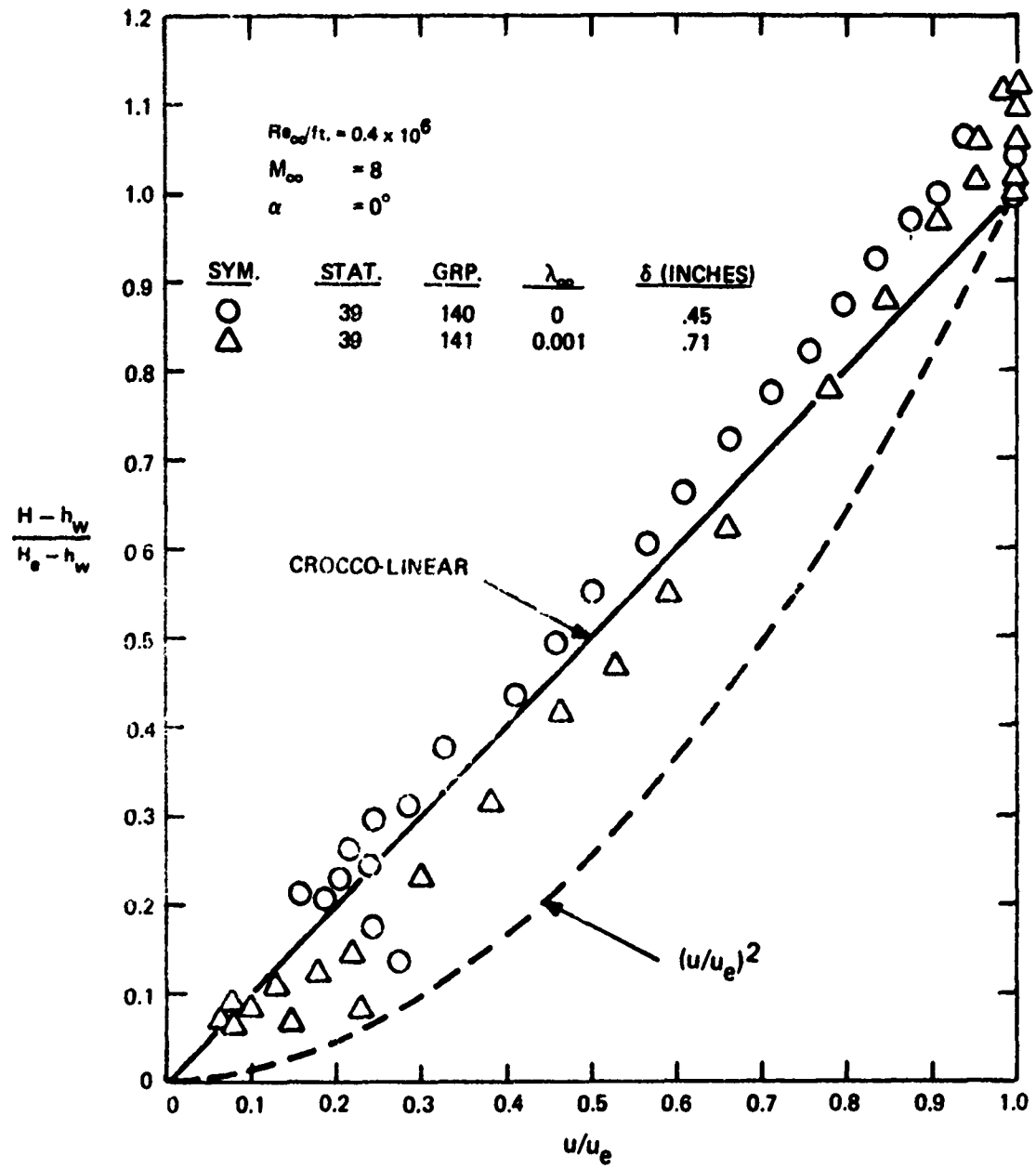

Figure 17. Crocco H-u with/without Blowing in Laminar Boundary Layer

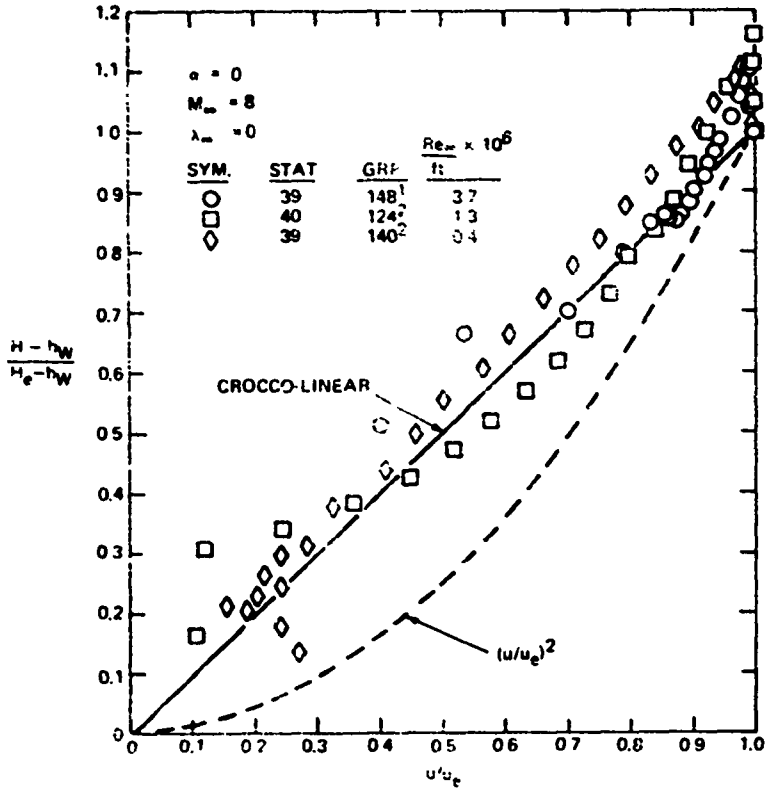

Figure 18. Crocco H-u with Reynolds Number Effects

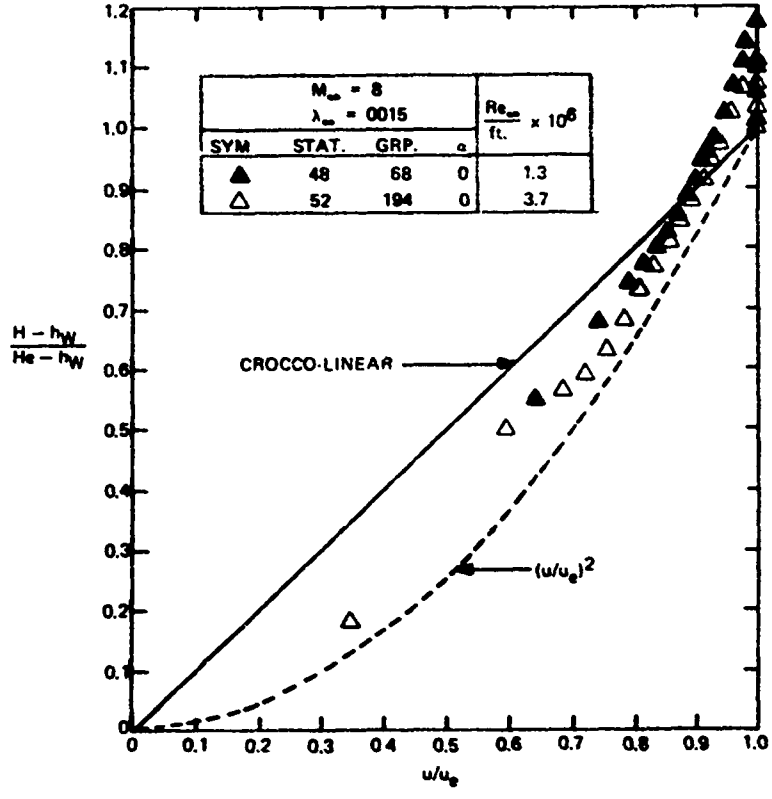

Figure 19. Crocco H-u with Blowing-Reynolds Numbers Effects

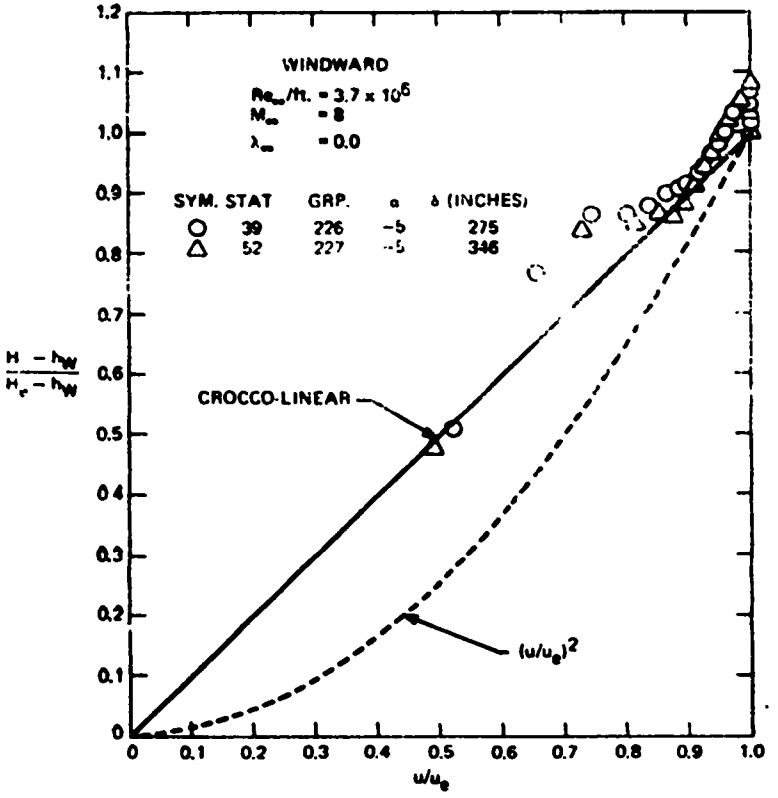

Figure 20. Crocco H-u with Angle of Attack (Windward) Effects

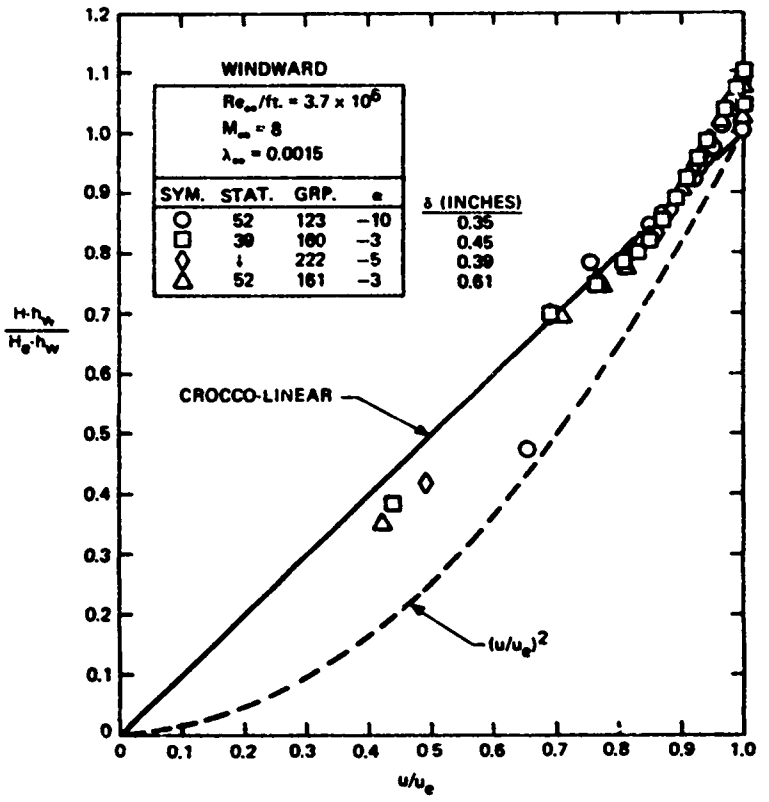

Figure 21. Crocco H-u with Angle of Attack and Blowing Effects

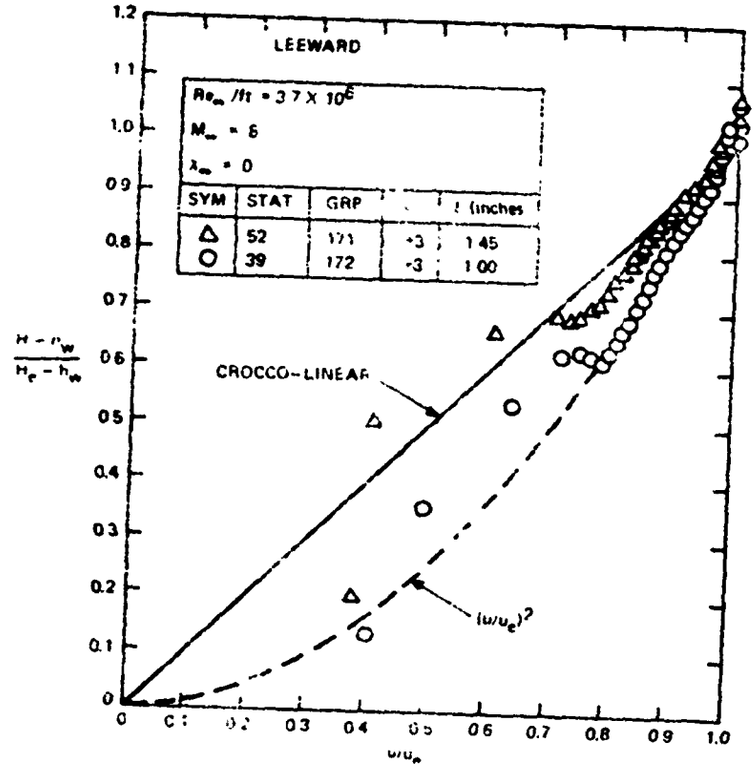

Figure 22. Crocco H-u with Angle of Attack (Leeward) Effects

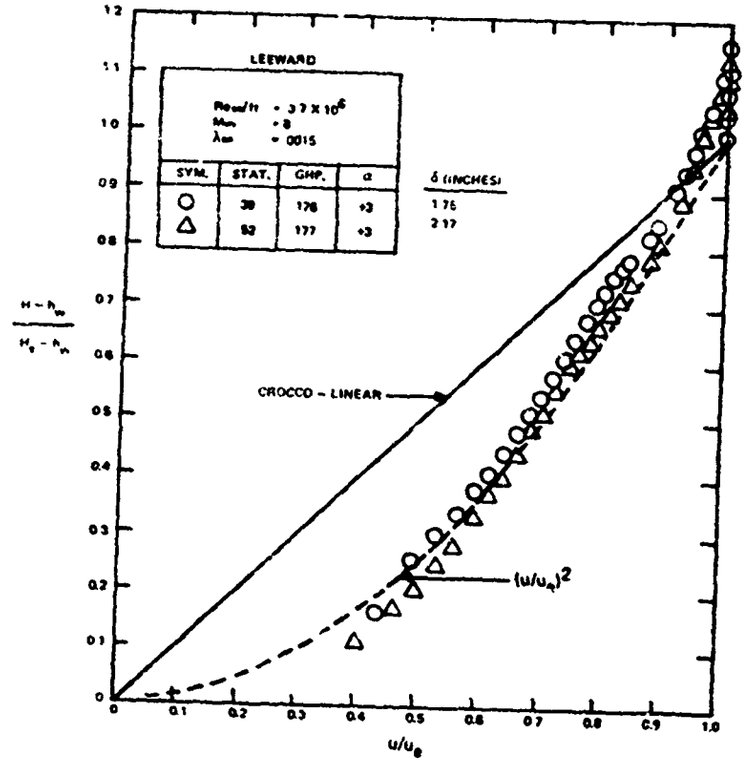

Figure 23. Crocco H-u with Angle of Attack (Leeward) and Blowing Effects

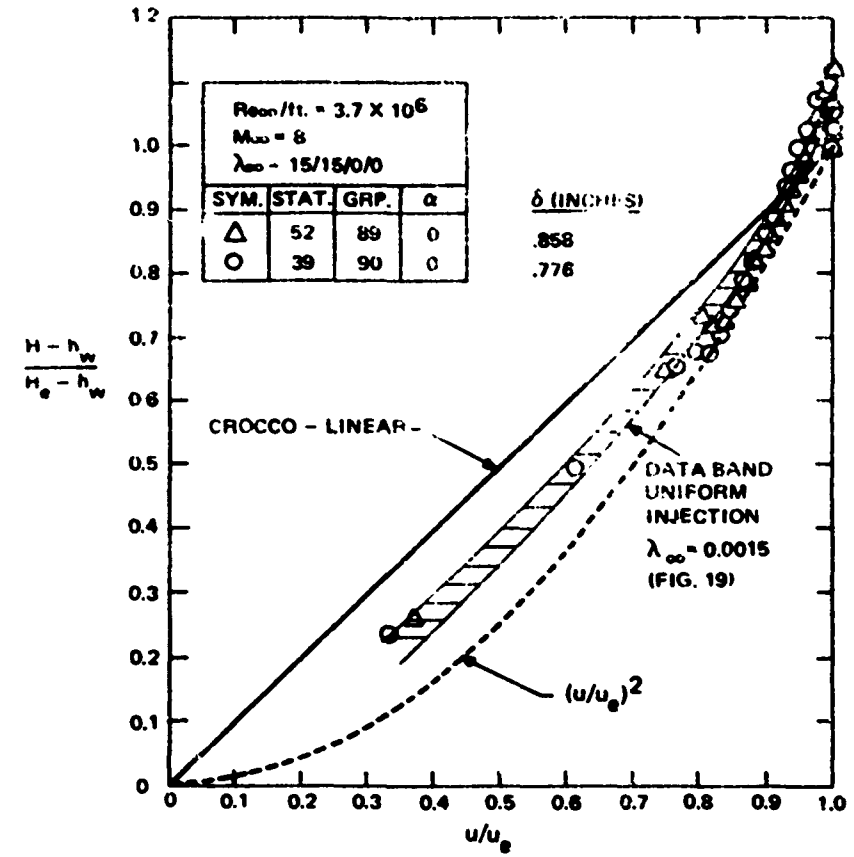

Figure 24. Crocco H-u with Non-Uniform Blowing Effects

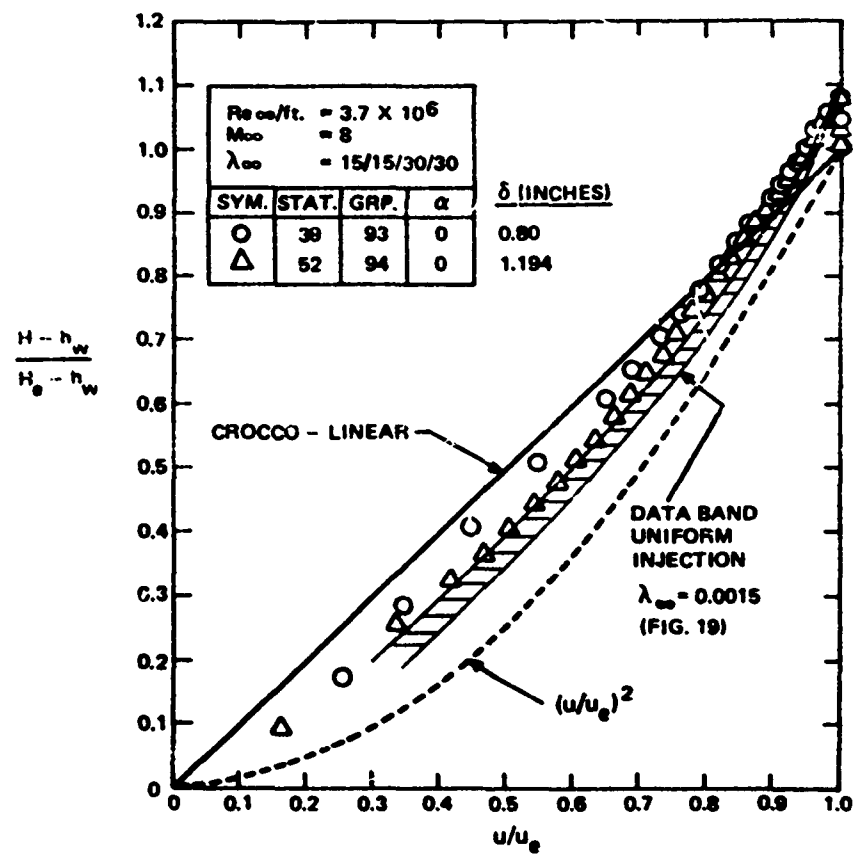

Figure 25. Crocco H-u with Non-Uniform Blowing Effects

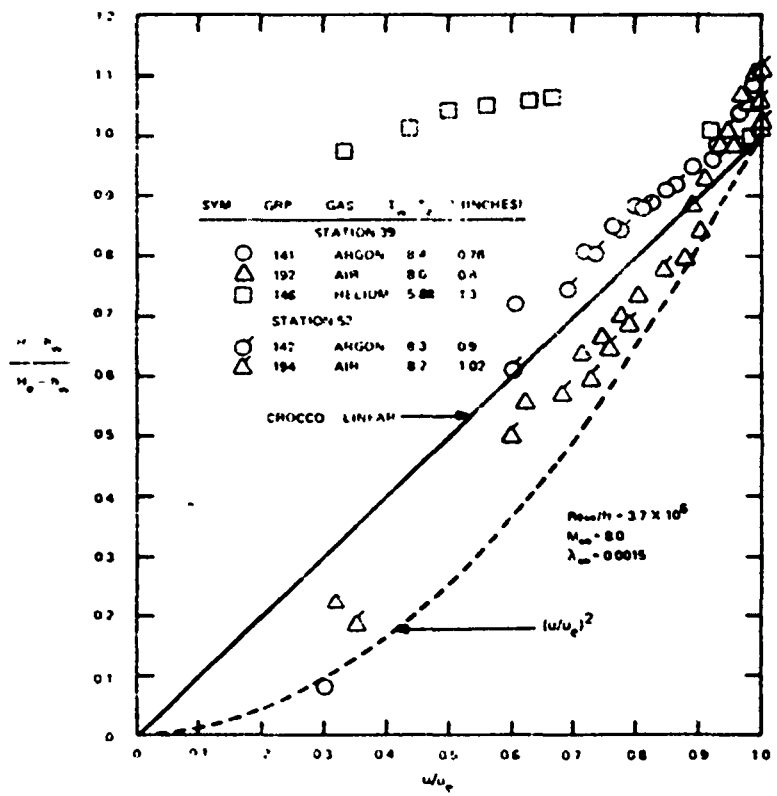

Figure 26. Crocco H-u with Molecular Weight Effects

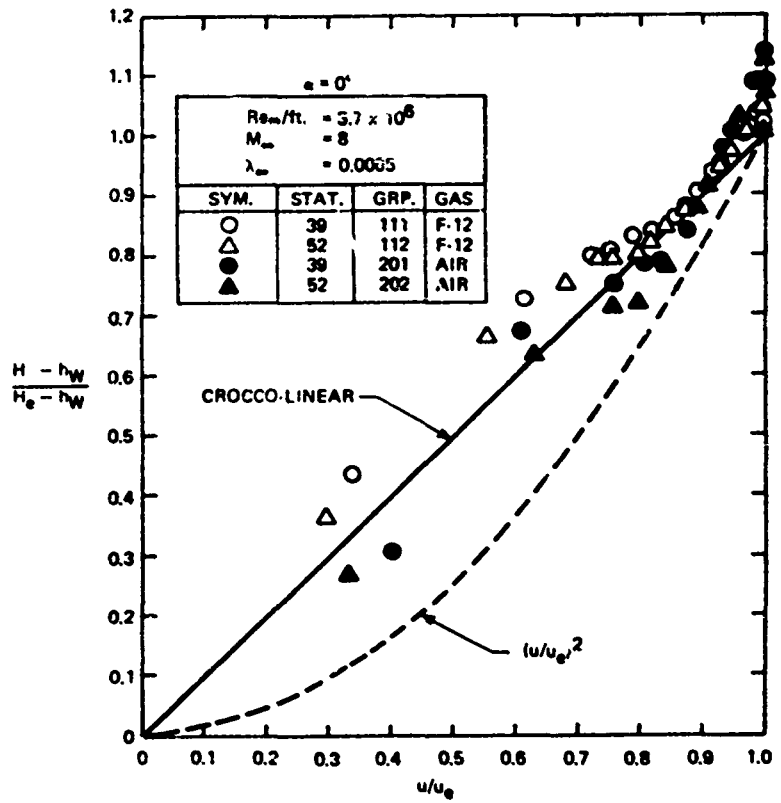

Figure 27. Crocco H-u with Molecular Weight Effects

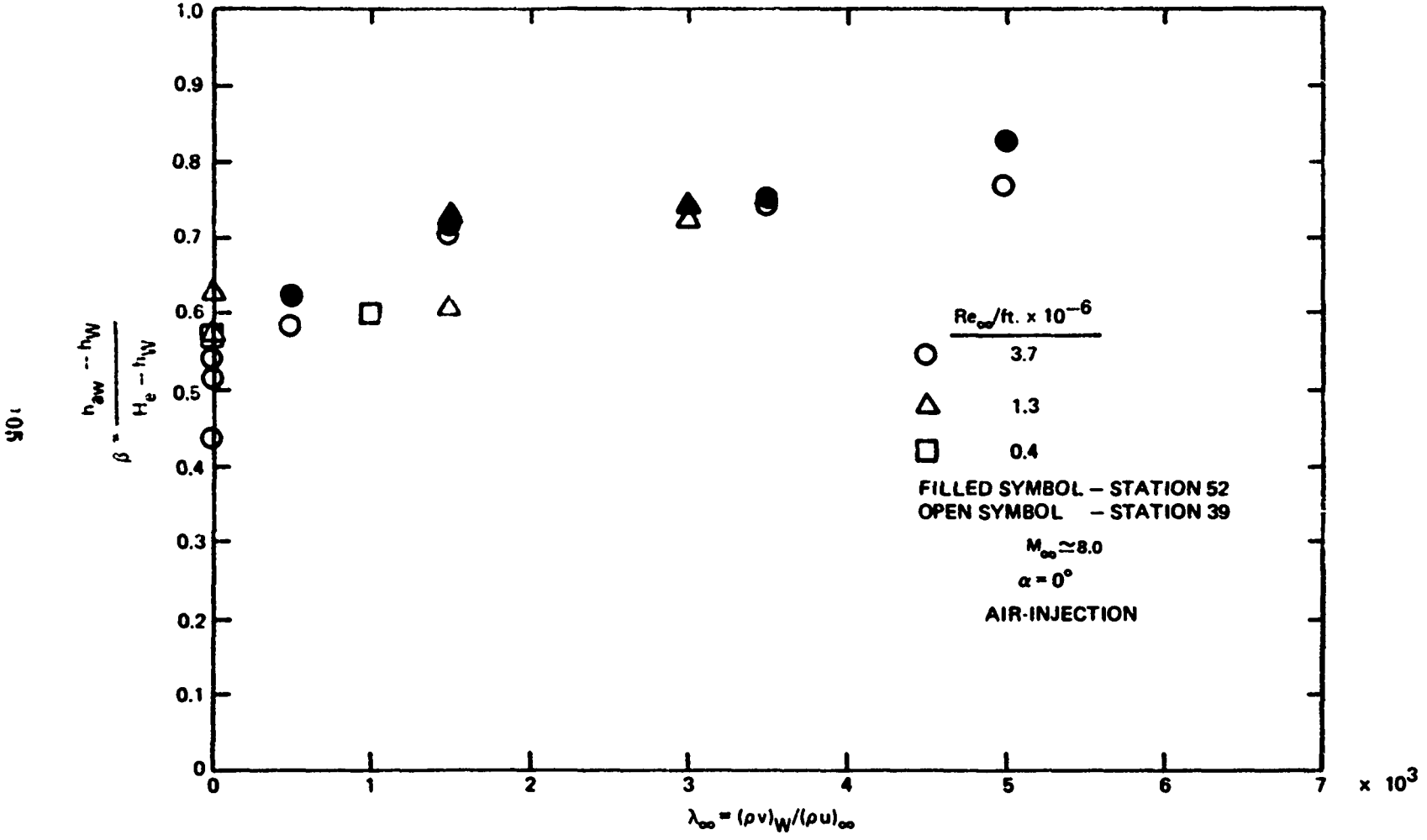

Figure 28. Variation of Compressibility Parameter with Blowing

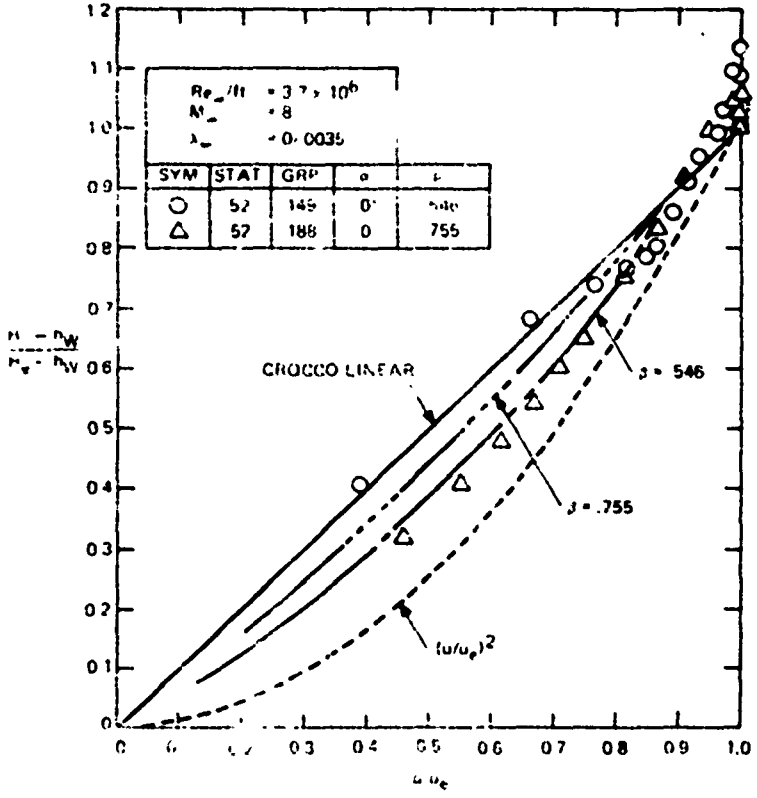

Figure 29. Crocco H-u Variation with Compressibility and Blowing

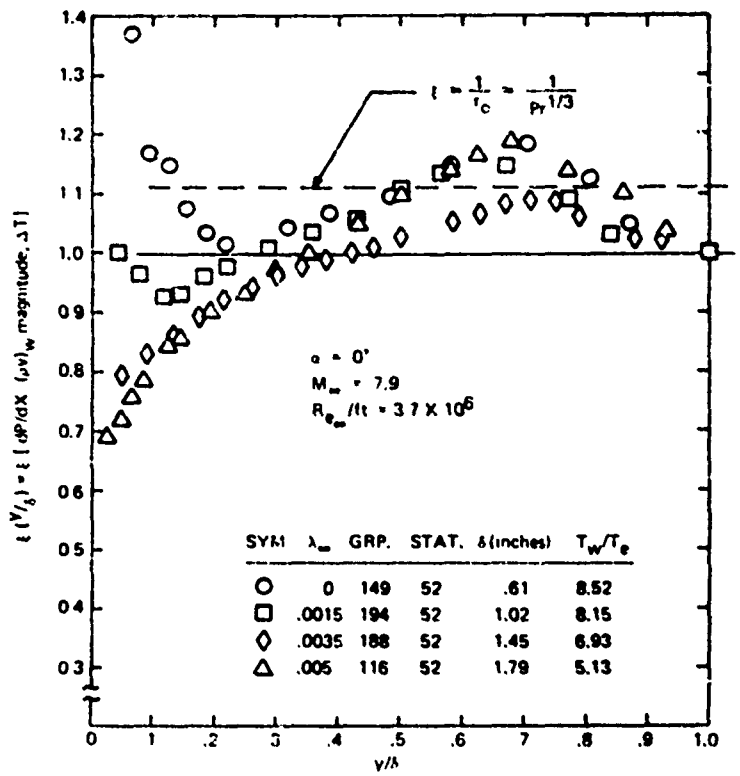

Figure 30A. Effect of Non-Similarity through the Boundary Layer with Blowing

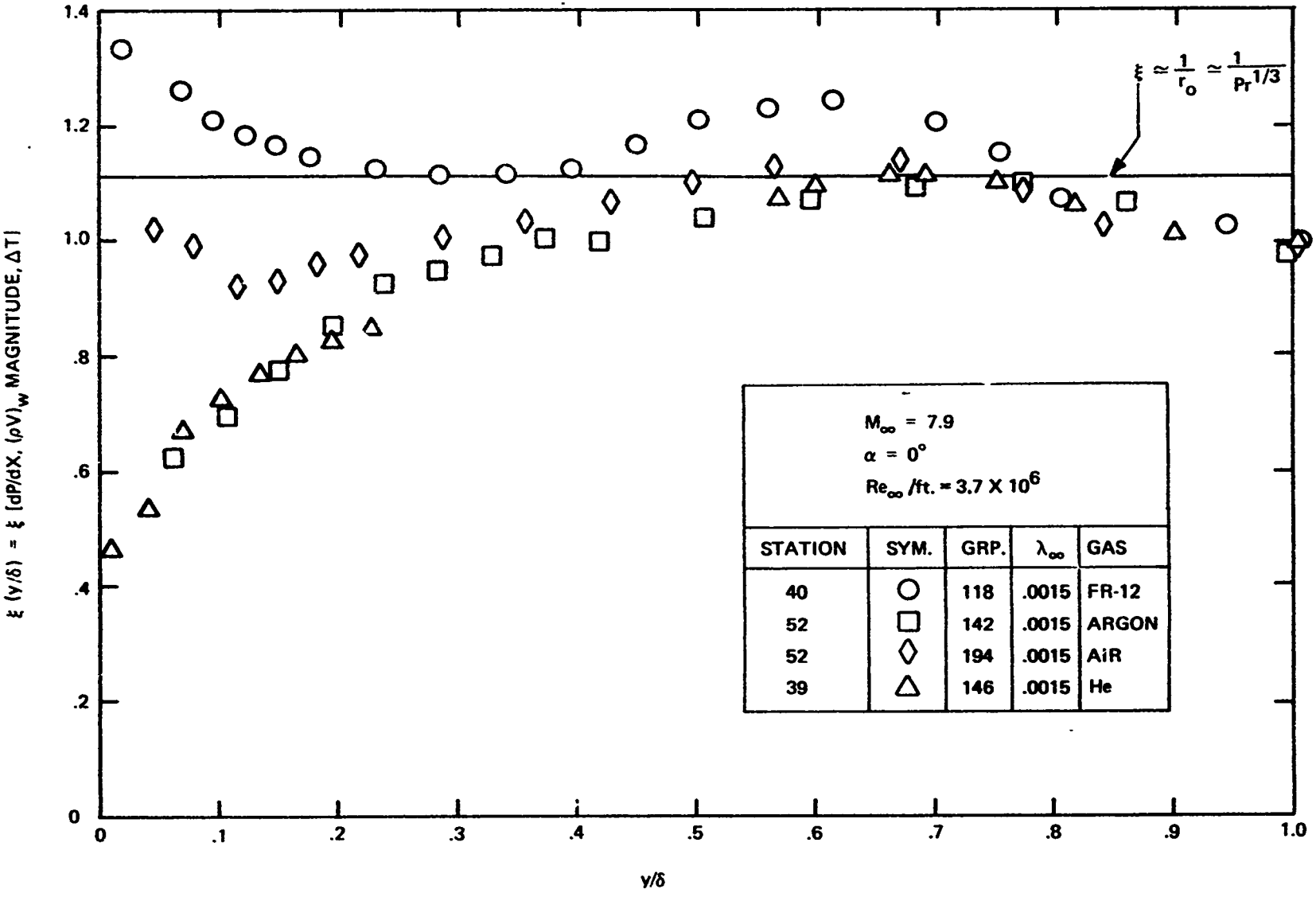

Figure 30B. Effect of Non-Similarity through the Boundary Layer with Molecular Weight

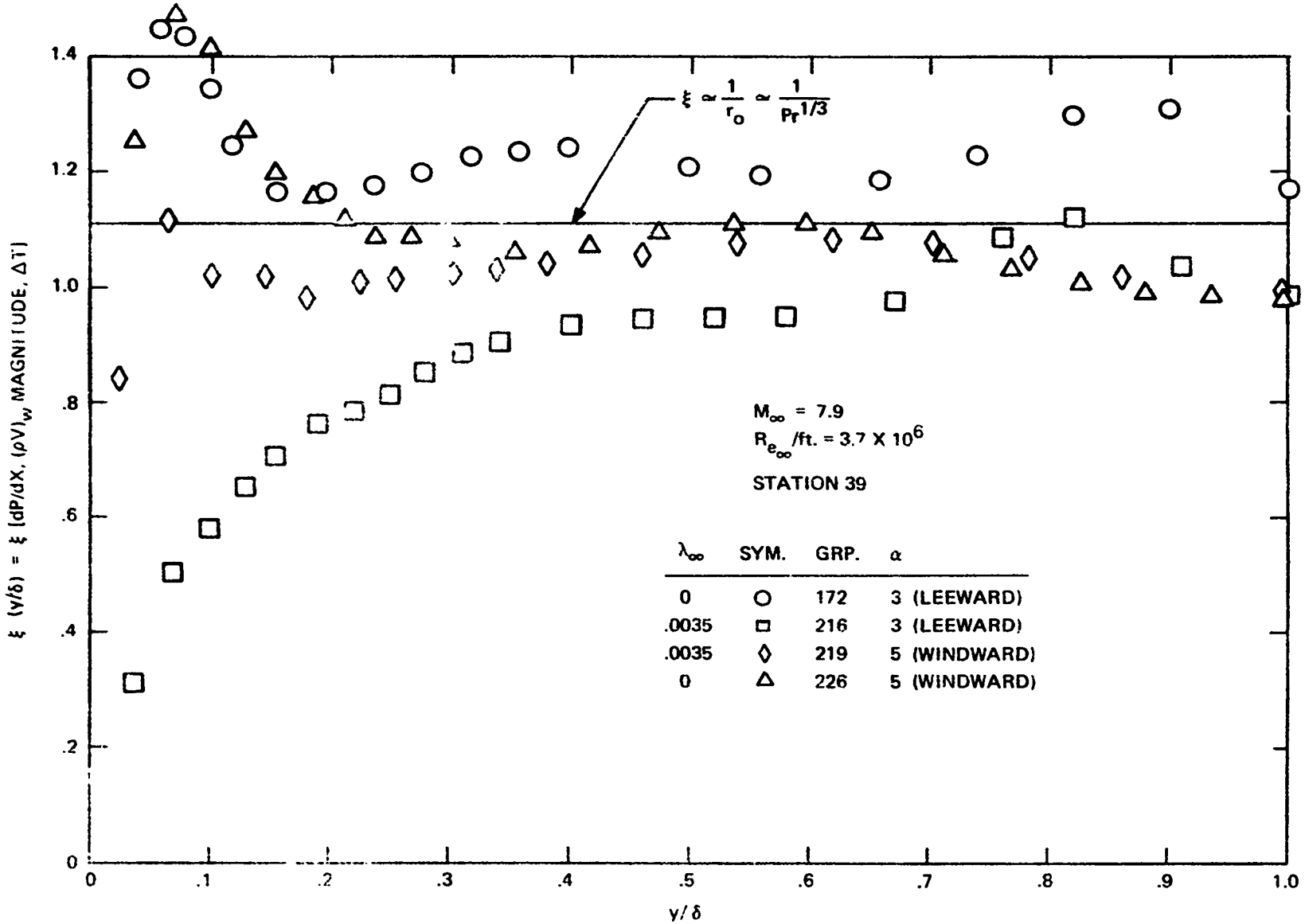

Figure 30C. Effect of Non-Similarity through the Boundary Layer with Angle of Attack

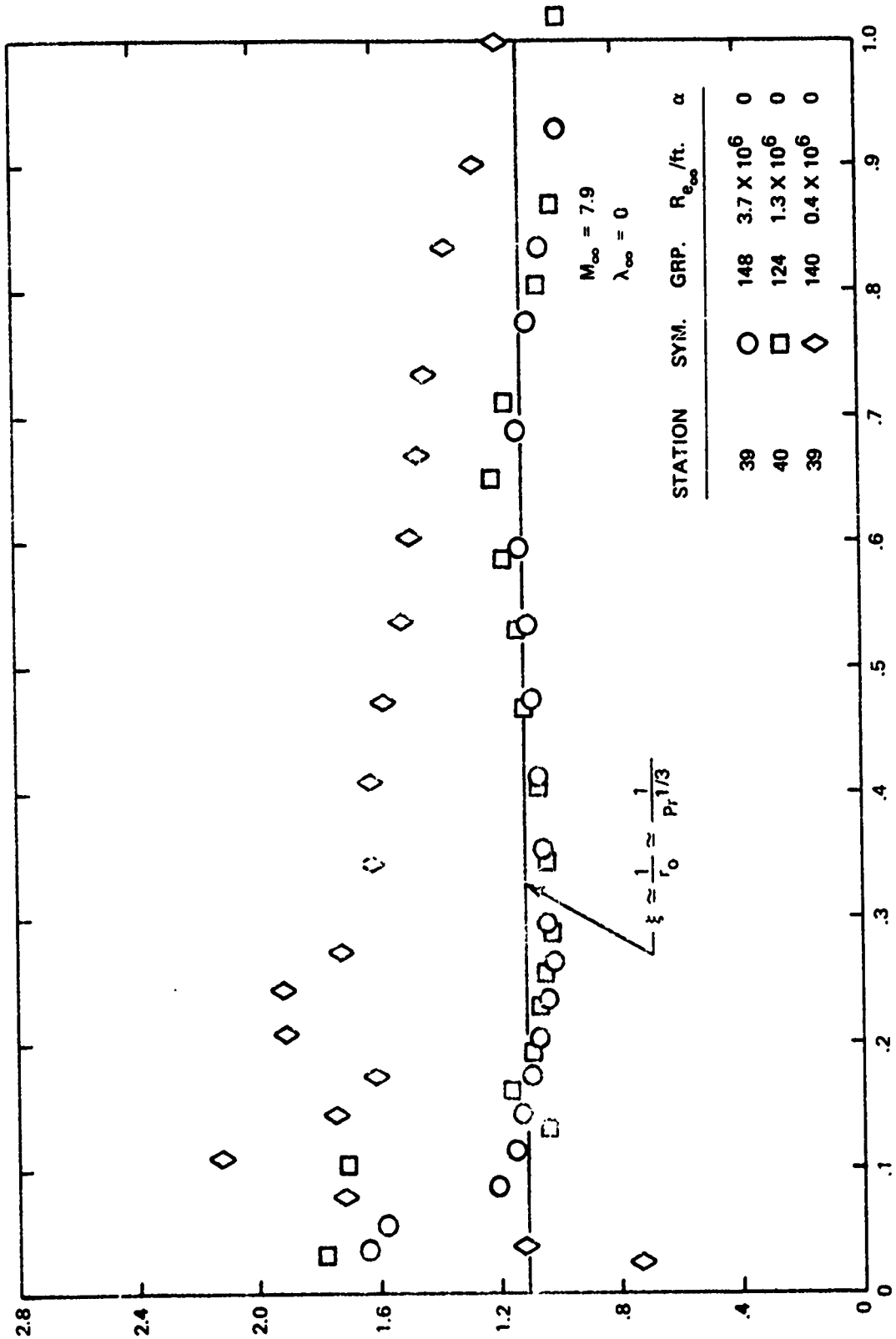

Figure 30D. Effect of Non-Similarity through the Boundary Layer with Reynolds Number

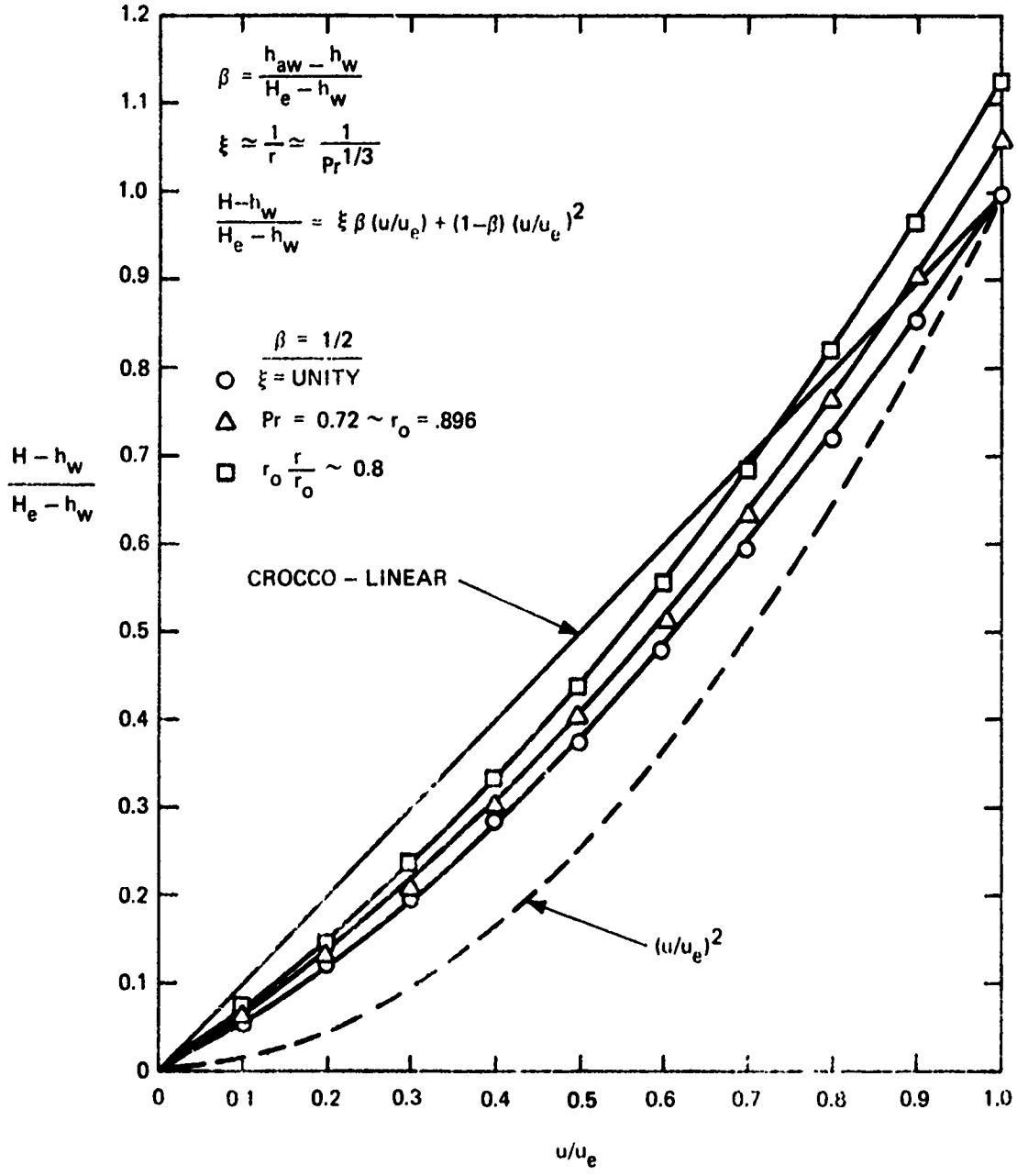

Figure 31. Crocco H-u with Non-Similarity and Compressibility

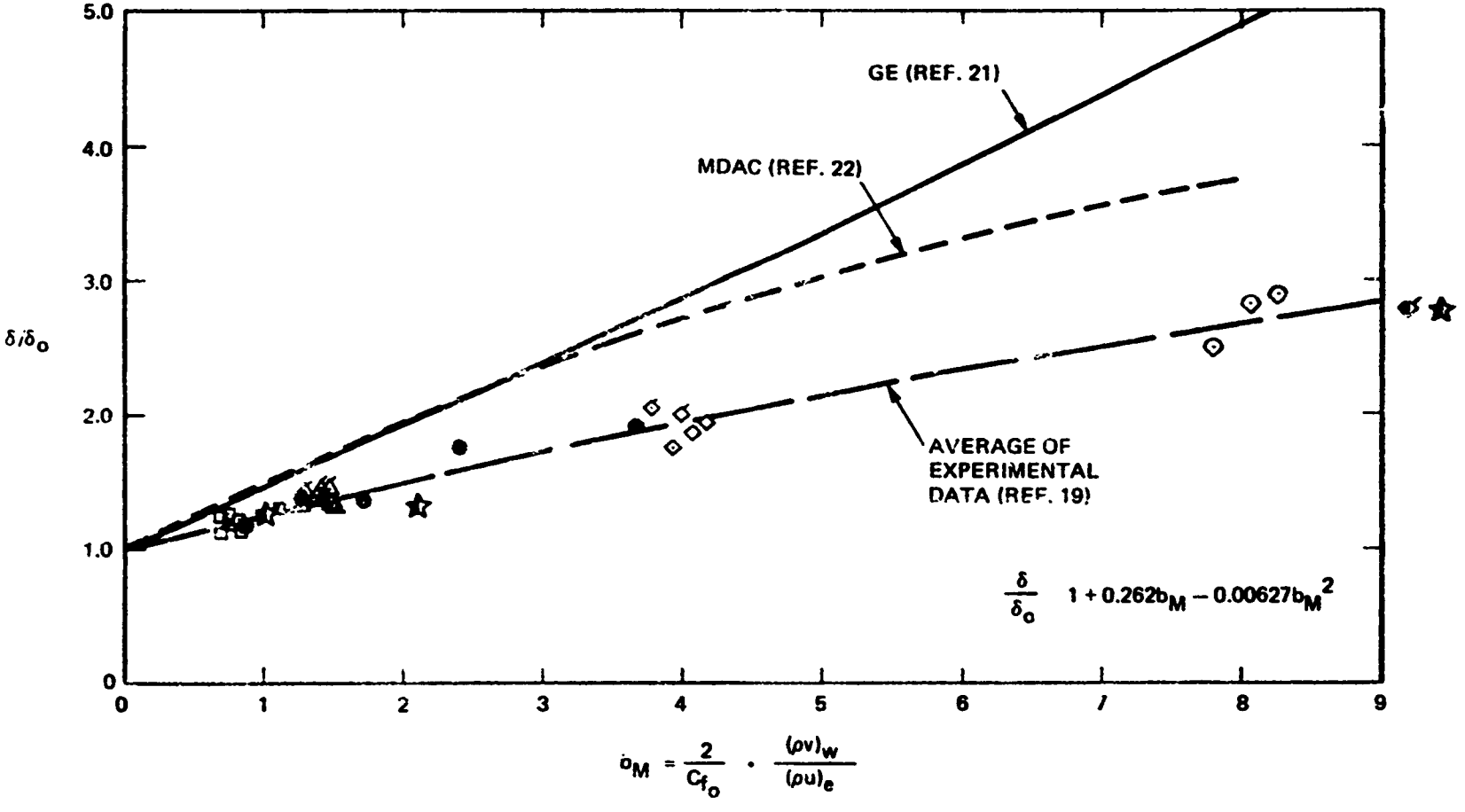

Figure 32. Effect of Mass Transfer on Boundary Layer Thickness ($\alpha = 0°$)

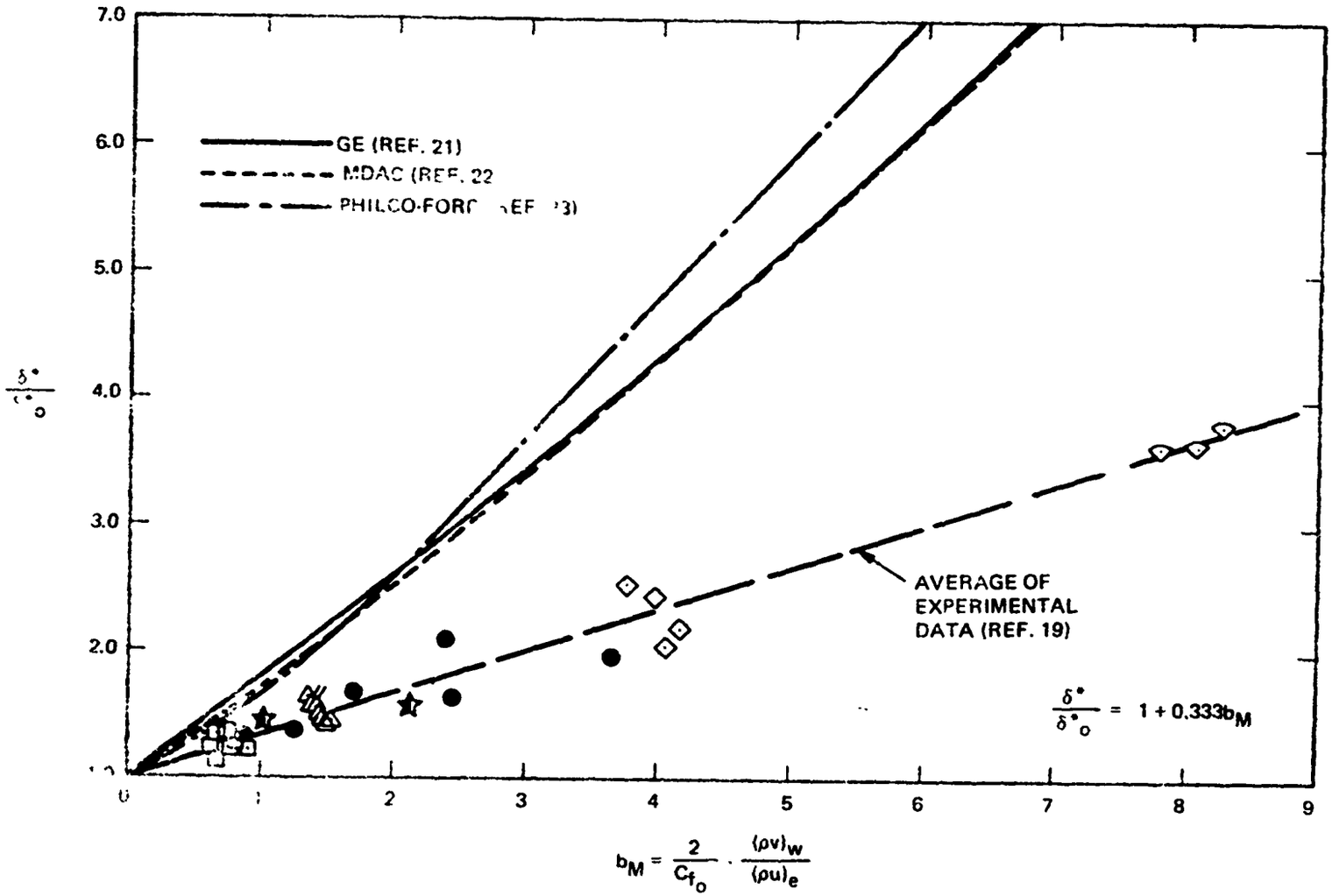

Figure 33. Effect of Mass Transfer on Displacement Thickness ($\alpha = 0°$)

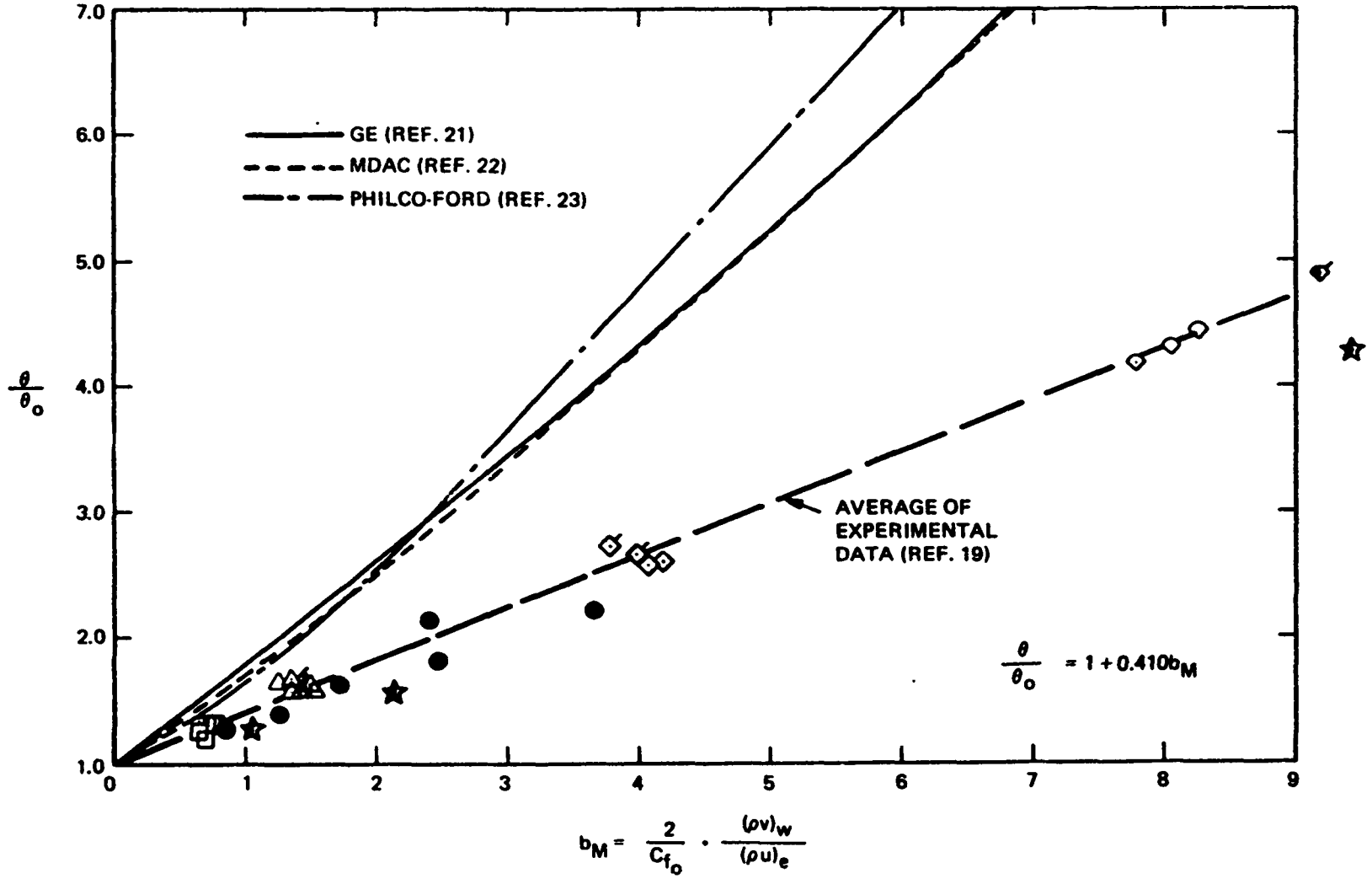

Figure 34. Effect of Mass Transfer on Momentum Thickness ($\alpha = 0°$)

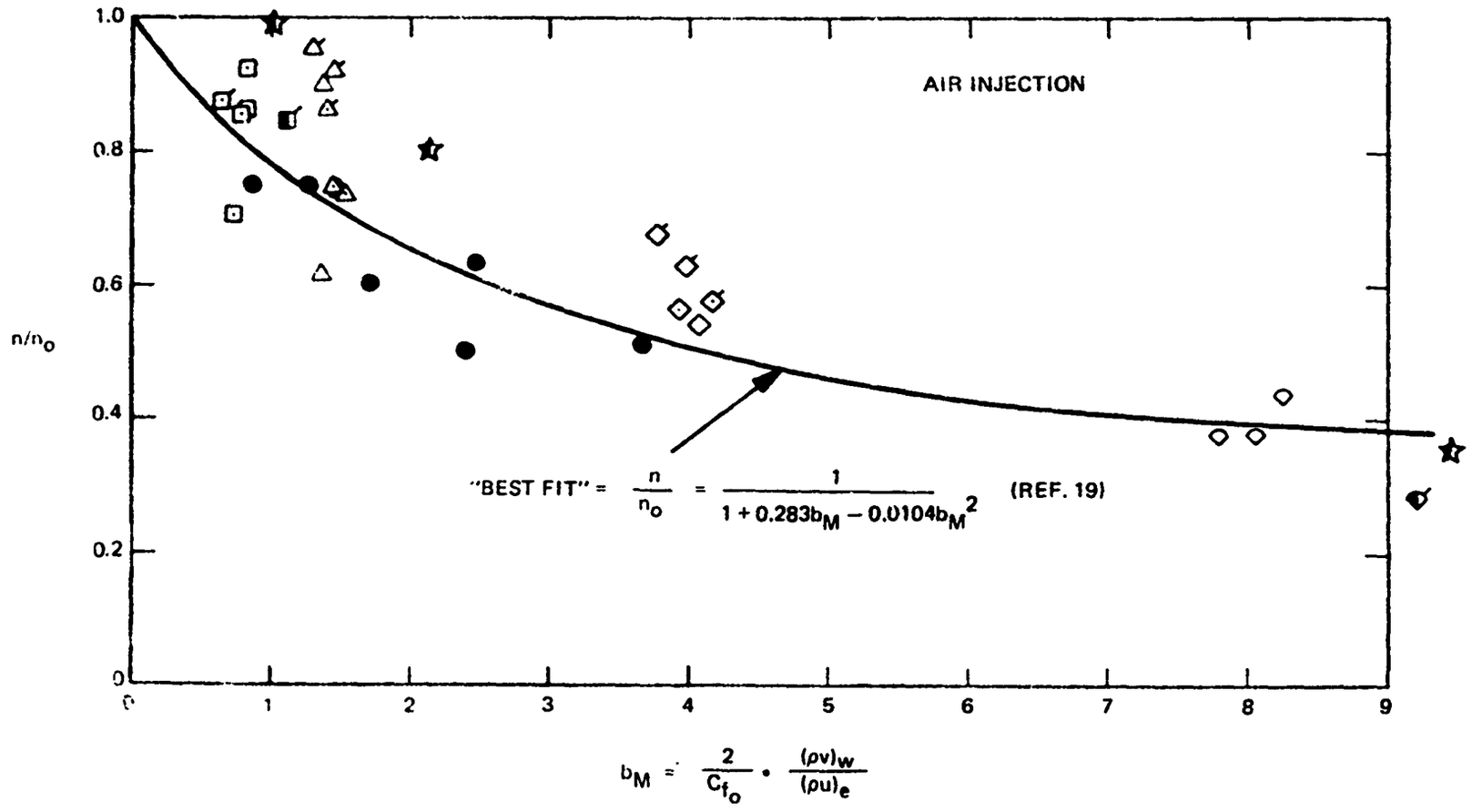

Figure 35. Effect of Mass Addition on Velocity Profile Exponent

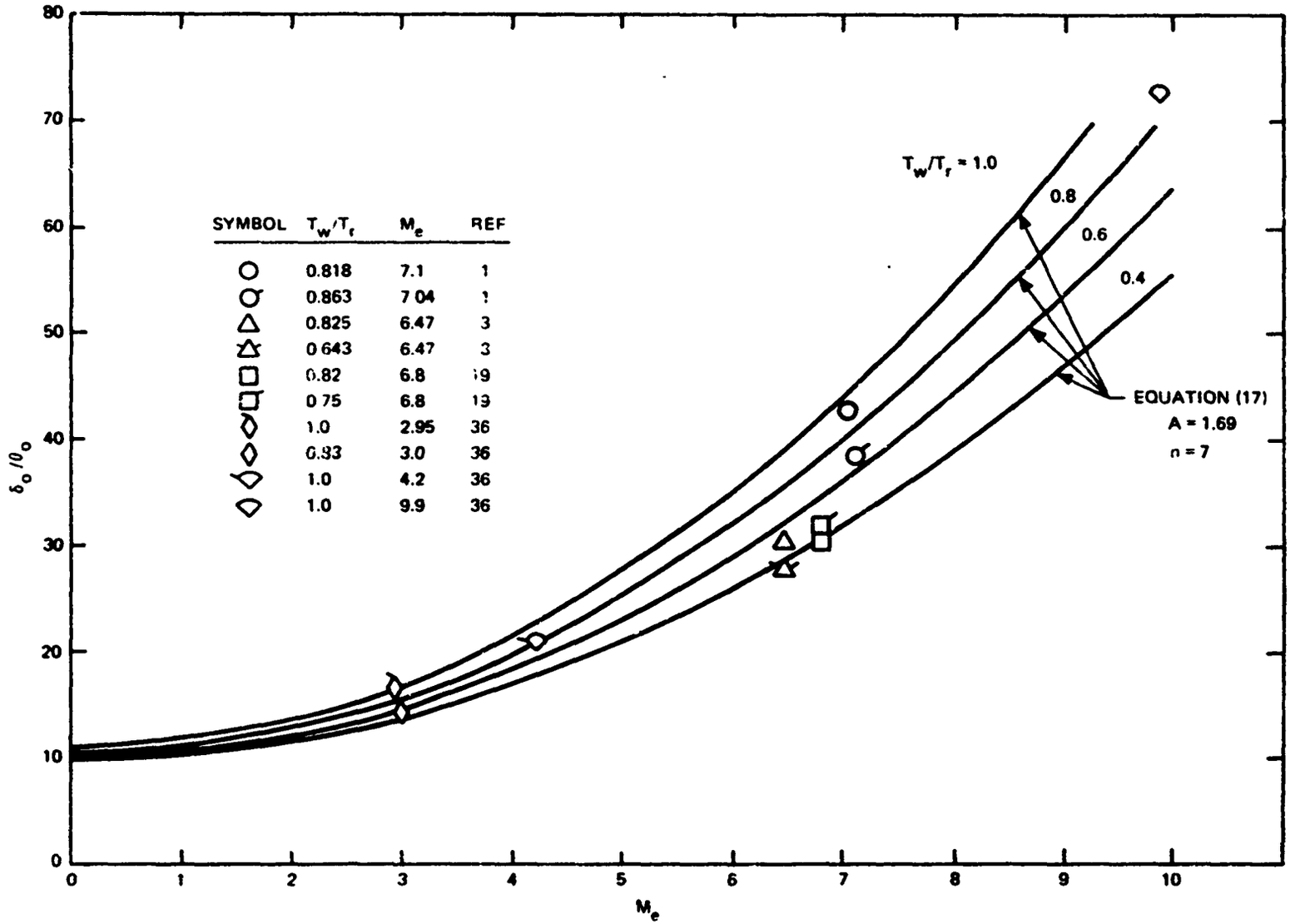

Figure 36. Boundary Layer Thickness Ratio Variation with Mach Number

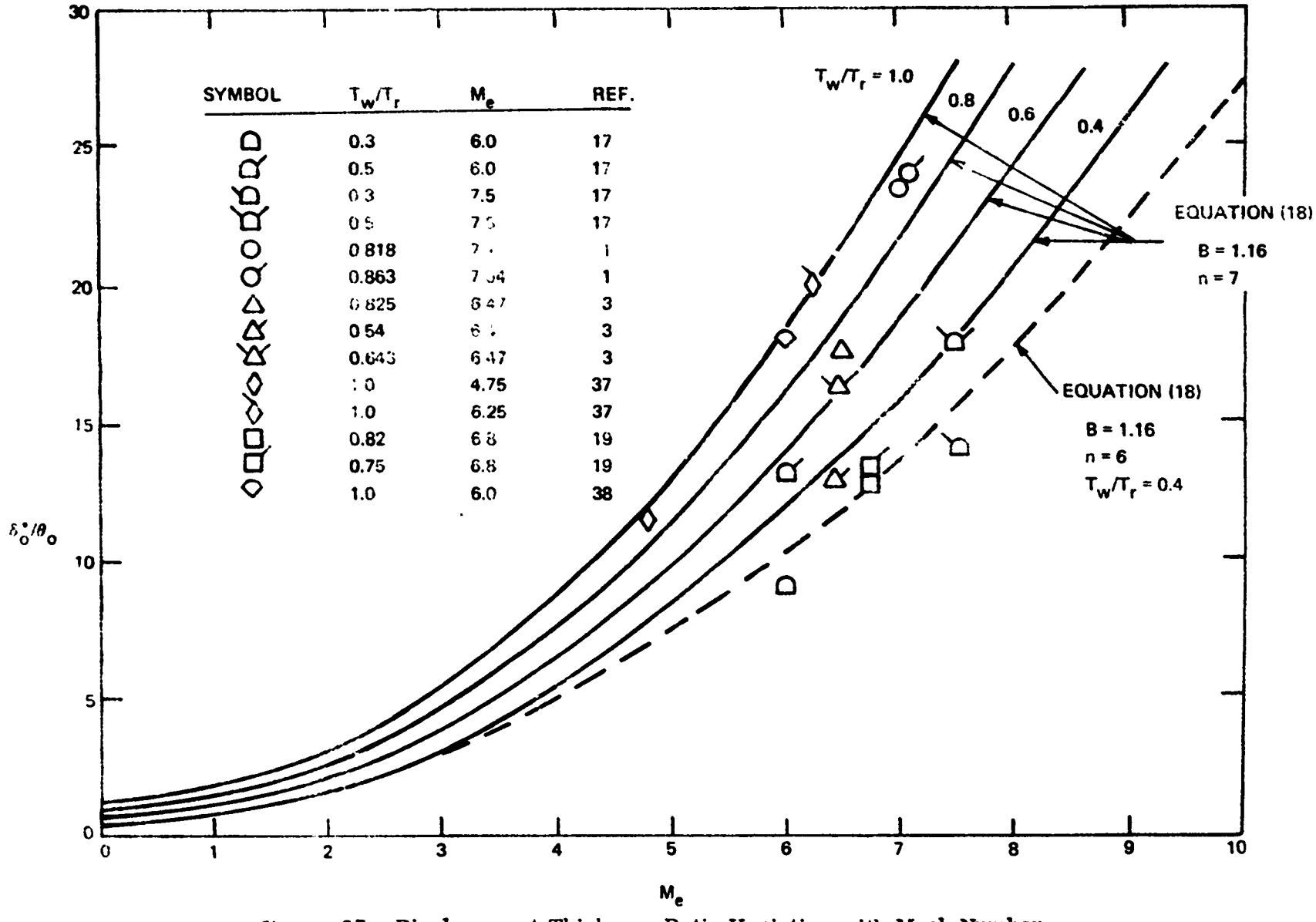

Figure 37. Displacement Thickness Ratio Variation with Mach Number

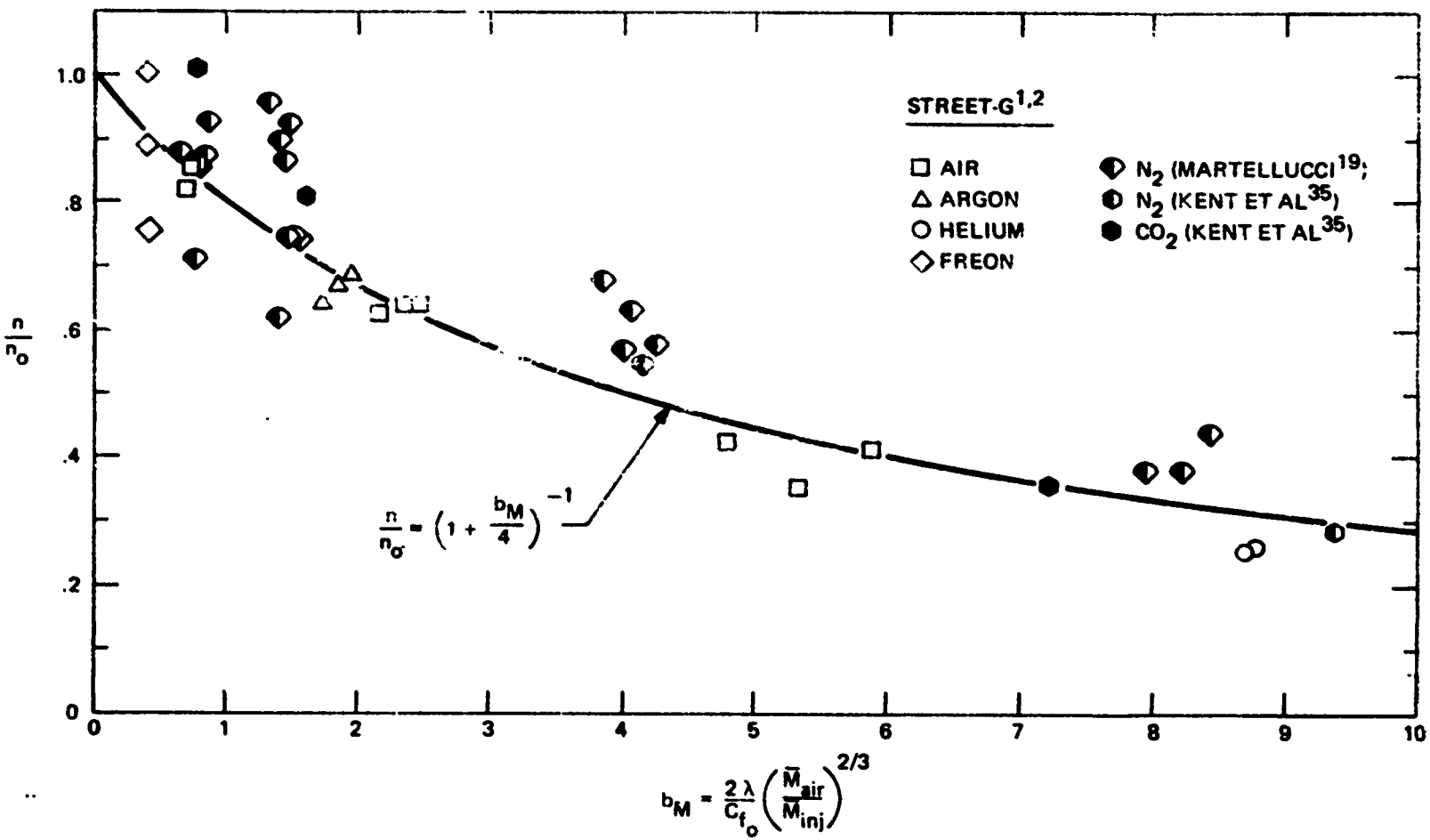

Figure 38. Effects of Mass Transfer on the Velocity Power Law Exponent

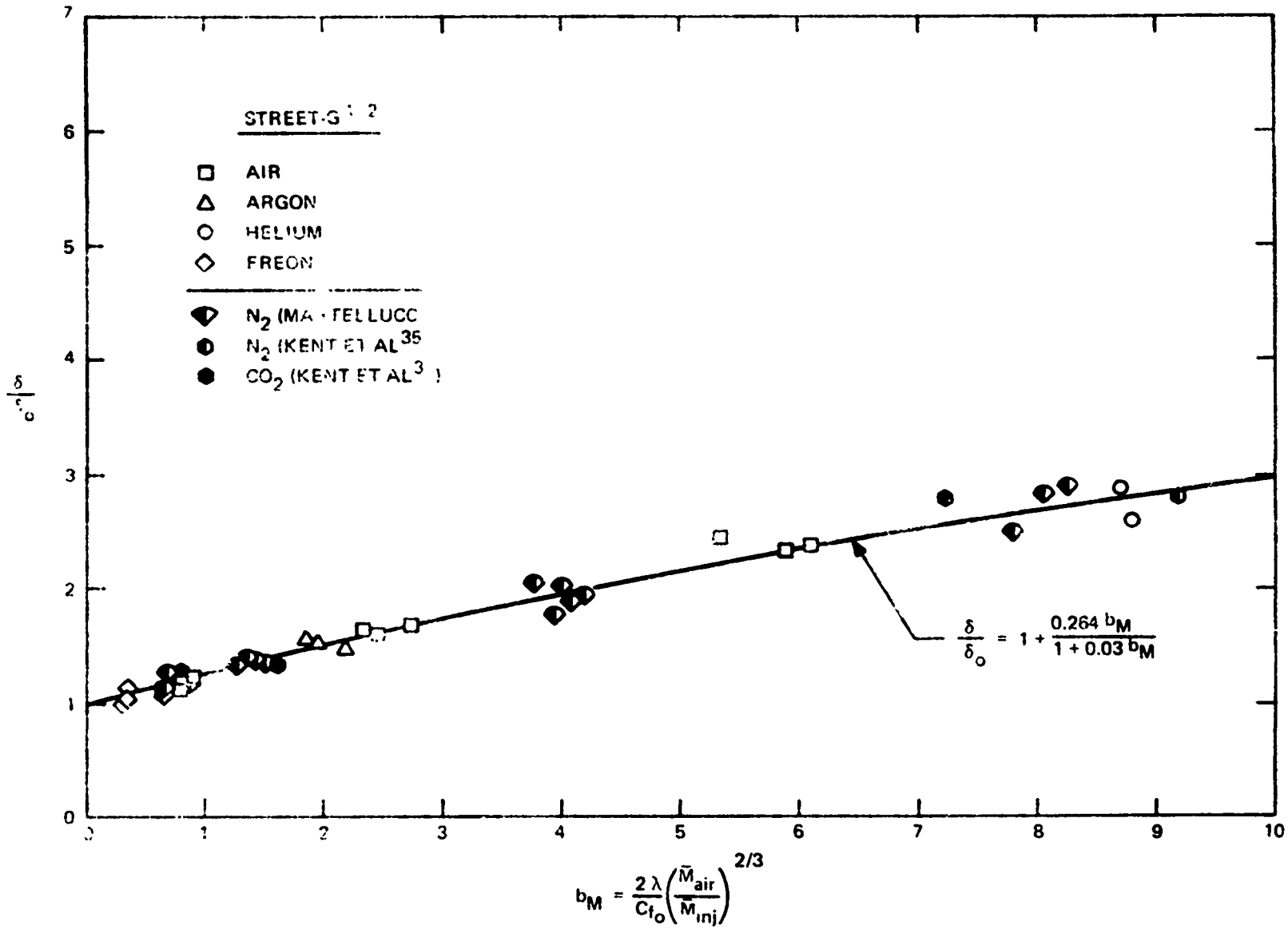

Figure 39. Effects of Mass Transfer on Boundary Layer Thickness ($\alpha = 0°$)

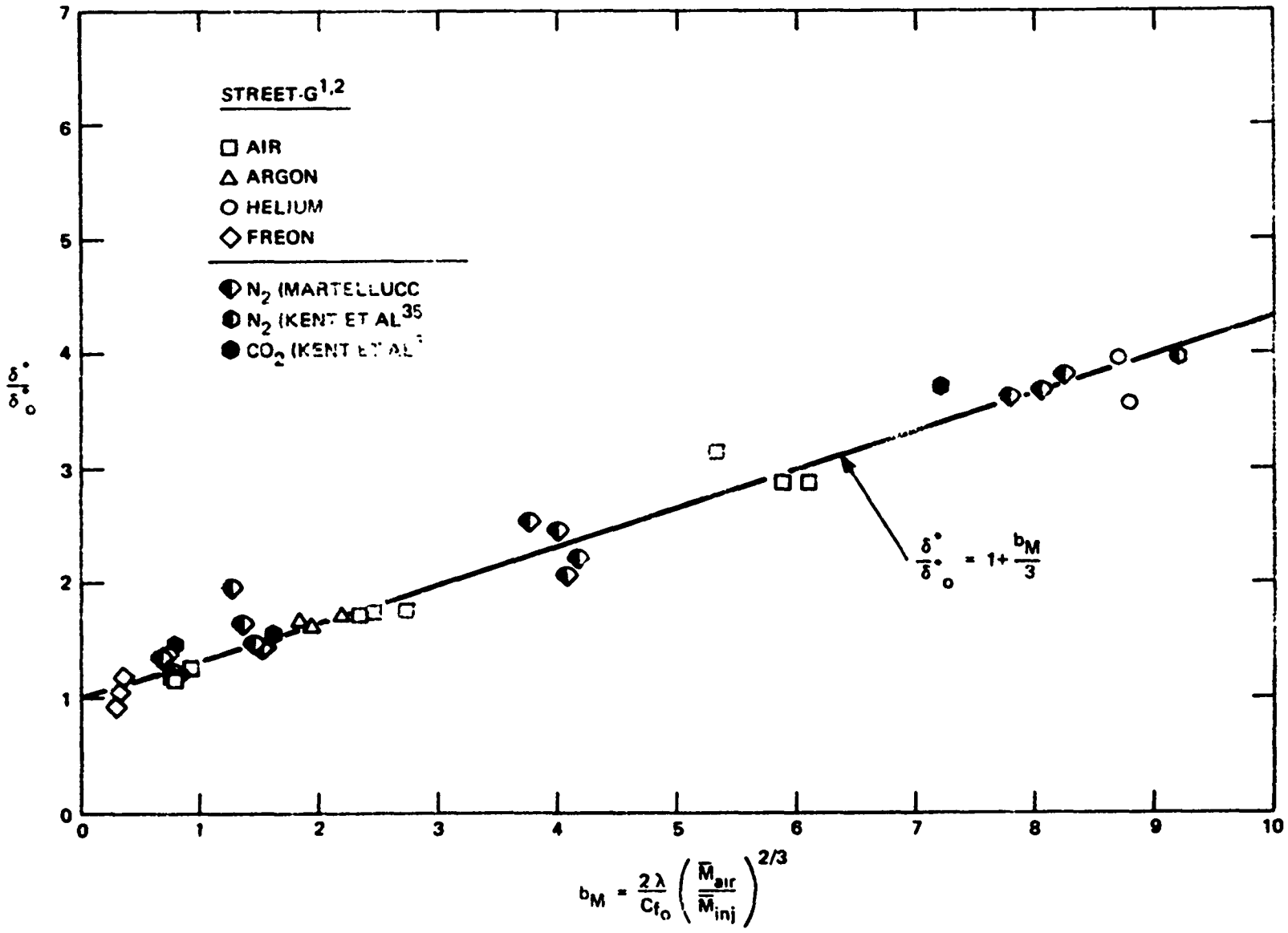

Figure 40. Effects of Mass Transfer on Displacement Thickness ($\alpha = 0°$)

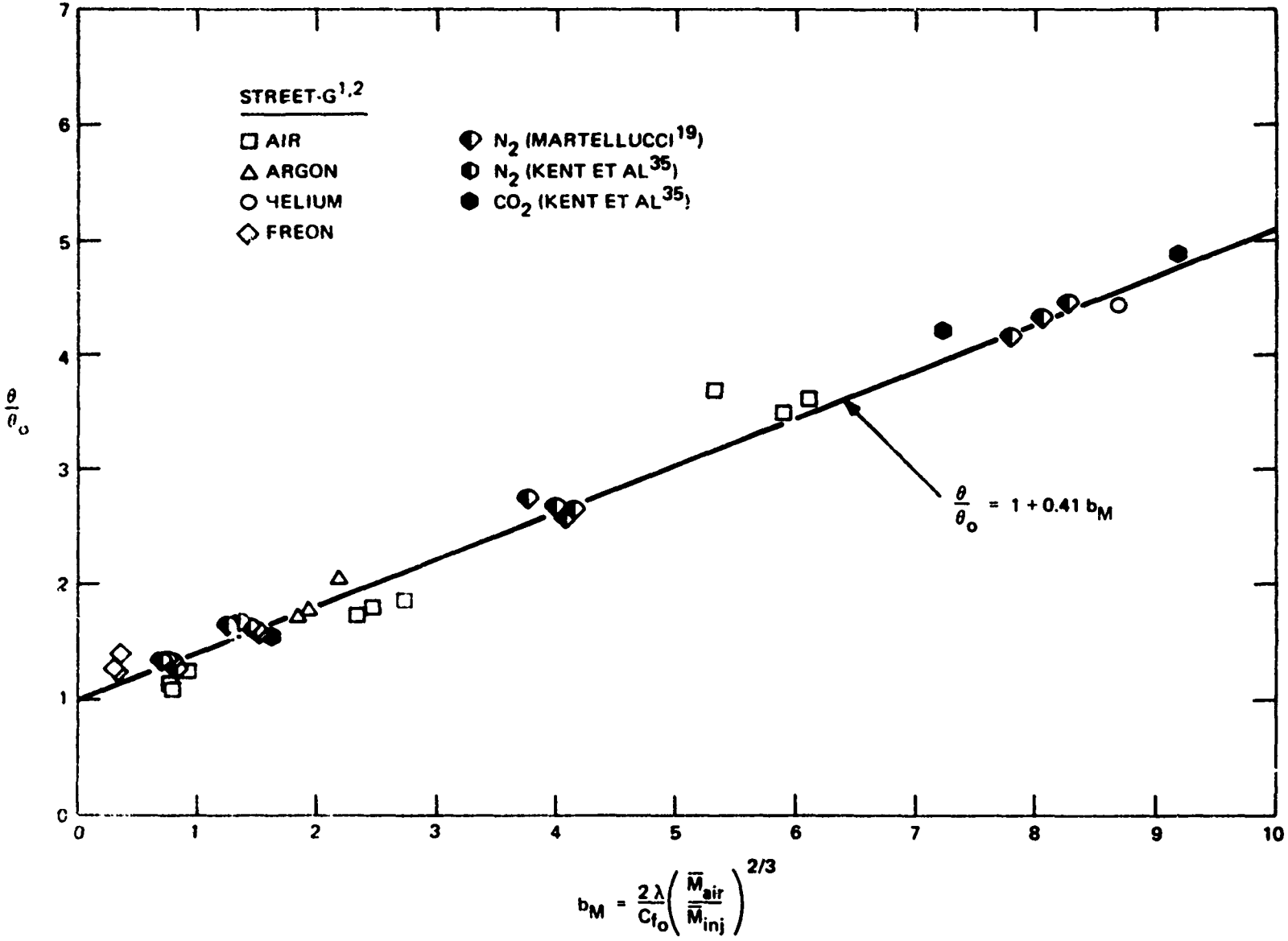

Figure 41. Effects of Mass Transfer on Momentum Thickness ($\alpha = 0°$)

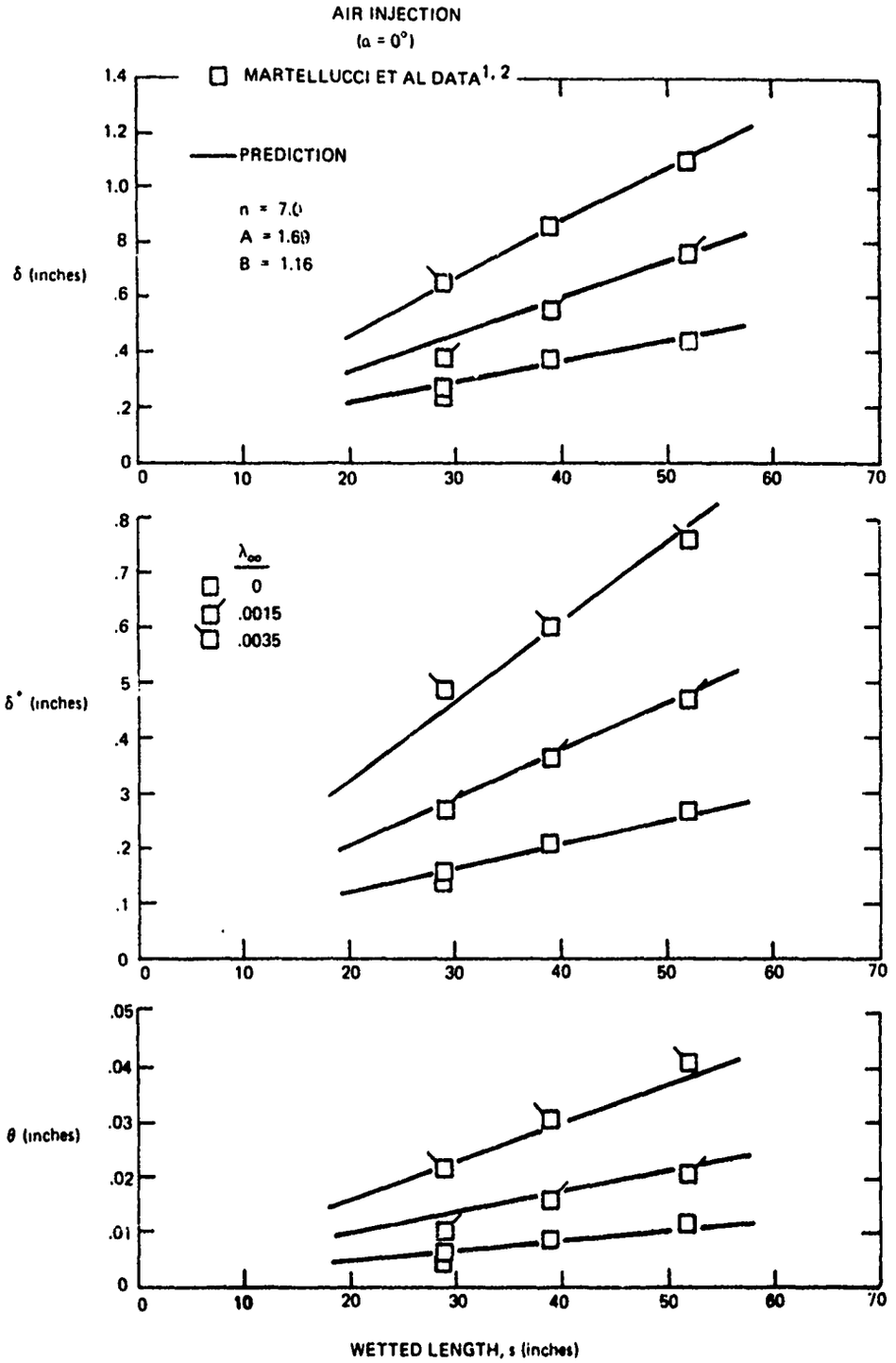

Figure 42. Viscous Layer Thickness Predictions Compared to Data

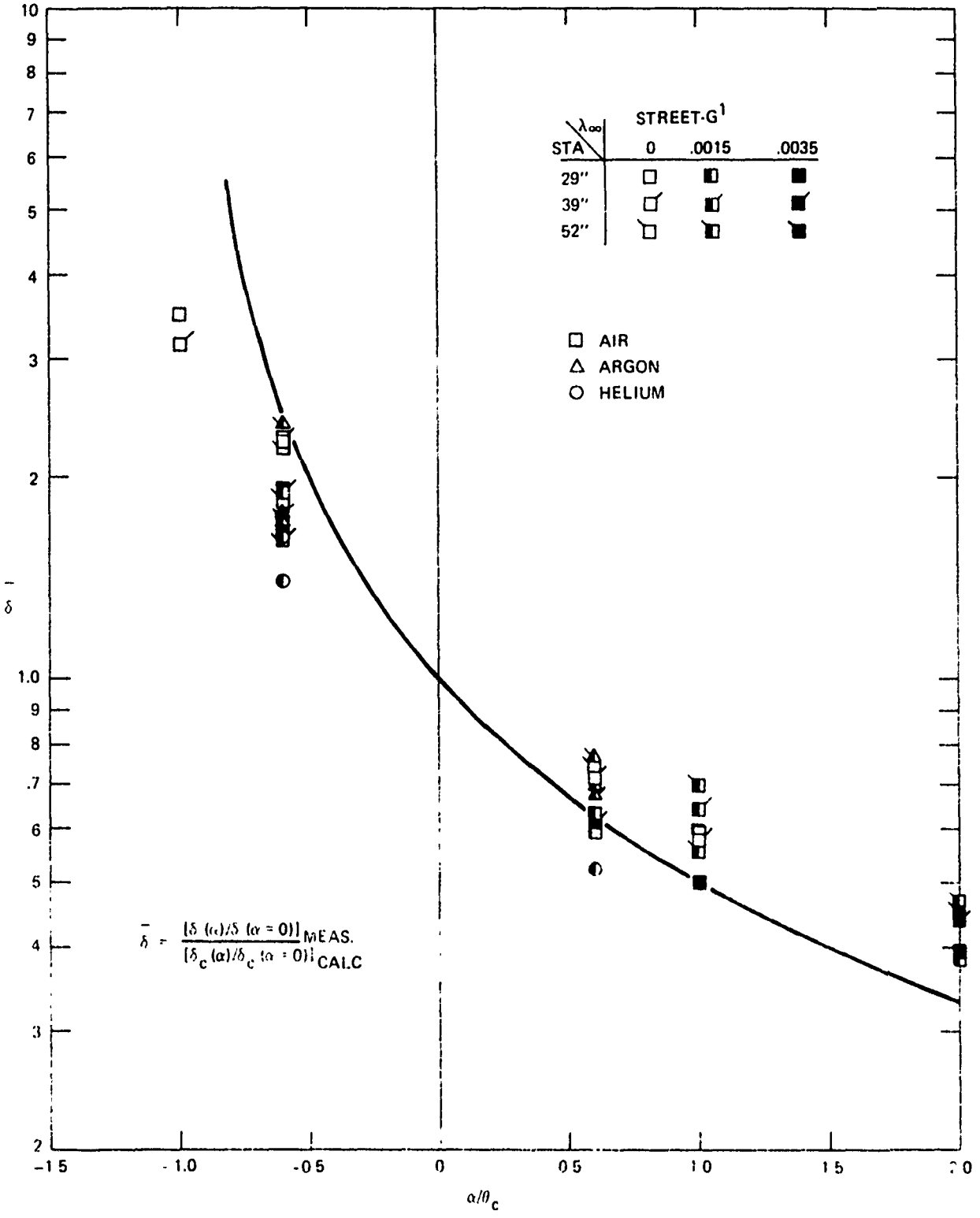

Figure 43. Correlation of Boundary Layer Thickness with Angle of Attack

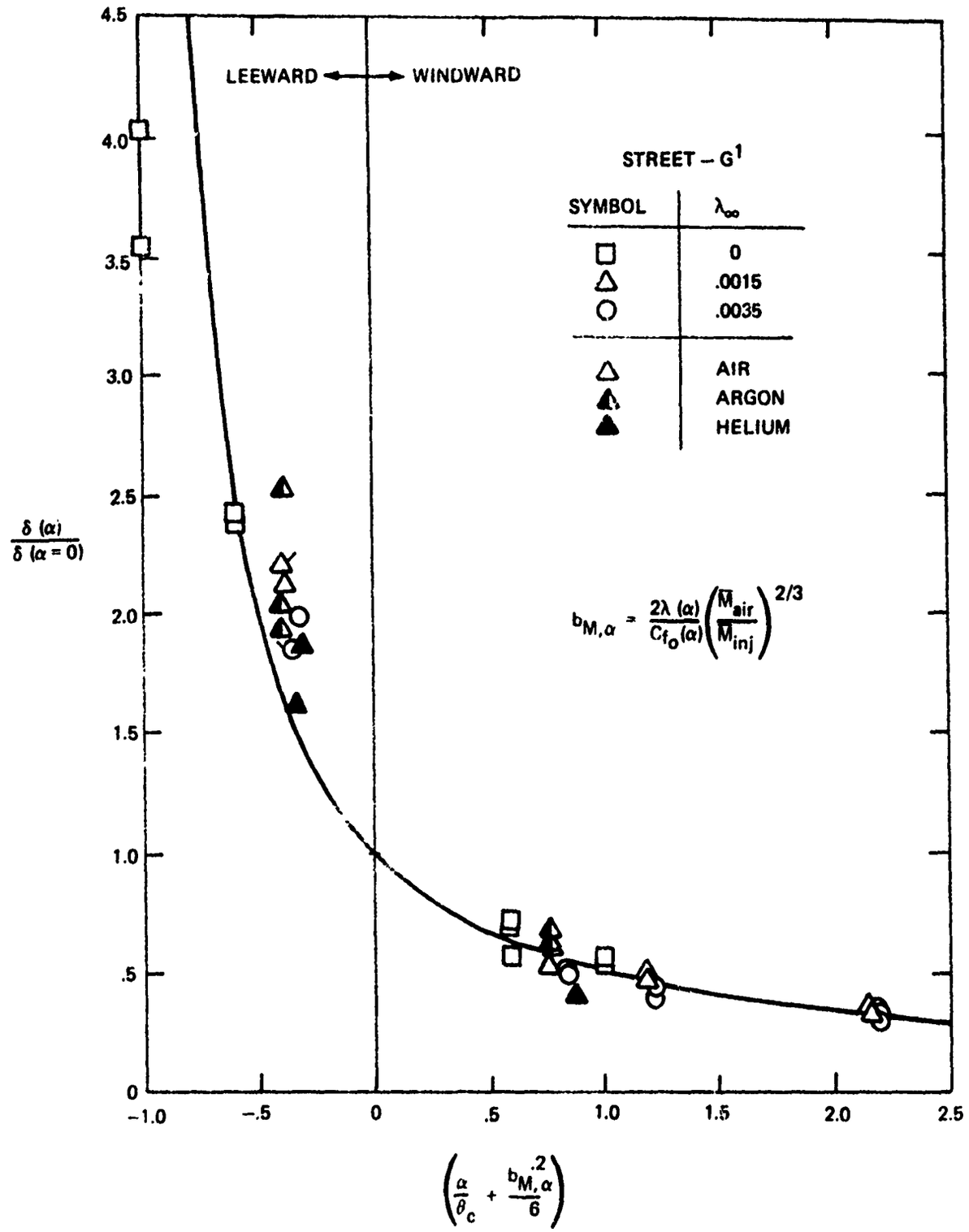

Figure 44. Correlation of Boundary Layer Thickness with Angle of Attack and Blowing

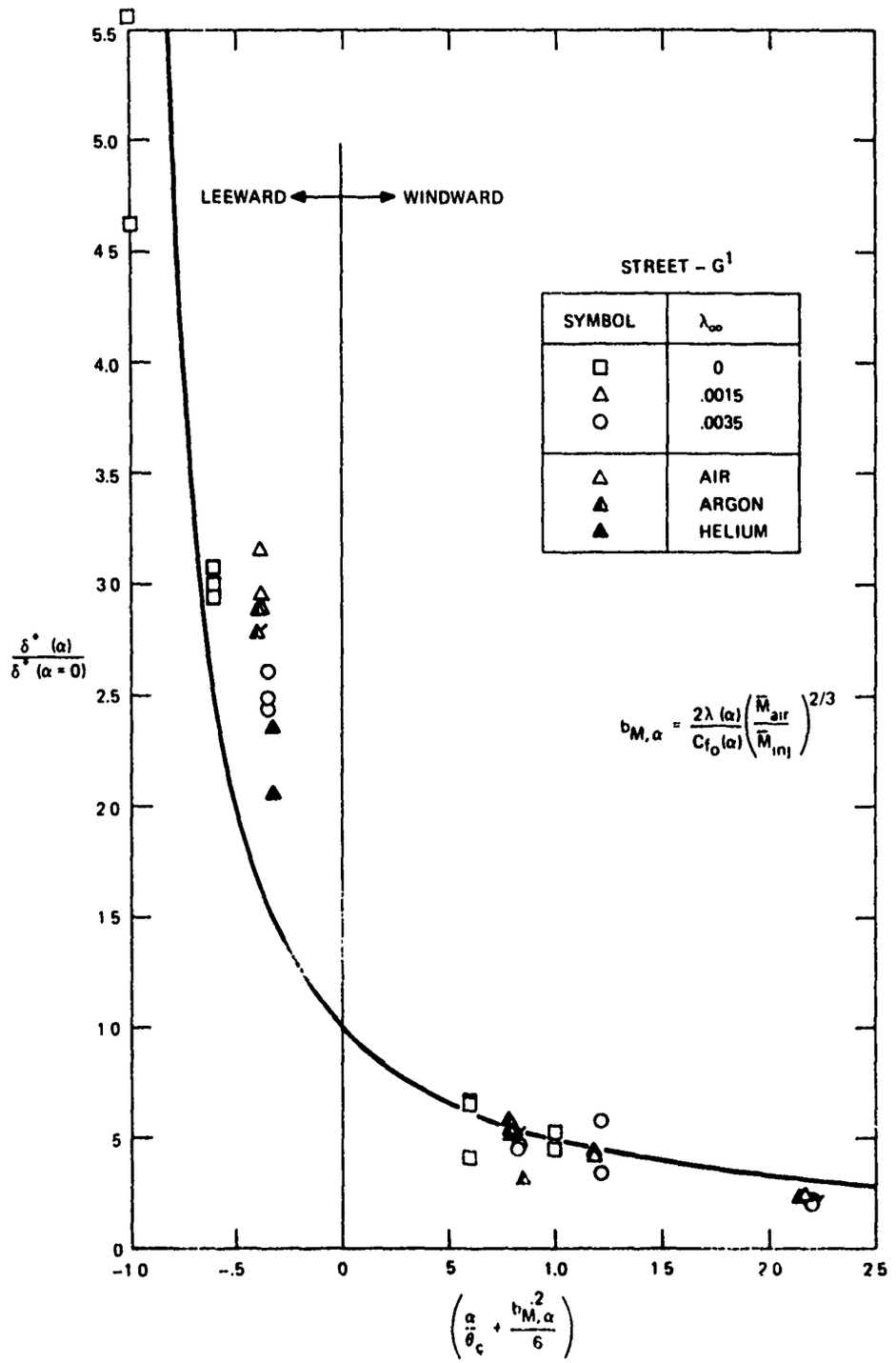

Figure 45. Correlation of Displacement Thickness with Angle of Attack and Blowing

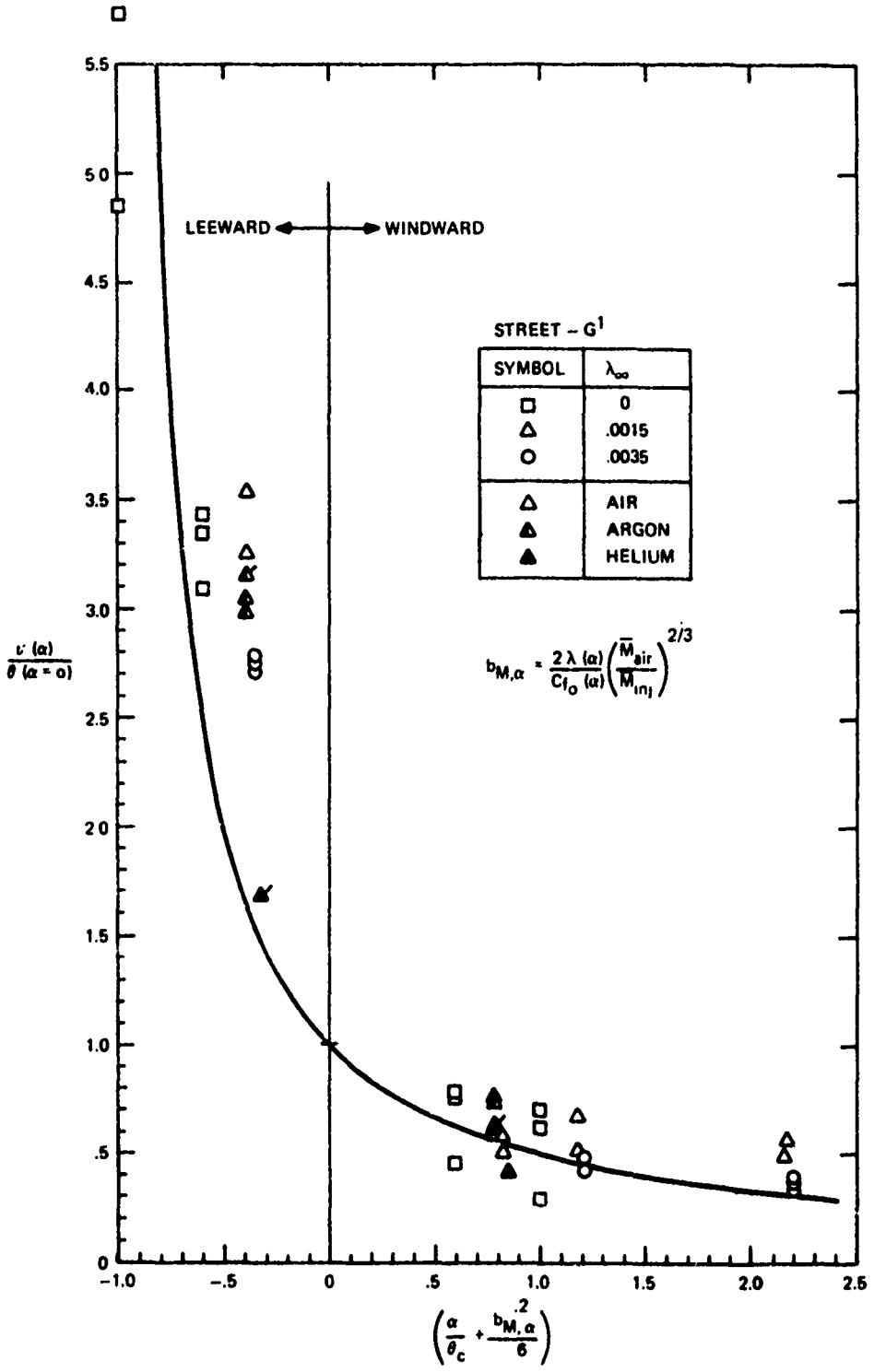

Figure 46. Correlation of Momentum Thickness with Angle of Attack and Blowing

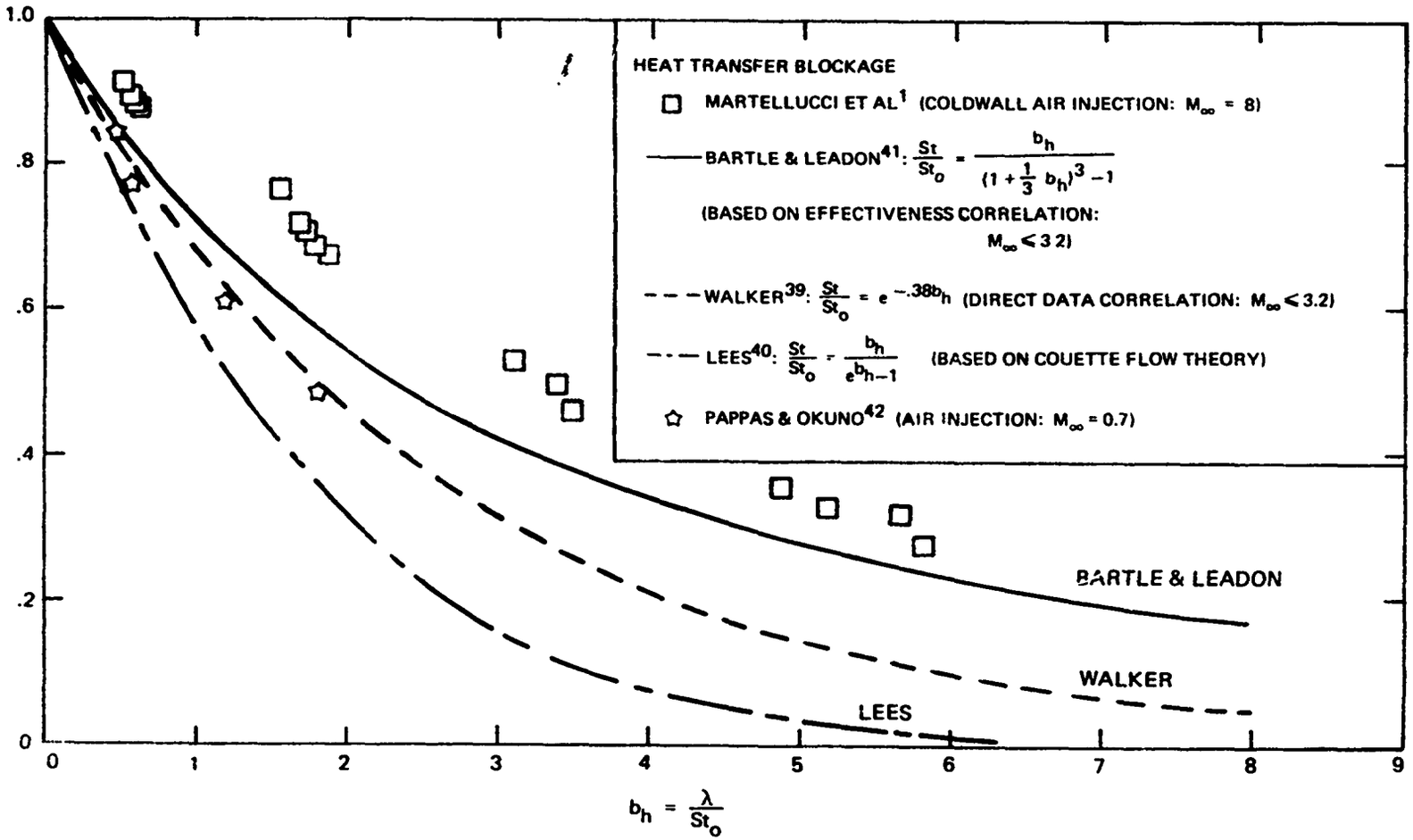

Figure 47. Empirical Heat Blockage Correlations of Previous Investigators

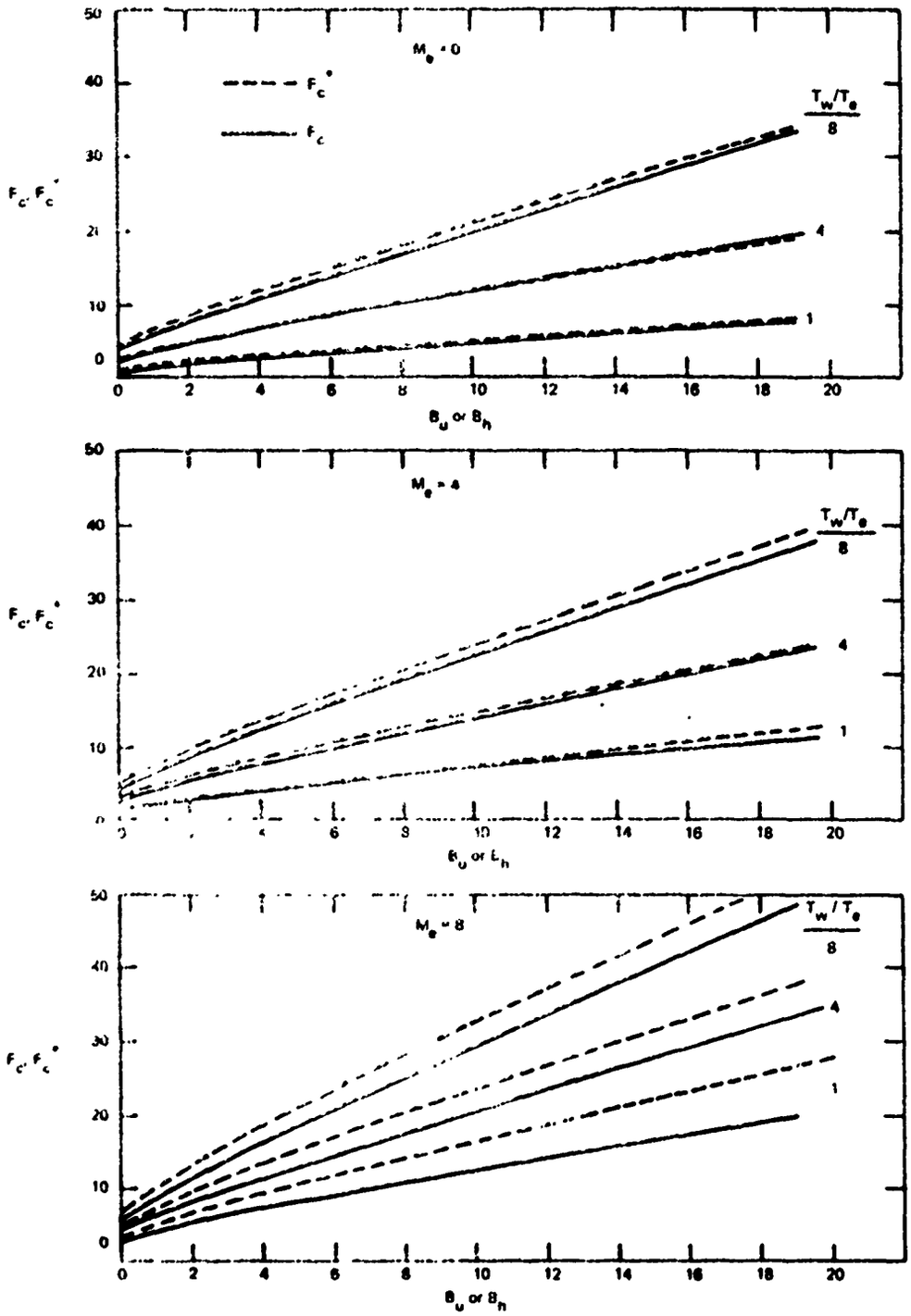

Figure 48. Verification of Compressibility Transformation Approximation

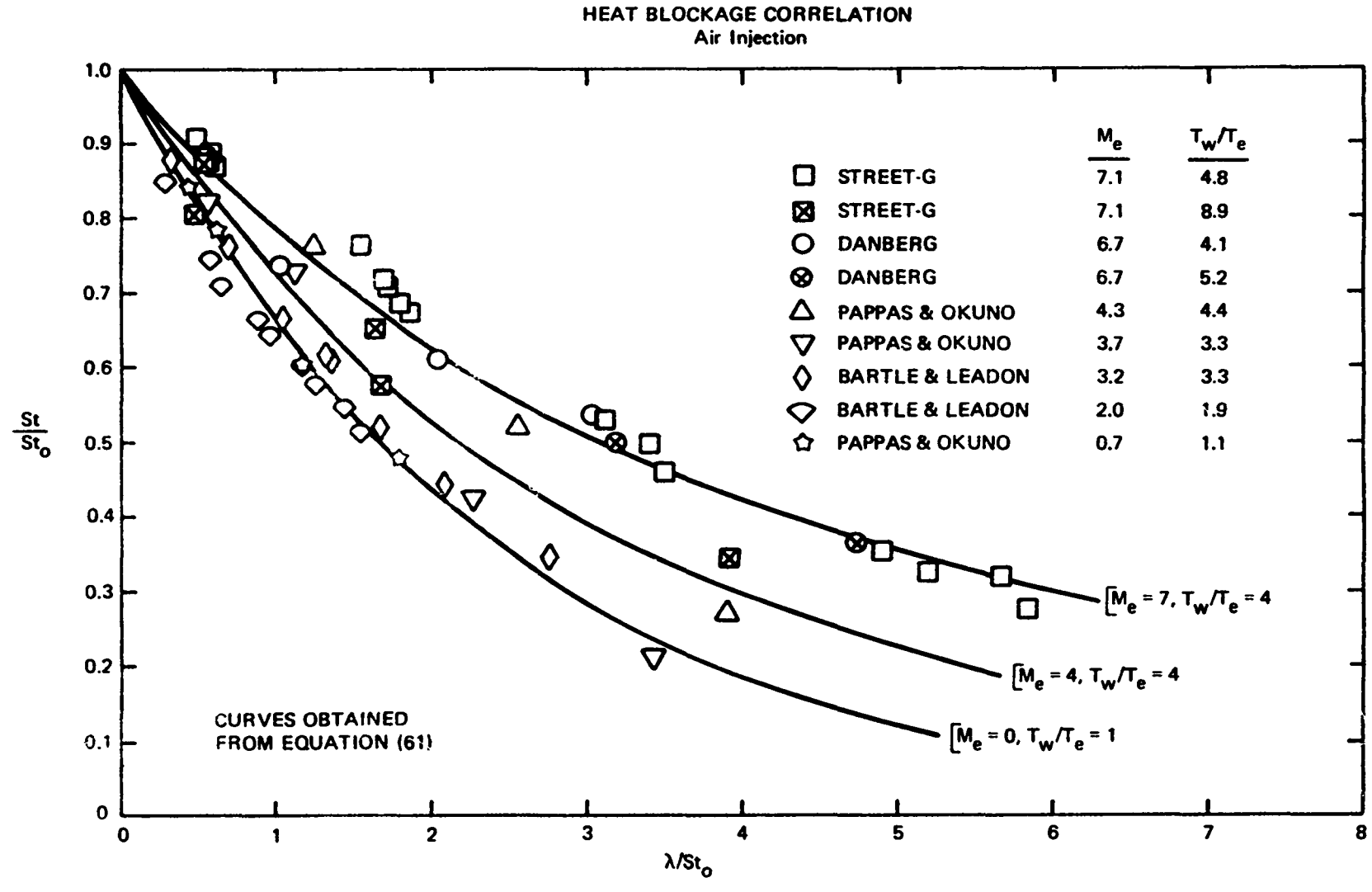

Figure 49. Verification of the Heat Blockage Correlation (Air Injection)

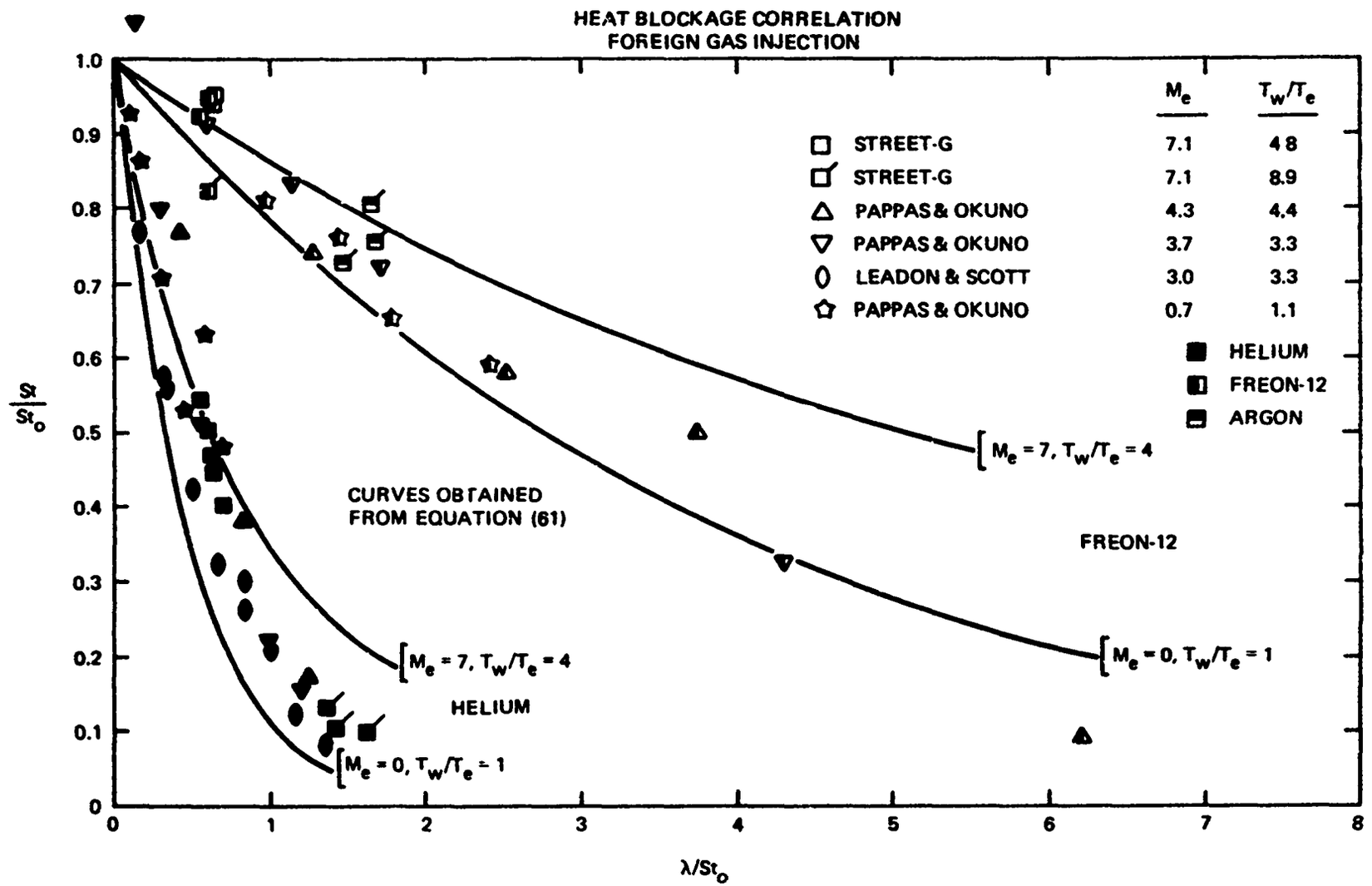

Figure 50. Verification of the Heat Blockage Correlation (Foreign Gas Injection)

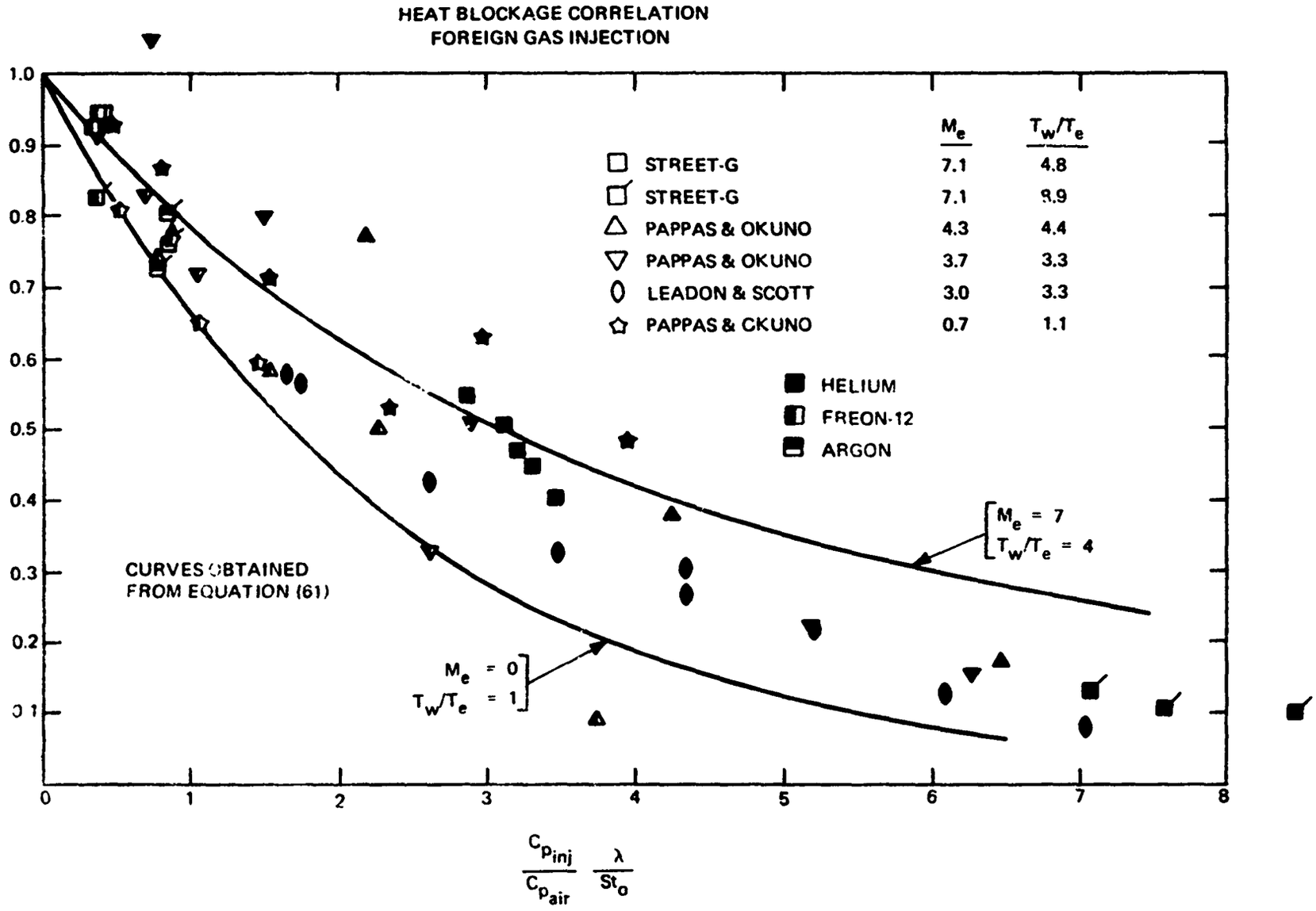

Figure 51. Verification of the Heat Blockage Correlation (Foreign Gas Injection)

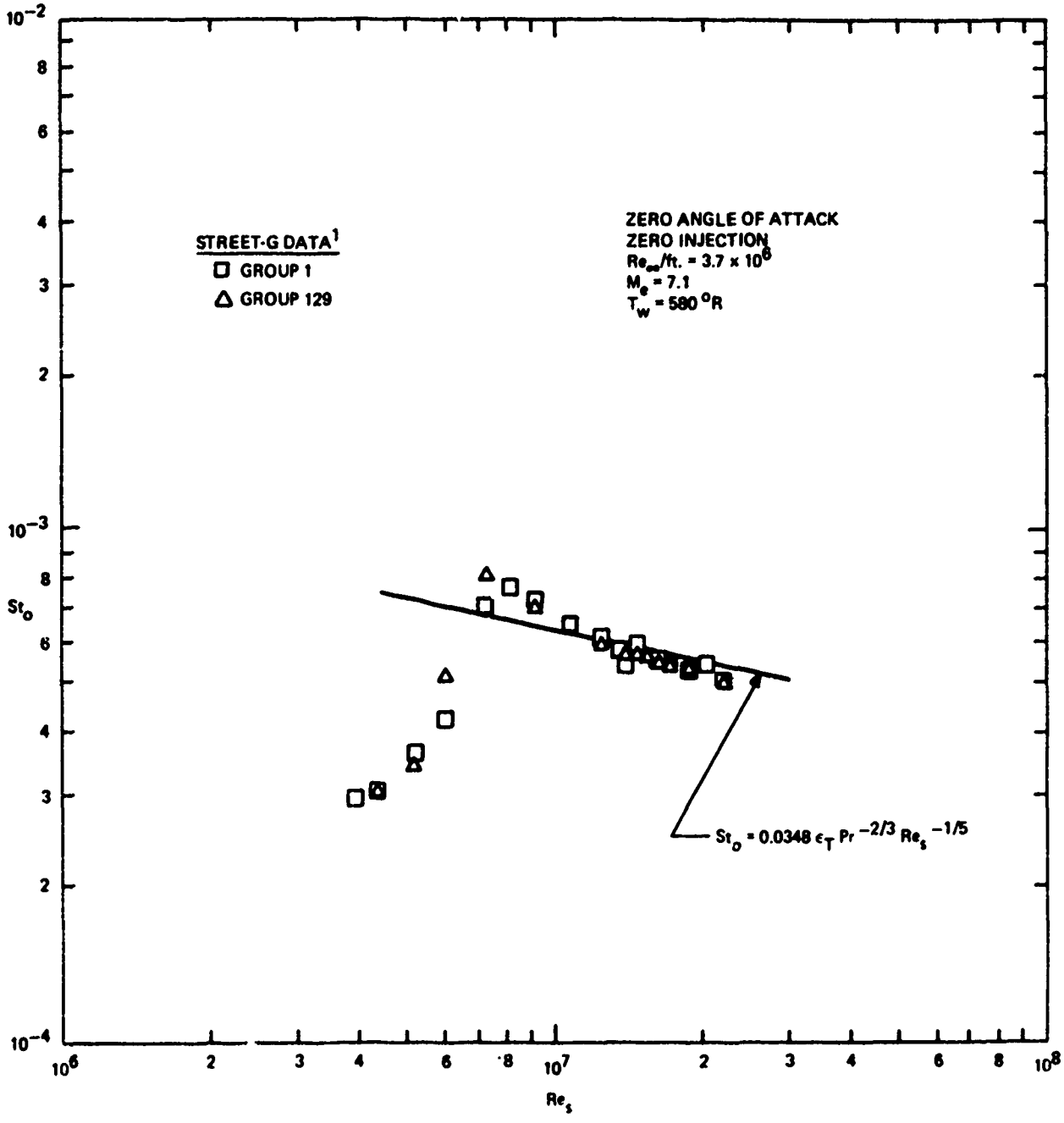

Figure 52. Comparison of Local Stanton Number Prediction with Data

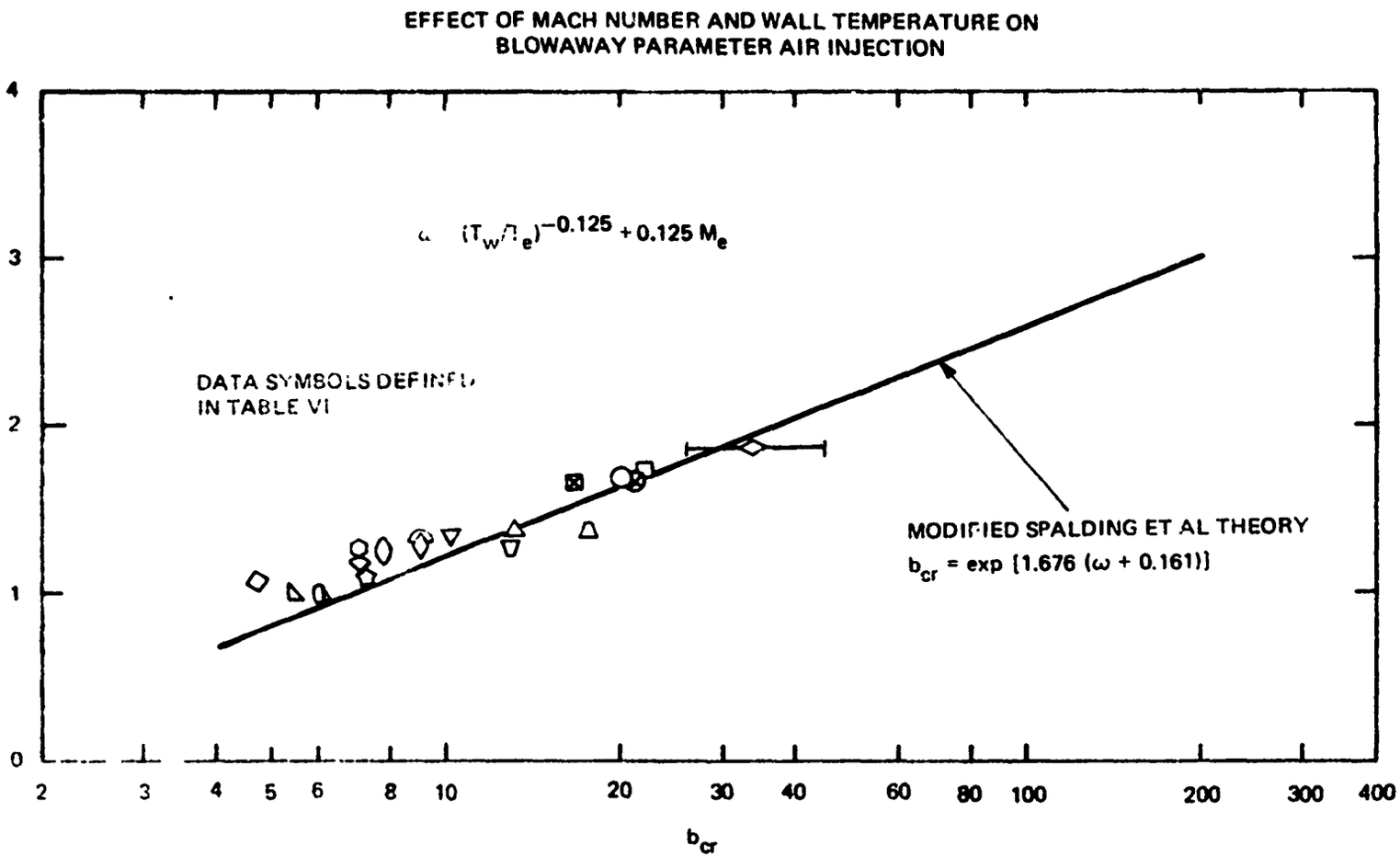

Figure 53. Effect of Mach Number and Wall Temperature on Blowaway Parameter (Air Injection)

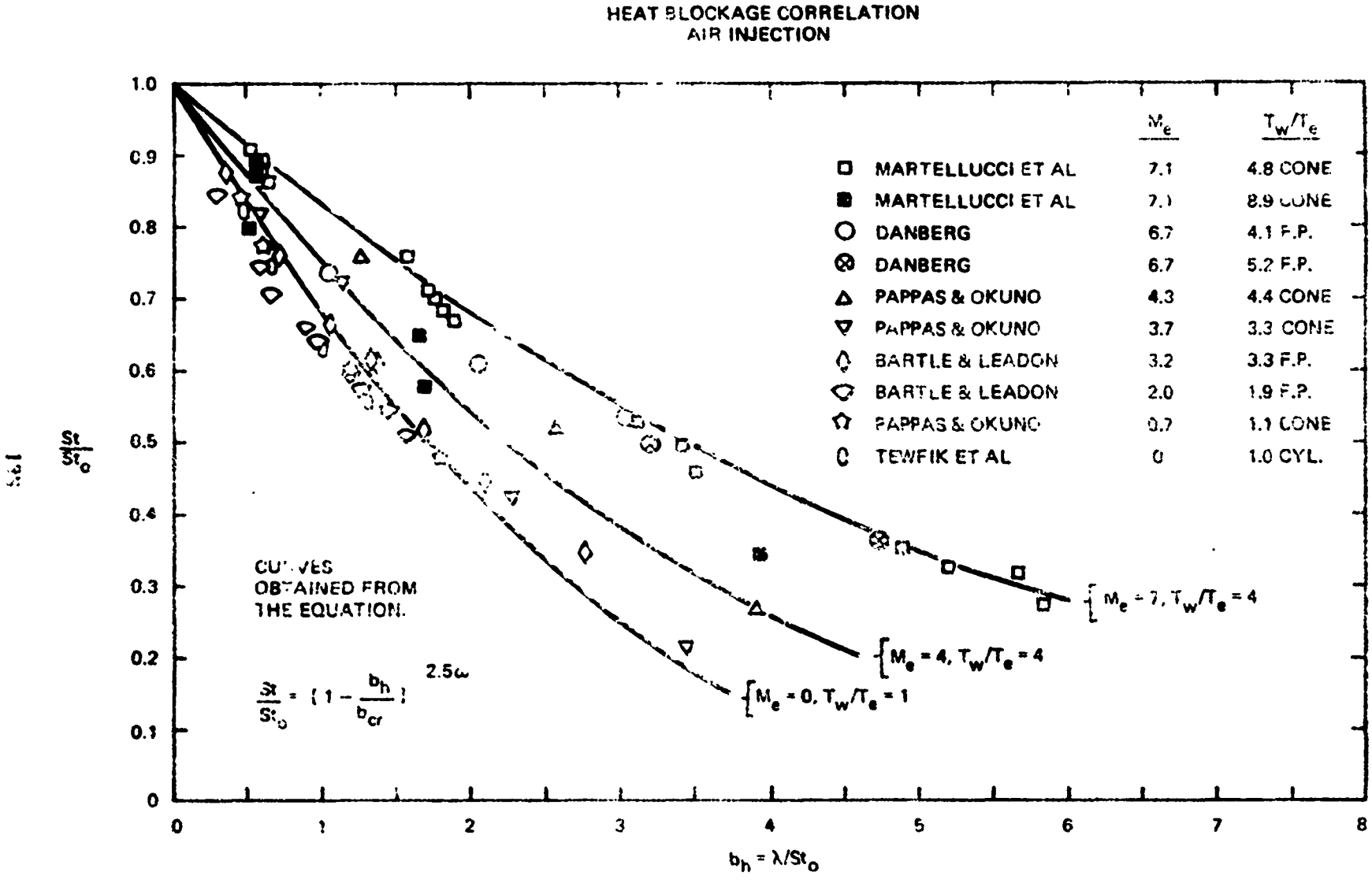

Figure 54. Comparison of Heat Blockage Correlation with Air Injection Data

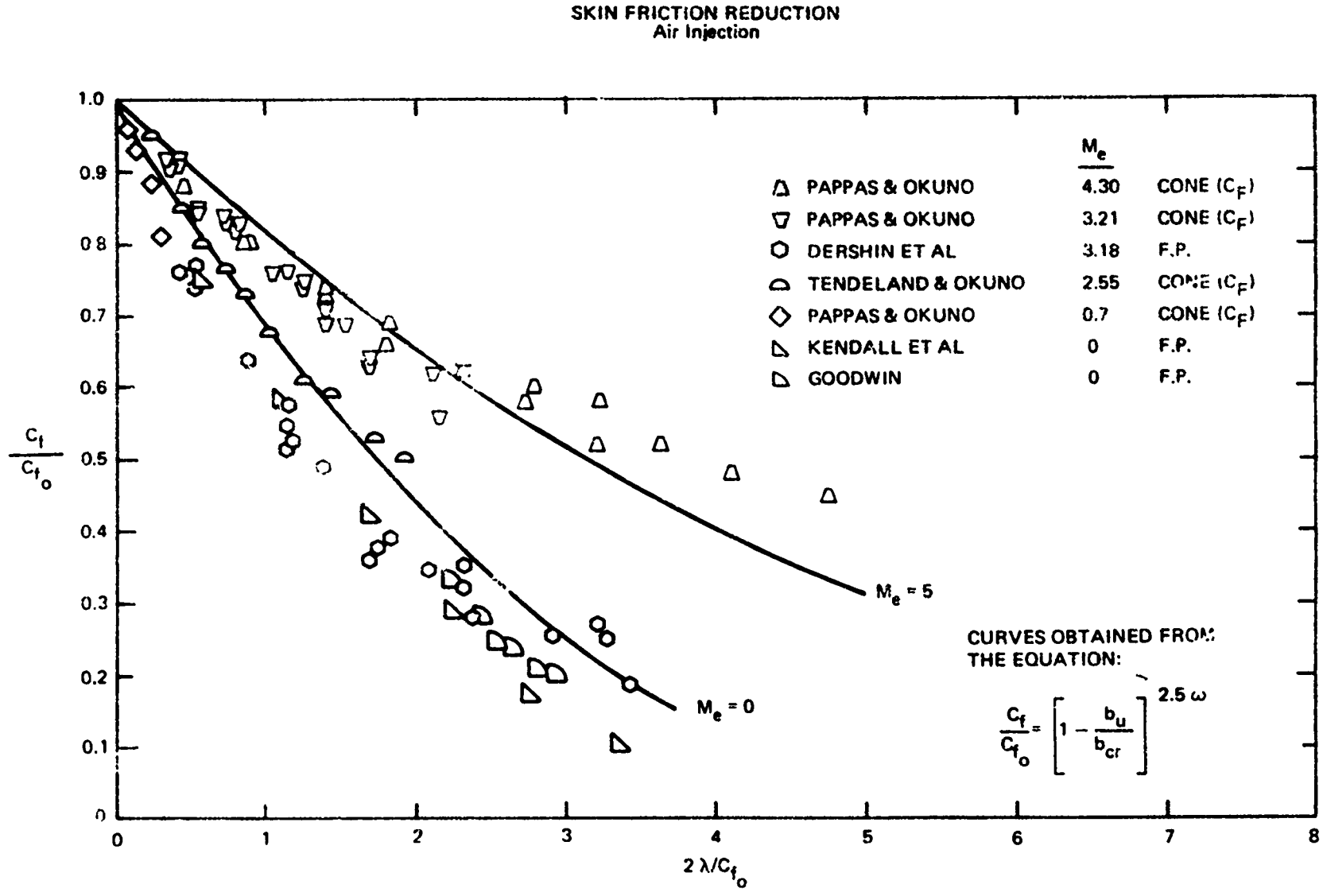

Figure 55. Comparison of Skin Friction Reduction Correlation with Air Injection Data

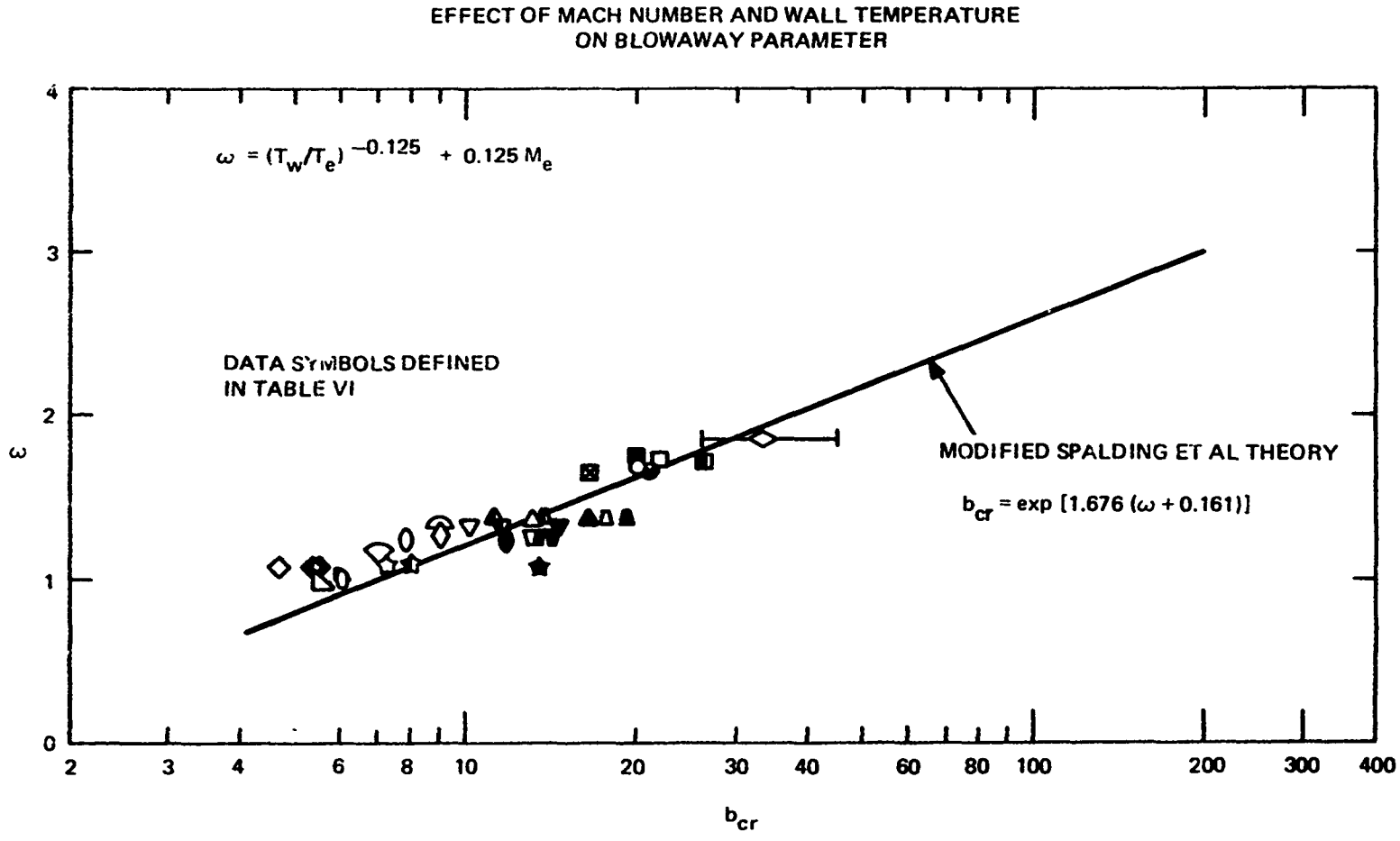

Figure 56. Effect of Mach Number and Wall Temperature on Blowaway Parameter (Foreign Gas Injection)

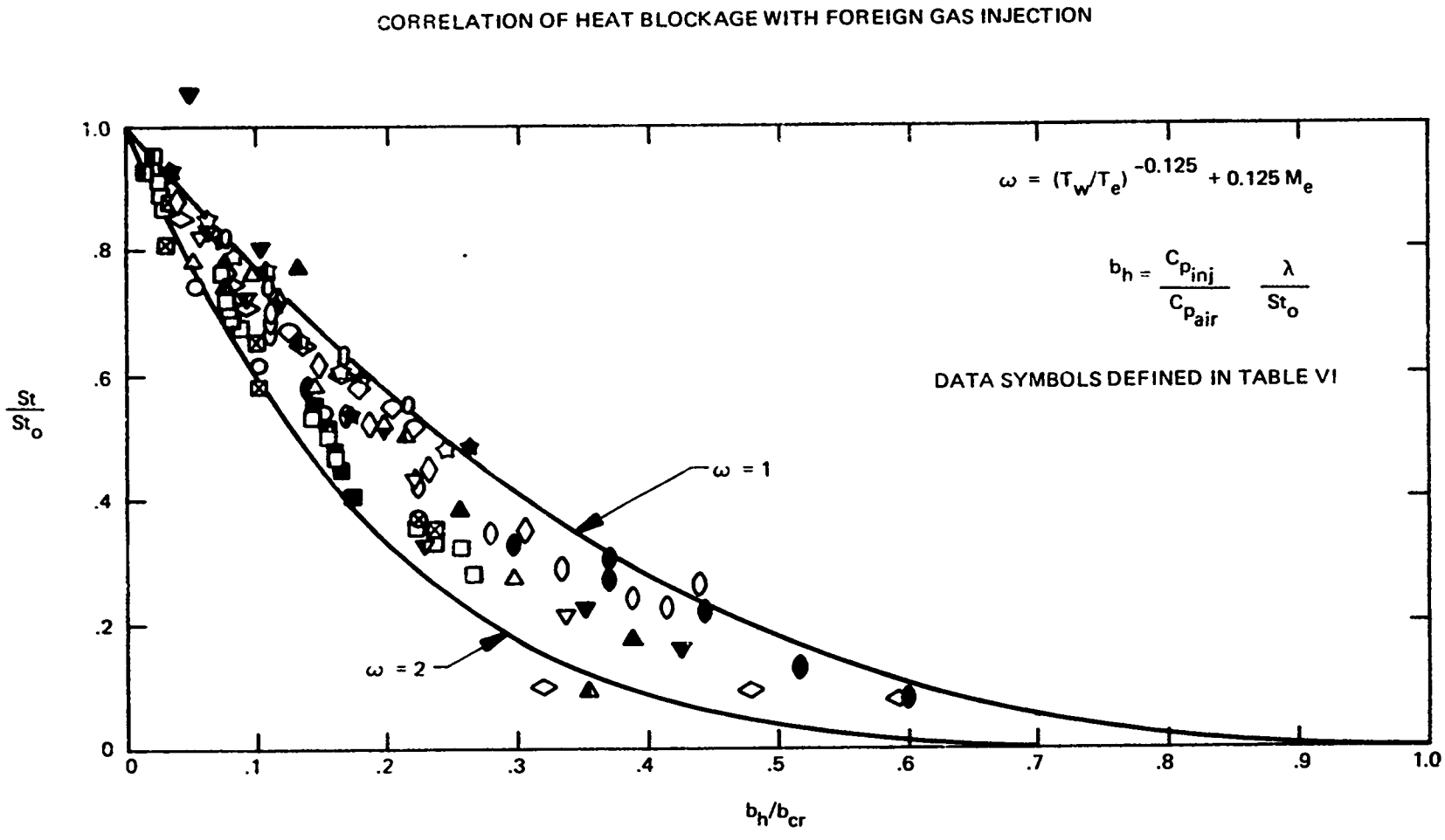

Figure 57. Correlation of Heat Blockage with Foreign Gas Injection

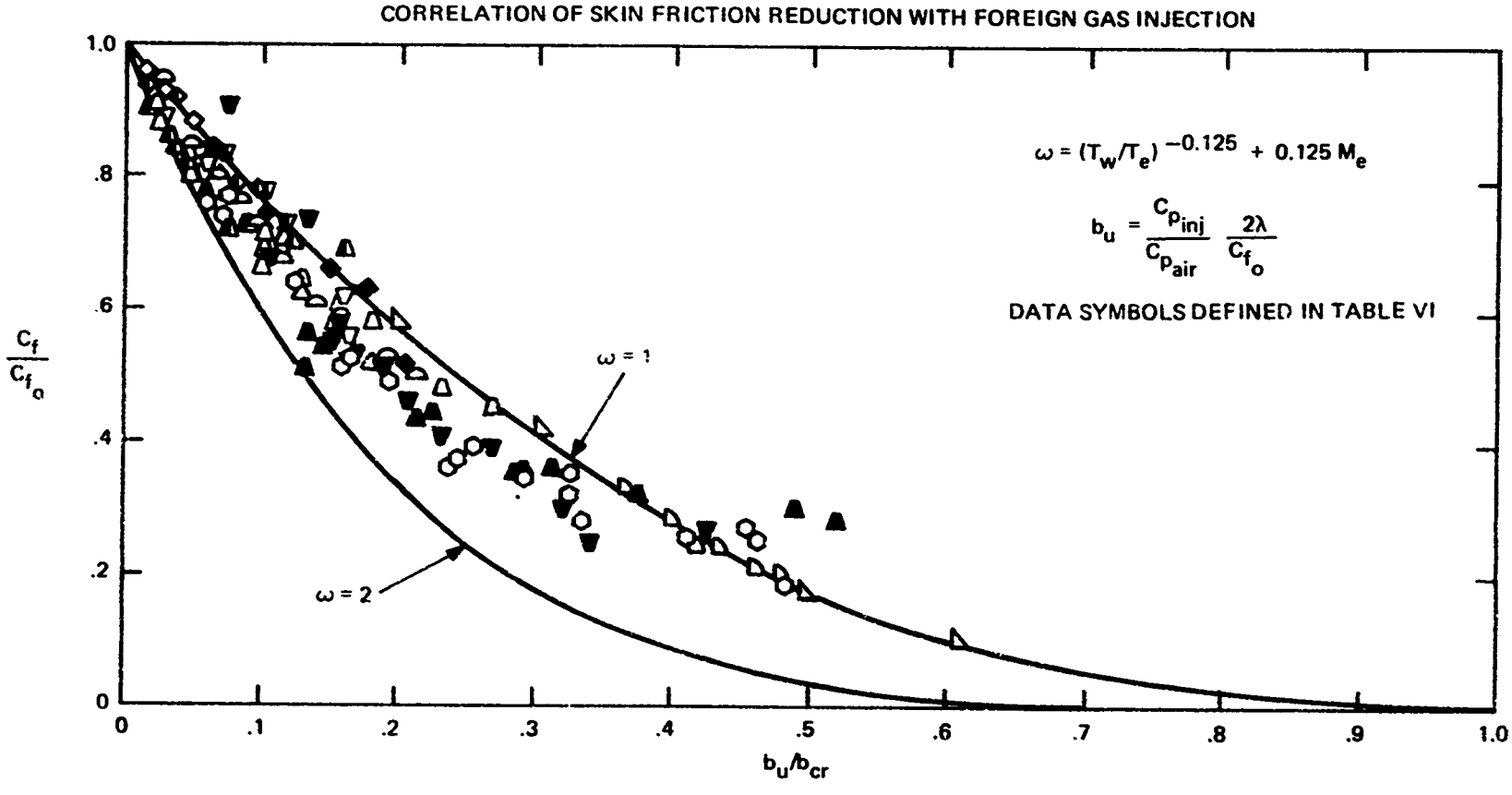

Figure 58. Correlation of Skin Friction Reduction with Foreign Gas Injection

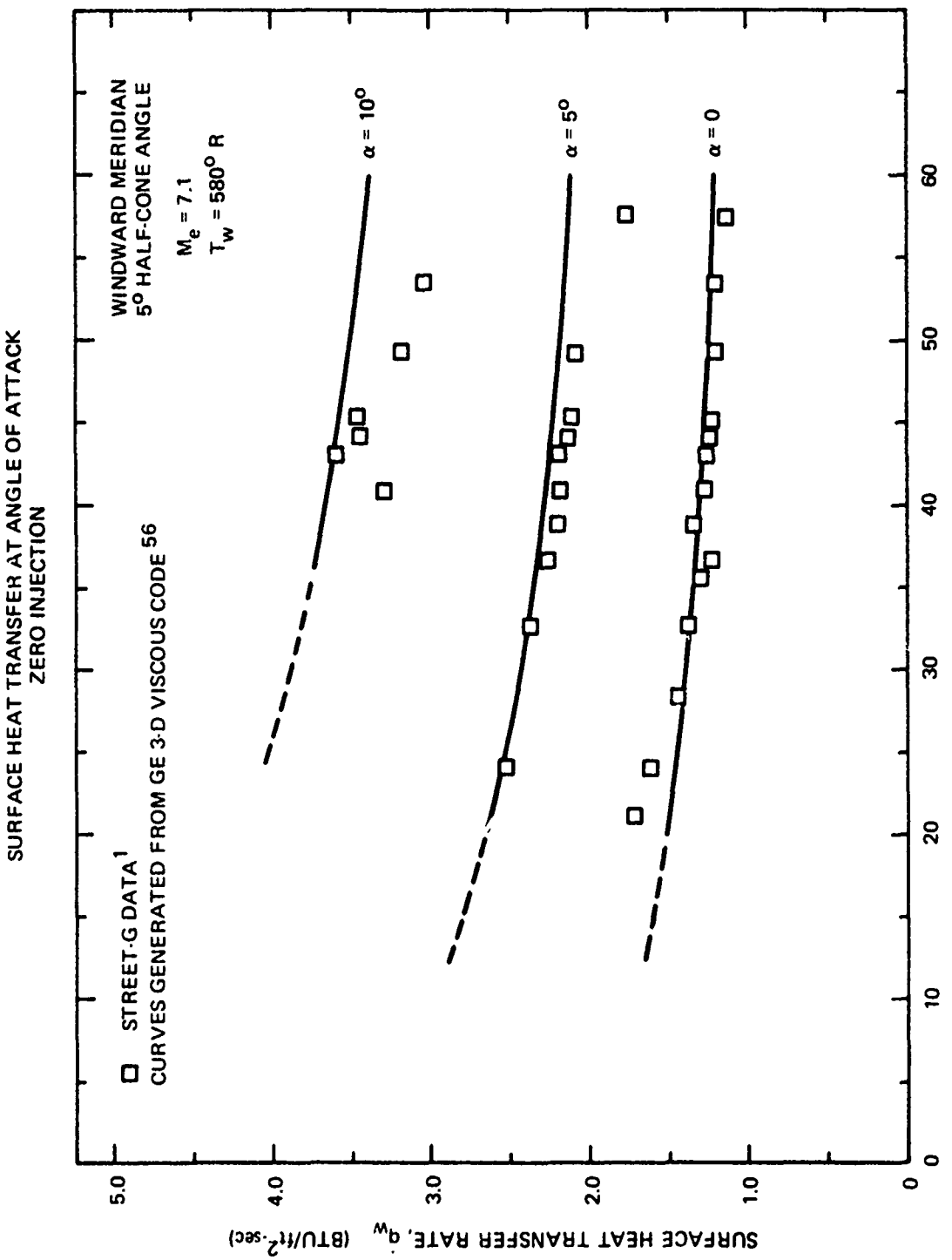

Figure 59. Surface Heat Transfer at Angle of Attack (Zero Injection)

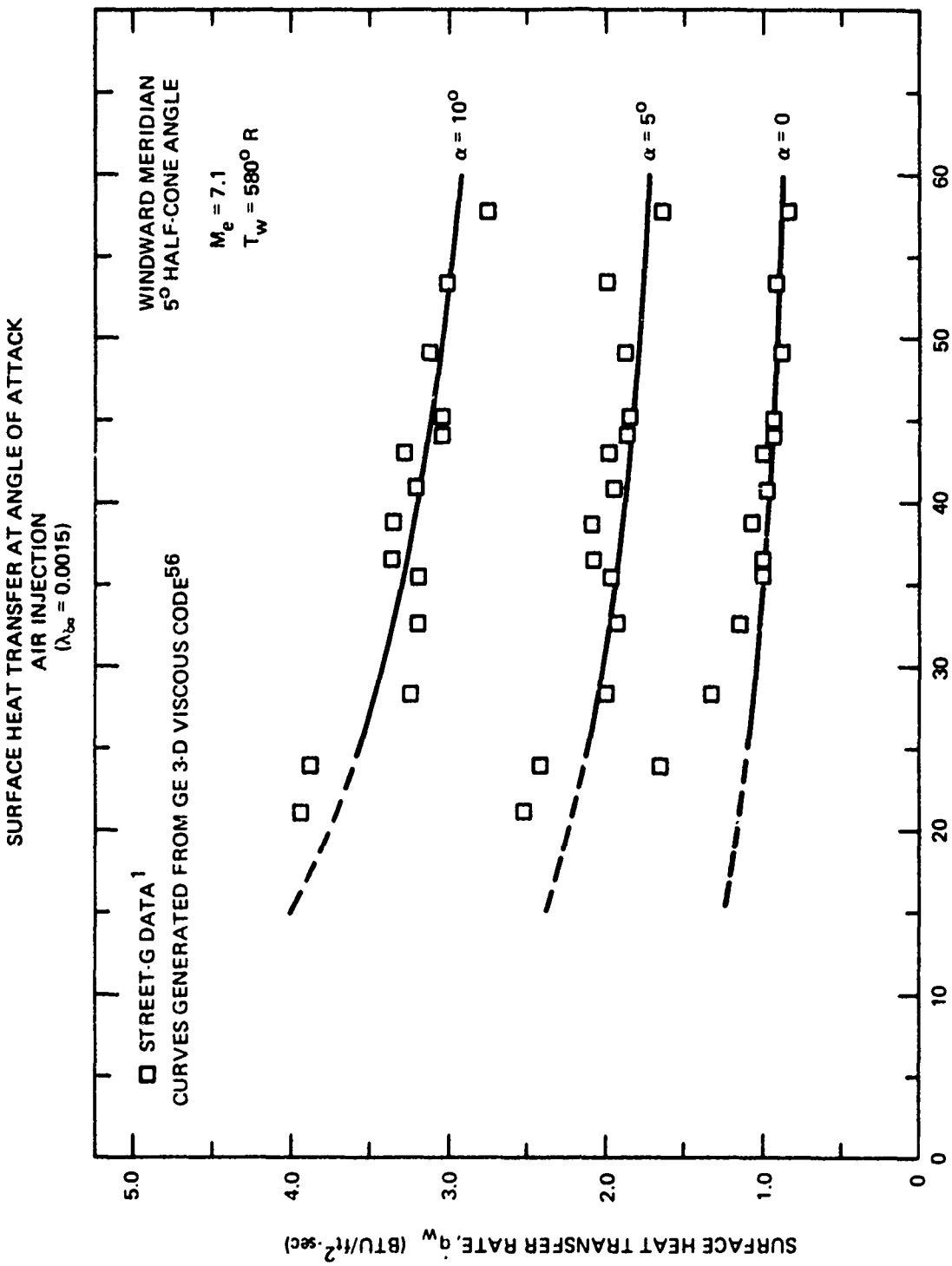

Figure 60. Surface Heat Transfer at Angle of Attack (Air Injection)

☆U.S.Government Printing Office: 1975 657-023/656